UNIVERSIDADE ESTADUAL DE CAMPINAS
FACULDADE DE ENGENHARIA DE ALIMENTOS
DEPARTAMENTO DE ENGENHARIA DE ALIMENTOS

PURIFICAÇÃO E CONCENTRAÇÃO DE ÁCIDO CLAVULÂNICO POR NANOFILTRAÇÃO

Andrea Limoeiro Carvalho
MSc. Engenharia Química
Engª. de Alimentos

Prof. Dr. Francisco Maugeri Filho
Orientador

Tese de Doutorado apresentada à Faculdade de Engenharia de Alimentos da Universidade Estadual de Campinas para a obtenção do título de Doutor em Engenharia de Alimentos na área de Bioengenharia e Biotecnologia

Campinas, março de 2011

FICHA CATALOGRÁFICA ELABORADA PELA
BIBLIOTECA DA FEA – UNICAMP

Carvalho, Andrea Limoeiro
C253p Purificação e concentração de ácido clavulânico por nanofiltração / Andrea Limoeiro Carvalho. -- Campinas, SP: [s.n], 2011.

Orientador: Francisco Maugeri Filho
Tese (doutorado) – Universidade Estadual de Campinas. Faculdade de Engenharia de Alimentos.

1. Nanofiltração. 2. Ácido clavulânico. 3. Purificação. 4. Biotecnologia. I. Maugeri Filho, Francisco. II. Universidade Estadual de Campinas.Faculdade de Engenharia de Alimentos. III. Título.

Título em inglês: Clavulanic acid concentration and purification by nanofiltration
Palavras-chave em inglês (Keywords): Nanofiltration, Clavulanic acid, Purification, Biotechnology
Titulação: Doutor em Engenharia de Alimentos
Banca examinadora: Francisco Maugeri Filho
Clóvis Sacardo da Silva
Luiz Antônio Viotto
Marco di Luccio
Raquel Cristine Kuhn
Data da defesa: 05/04/2011
Programa de Pós Graduação: Programa em Engenharia de Alimentos

COMISSÃO EXAMINADORA

Este exemplar corresponde à redação final da tede defendida em ___/___/_____ por Andrea Limoeiro Carvalho aprovado pela comissão julgadora em ___/___/_____.

_____

Prof. Dr. Francisco Maugeri Filho (Orientador)

_____

Dr. Clóvis Sacardo da Silva (Membro)

_____

Prof. Dr. Luiz Antônio Viotto (Membro)

_____

Prof. Dr. Marco di Luccio (Membro)

_____

Dra. Raquel Cristine Kuhn (Membro)

_____

Profa. Dra. Beatriz Vahan Kilikian (Membro Suplente)

_____

Profa. Dra. Leila Peres (Membro Suplente)

_____

Prof. Dr. Marlei Barboza Pasotto (Membro Suplente)

"A alegria que se tem em pensar e aprender faz-nos pensar e aprender ainda mais."

(Aristóteles)

"Toda a nossa ciência, comparada com a realidade, é primitiva e infantil - e, no entanto, é a coisa mais preciosa que temos."

(Albert Einstein)

Este trabalho é dedicado ao César,
companheiro nas horas mais difíceis
e grande incentivador de meus pensamentos.

AGRADECIMENTOS

À Deus por iluminar os meus caminhos.

Ao meu pai, Joselito, meus irmãos, Ana Paula e André Luiz, e meus cunhados, João Otávio e Graciela, pelo carinho e apoio incondicional.

Ao Prof. Francisco pela orientação e incentivo ao desenvolvimento da tese, pela paciência e exemplo de profissional, sempre aguçando a nossa curiosidade científica.

Al Prof. Pedro, profesional de excelente calidad, persona de espirito elevado y ejemplo de profesor y orientador.

Aos membros da Comissão Examinadora pela contribuição e auxílio.

À Fifa, pessoa iluminada que eu tive o prazer de conhecer e de contar nesses 5 anos de LEB, um grande exemplo de ser humano.

À Prof. Maria Isabel pelo apoio e colaboração nos planejamentos.

A los profesores Laura, António y José Ignacio por la ayuda y atención que me dedicarón en Valladolid.

À minha prima e amiga Luciana pelas conversas e pelo carinho.

Aos amigos de longa data, Elizama, Abraão, Geraldo e Alexandre por ainda fazerem parte de minha vida.

Aos meus amigos, Priscilla, Irede, Luiz, Carol, Marquinhos, Remi, Fabi, Aninha, Giba, Lizi, Marcão, Lucas (Carioca), Claudinha, preciosidades que cruzaram o meu caminho aqui em Campinas e que jamais deixarão o meu coração.

Aos meus amigos, Nenis, Lucielen, Louise, Douglas e Marcelo (Cais), pessoas maravilhosas que conheci aqui em Campinas e que me dão alegria todas as vezes que encontro ou falo, nem que seja pela internet.

A Verónica, Noemí, Montse y Noelia, amigas queridas que conocí durante me pasantía en España y que guardaré conmigo por toda la vida.

Aos amigos do LEB, Raquel, Rô, Mónica, Ana, Cris, Dani, Gi, Rafael (FEQ), Susan, Susana e Bárbara, pelo companherismo, apoio, risadas e amizade, momentos muito alegres em que eu agradecia a oportunidade de trabalhar nesse ambiente.

Ao Departamento de Engenharia de Alimentos da Unicamp, ao Departamento de Física Aplicada da Universidad de Valladolid, à FAPESP, à CAPES e ao CNPq por tornarem possível a realização deste trabalho.

À Filmtec™ e à Microdyn Nadir®, por haverem fornecido as amostras de membranas.

E a todos que tornaram possível a realização desse trabalho.

SUMÁRIO

Índice de Tabelas ..... **xii**
Índice de Figuras ..... **xiv**
Resumo ..... **xvii**
Summary ..... **xix**

1. Introdução Geral **1**
2. Objetivos **3**
2.1. Objetivos específicos 3
3. Referências Bibliográficas **4**
4. Capítulos **6**

CAPÍTULO 1 ..... **6**

Nanofiltration process, its characterization and application to the concentration and purification of clavulanic acid: a review **6**
Abstract 6
1. Introduction 7
2. β-lactam antibiotics 8
2.1. Clavulanic acid 10
3. Purification of biotechnology products 10
4. Nanofiltration 12
4.1. Membrane Characterization 13
4.1.1. Morphology characterization 13
4.1.2. Electric characterization 15
4.1.3. Functional characterization 16
4.2. SEDE Model 17
4.3. Scale up 19
5. Conclusions 21
6. References 21

CAPÍTULO 2 25

AFM analysis of the surface of nanoporous membranes: application to the nanofiltration of potassium clavulanate 25

Abstract 25
1. Introduction 26
2. Methodology 29
2.1. Membrane and chemicals 29
2.2. Nanofiltration experiments 30
2.3. Atomic Force Microscopy 31
2.4. Surface Analysis 33
3. Results and Discussion 36
3.1. Filtration processes 36
3.2. AFM Characterization 36
3.2.1. Pore size distribution for clean membranes 36
3.2.2. Surface analysis 41
4. Conclusions 48
5. References 49

CAPÍTULO 3 54

Nanofiltration membrane selection and process modelling in clavulanic acid separation 54

Abstract 54
1. Introduction 55
2. Methodology 57
2.1. Material 57
2.2. Experimental procedure 59
3. Mathematical Considerations 59
3.1. Electric characterization 59
3.2. Structural and functional characterization 60

3.3. Model resolution 61
4. Results and Discussion 62
4.1. Membrane charge results 62
4.2. pH characterization 64
4.3. Concentration polarization effect 66
4.3.1. Mass transfer coefficient determination 66
4.4. KCl and CA rejection results 68
4.4.1. SEDE-VCh model results 71
4.4.2. Membrane selectivity for clavulanic acid 72
5. Conclusions 73
6. References 74

CAPÍTULO 4 77

Nanofiltration membrane technology applied to the concentration and purification of clavulanic acid: Effect of pore size and permeability 77
Abstract 77
1. Introduction 78
2. Methodology 79
2.1. Material 79
2.2. Experimental procedure 81
2.3. Mathematical considerations 82
2.4. Analytical methodology 83
3. Results and Discussion 83
3.1. Membrane selection and process optimization 83
3.2. Validation 87
3.3. Membrane selectivity 89
4. Conclusions 93
5. References 94

CAPÍTULO 5 97

Nanofiltration process scale up: purification of clavulanic acid 97

Abstract 97

1. Introduction 98

2. Methodology 100

2.1. Material 100

2.2. Experimental procedure 102

2.3. Mathematical considerations 102

2.4. Analytical methodology 103

3. Results and Discussion 103

3.1. Experiments in the stirred dead-end cell and the pilot plant 103

3.2. Scale up procedure 108

4. Conclusions 108

5. References 109

5. Conclusões Gerais 111

6. Sugestões para Trabalhos Futuros 114

CAPÍTULO 1

Table 1 – β-lactams antibiotics, its structure and producers microorganisms. 9
Table 2 – SEDE-VCh equations summarized 18

CAPÍTULO 2

Table 1 – Characteristics of the membranes used here as given by their manufacturers..29
Table 2 – Water permeability for each membrane evaluated, before and after KCA permeation 36
Table 3 – Membrane thickness in micrometer as obtained from the comparison of theoretical and experimental water permeabilities in Fig. 6 40
Table 4 – Fractal dimension for the clean and fouled membranes.....46

CAPÍTULO 3

Table 1 – Characteristics of the membranes used 57
Table 2 – SEDE-VCh equations summarized 61
Table 3 – KCl real rejection for all membranes studied at the maximum TMP applied for each one 69
Table 4 – Dielectric constant inside the pores for all membranes studied.....71

CAPÍTULO 4

Table 1 – Characteristics of the membranes used 80
Table 2 – Independent variables and their levels for membrane selection 81
Table 3 – Independent variables and levels for the purification assays 82
Table 4 – Template for the planning and results obtained in the membrane selection experiments 84
Table 5 – Results of the Tukey test for both membranes.....89
Table 6 – 2^{4-1} fractional factorial design for the membrane selectivity studies 90

CAPÍTULO 5

Table 1 – Characteristics of the membrane NF 101

Conclusões Gerais

Tabela 1 – Melhores condições operacionais para as membranas estudadas 111
Tabela 2 – Melhores resultados obtidos para as quatro membranas estudadas 111
Tabela 3 – Permeabilidade a água para cada membrana avaliada, antes e depois do seu uso para permear clavulanato de potássio 112

CAPÍTULO 1

Figure 1 – Molecular structures of clavulanic acid and potassium clavulanate. 12
Figure 2 – Tip action over the membrane surface 14
Figure 3 – Schematic representation of the streaming potential measurements cell. 15
Figure 4 – Schematic representation of the bench-scale stirred cell. 19
Figure 5 – Schematic representation of the pilot plant 20

CAPÍTULO 2

Figure 1 – Molecular structures of clavulanic acid and potassium clavulanate 28
Figure 2 – Schematic representation of a crossflow nanofiltration experimental setup at laboratory scale. 30
Figure 3 – Examples of the AFM images of the membranes with scanned areas of (40 × 40) nm^2 used to obtain the pore size distribution for: (a) NF90 (b) NF, (c) NP030 and (d) NP010 37
Figure 4 – Pore size distribution for the membranes NF90, NF, NP030 and NP010. They have been fitted to a Gaussian distribution showing the mean pore dimeter along with the standard deviation of the corresponding distribution 38
Figure 5 – Experimental water permeability versus mean pore diameters as obtained from AFM images 39
Figure 6 – Experimental permeability versus that calculated from the distributions shown in Fig. 4 and the Hagen-Poiseuille equation 40
Figure 7 – 3D-AFM images corresponding to scanned areas of (5 × 5) μm^2 for: (a) NF90 clean and (b) used, (c) NF clean and (d) used, (e) NP030 clean and (f) used, and (g) NP010 clean and (h) used 42
Figure 8 – Roughness, S_q, as a function of the length scale, L, (side of the square scanned area) for all the membranes studied before (a) and after (b) fouling with KCA. The insert shows a detail of the three membranes with low and very similar roughness (NF90, NP030 and NP010) 43

Figure 9 – Scheme of the cross section for the deposition of KCA (black balls) according to the fouling mechanism assumed on the surface (gray line) of each membrane studied 45
Figure 10 – Experimental water permeability versus roughness, S_q, as obtained from images with scanned areas of (2.5 x 2.5) μm^2 of the clean membranes.....46
Figure 11 – 2D Power Spectra Density of NF clean membrane with several scan sizes. The fitted line (which slope determines the fractal dimension) corresponds to the best fitting to the three length scales (side of the square scanned area) shown.....47
Figure 12 – Percent reduction of the permeability due to the KCA adsorption versus the difference of the fractal dimension of the clean membrane, D_i and the used one D_f.....48

CAPÍTULO 3

Figure 1 – Schematic representation of the streaming potential measurements cell. 58
Figure 2 – Schematic representation of the bench-scale stirred dead-end cell. 58
Figure 3 – Membrane charge versus KCl concentration for all evaluated membranes 63
Figure 4 - Chart of zeta potential versus pH solution for the four membranes.....65
Figure 5 - Chart of membranes charges versus pH solution to the four membranes studied 65
Figure 6 – Mass transfer coefficient for all membranes evaluated 68
Figure 7 – Real rejection versus permeate flux for all of the membrane at (a) $1x10^{-4}$ M and (b) $1x10^{-3}$ M KCl concentration 69
Figure 8 – KCl real rejection versus pH value for all membranes evaluated.....70
Figure 9 – KCl/CA selectivity as function of applied pressure, for $C_{KCl}/C_{CA} \approx 0.1$ 72

CAPÍTULO 4

Figure 1 – Schematic representation of the bench-scale stirred dead-end cell 80
Figure 2 – Retention coefficients (R_C) for the NF and NF90 membranes 86
Figure 3 – Productivity ($[CA]_{RET}/[CA]_0$.L.h) for the NF and NF90 membranes.....87
Figure 4 – Responses for NF and NF90 membranes, with their respective repetitions and averages: (a) retention coefficient and (b) productivity ($[CA]_{RET}/[CA]_0$.L.h) 88

Figure 5 – Retention coefficients for both membranes 91
Figure 6 – Productivities ($[CA]_{RET}/[CA]_0$.L.h) for both membranes 92
Figure 7 – Purification factor for both membranes 93

CAPÍTULO 5

Figure 1 – Schematic representation of the bench-scale stirred dead-end cell 100
Figure 2 – Schematic representation of the pilot plant..... 101
Figura 3 – Retention coefficient (R_C) as a function of permeate flux (J_V) for the different processes..... 104
Figura 4 – Productivity for both processes as a function of permeate flux (J_V)..... 105
Figura 5 – Retention coefficient and productivity as a function of the permeate flow (J_V) for the pilot plant with and without the addition of peptone in the CA solution, in applied pressure of 1.5MPa and 2 MPa 107
Figura 6 – Flow of permeate (J_V) for the pilot plant as a function of transmembrane pressure..... 107

RESUMO

A nanofiltração é um processo com membrana por diferença de pressão, enolvendo também mecanismos de sorção e difusão, que pode ser aplicado na etapa de concentração do caldo clarificado na produção de ácido clavulânico. No presente trabalho, o ácido clavulânico foi concentrado, avaliou-se a eficiência do processo e estudaram-se os parâmetros envolvidos na transferência de massa e aplicados ao modelo matemático SEDE-VCh, assim como avaliou-se a ampliação de escala do processo. Esse estudo foi dividido nas seguintes etapas: seleção e caracterização das membranas; aplicação do modelo matemático, nos quais foram realizados experimentos para avaliar o desempenho das membranas NF e NF90 (ambas da Filmtec™), e NP010 e NP030 (ambas da Microdyn Nadir®); ampliação de escala do processo, na qual a membrana que apresentou os melhores resultados nas etapas anteriores foi utilizada. Quanto à seleção da membrana, as respostas avaliadas foram o coeficiente de retenção, a produtividade e o fator de purificação. Na etapa de caracterização da membrana, foi avaliada a morfologia de superfície das quatro membranas, obtendo-se o tamanho e a distribuição de poros, a rugosidade, a dimensão fractal e a permeabilidade das mesmas, além de estudos que forneceram dados referentes aos efeitos estéricos e elétricos sobre o transporte através das membranas, como suas densidades superficiais e volumétricas de carga, a concentração do soluto nas suas superfícies externas e o coeficiente de transferência de massa do processo. A partir desses dados foi gerado um modelo para explicar o transporte através das membranas. Por fim foram feitos experimentos para verificar o comportamento do processo em uma escala piloto. Os resultados obtidos demonstram que a membrana NF é a melhor para o processo de concentração de ácido clavulânico com coeficiente de retenção médio de 0,988 em escala de bancada e aproximadamente 1,0 em escala piloto. As quatro membranas apresentaram raios de poro inferiores a 1 nm e ponto isoelétrico em pH entre 5 e 6. A membrana NP010 apresentou maior permeabilidade à água, e as demais na seguinte ordem: NP010 > NP030 > NF > NF90. Esse parâmetro se relaciona de forma linear com o diâmetro médio de poros e sua redução aumenta com a diferença entre a dimensão fractal antes e depois do uso das membranas. Foi possível verificar também que em altas adsorções a rugosidade das membranas tendem a ser similares. A membrana NF90 apresentou um maior coeficiente de transferência de massa, seguido da NF, NP010 e NP030, nessa ordem, sendo que a rejeição variou com o pH para as membranas NF e NF90. A constante dielétrica dentro dos poros aumenta inversamente ao tamanho médio dos poros das membranas até quando a mesma atinge o valor da água livre. A seletividade da membrana ao KCl e ácido clavulânico apresenta a mesma tendência da densidade volumétrica de

cargas: NF > NF90 > NP030 ≈ NP010. Com os estudos de ampliação de escala foi possível determinar que o sistema convencional que simula o processo de fluxo tangencial pode ser usado em outros estudos de avaliação de processos e de seleção de membranas visando à aplicação industrial, e que peptídeos e aminoácidos podem atuar melhorando o processo de concentração de ácido clavulânico por nanofiltração. A produtividade final obtida foi de até 6.4 $[CA]_{RET}/[CA]_0$.L.h.

SUMMARY

Nanofiltration is a pressure driven membrane process, with desorption and diffusion, which is also applied to the concentration of clavulanic acid from a clarified juice. In this study, clavulanic acid was concentrated, and the process had its efficiency evaluated and its mass transfer parameters studied and applied to the mathematical model SEDE-VCh, and in addition scale up was also evaluated. This study was divided into the following stages: selection and characterization of the membranes, and the application of the model, in which experiments were performed to evaluate the performance of the NF and NF90 membranes (both Filmtec™), and NP010 and NP030 (both Microdyne Nadir®), and the scale up of the process, in which the membrane that showed the best results in the previous steps was used. Concerning the selection of the membrane, the evaluated responses were the retention coefficient, productivity and purification factor. In the characterization of the membrane step, we evaluated the surface morphology of the four membranes, targeting the pore size and pore size distribution, roughness, fractal dimension and permeability, in addition to studies that provided data on the electrical and steric effects over the transport through the membranes, as their surface and volumetric density charges, the concentration of solute in its external surfaces and the mass transfer coefficient of the process. From these data a model was created to explain the transport through the membranes. Finally experiments were carried out to verify the behavior of the process in a pilot scale. The results showed that the NF membrane is best for the process of concentration of clavulanic acid with retention coefficient average of 0.988 in bench scale and almost 1.0 in the pilot plant. All the four membranes had pore radii below 1 nm and an isoelectric point between pH 5 and 6. The NP010 membrane showed the higher water permeability, in the following order: NP010 > NP030 > NF > NF90. This parameter is related linearly with the average pore size and its reduction increases with the difference between the fractal dimension before and after the use of the membranes. It was also verified that at high adsorption the roughness of the membranes tends to be similar. The NF90 membrane showed a higher mass transfer coefficient, followed by NF, NP010 and NP030, in that order and the rejection varied with the pH for the NF and NF90 membranes. The dielectric constant inside the pores increases inversely with pore size of the membranes even when it reaches the value of free water. The selectivity of the membrane to KCl and clavulanic acid shows the same trend as the volumetric density charge: NF > NF90 > NP030 ≈ NP010. By means of the studies of scale up it was determined that the conventional system with a stirrer that promotes the convection movement in the process can be used in other studies of process evaluation and selection of membranes in

view of industrial application, and also that peptide and mino acid substances improve the process concentration of clavulanic acid by nanofiltration. The final productivity was about 6.4 $[CA]_{RET}/[CA]_0$.L.h.

1. INTRODUÇÃO GERAL

O ácido clavulânico (AC) é um inibidor da enzima β-lactamase, sua utilização combinada com penicilinas sensíveis à β-lactamase protege o anel β-lactâmico do antibiótico à hidrólise (Bersanetti *et al*., 2005; Cavaco Morão *et al*., 2006a). O ácido clavulânico é produzido industrialmente via fermentação por *Streptomyces clavuligerus*, e apresenta baixos rendimentos em seu processo de produção, particularmente na etapa de separação e purificação, devido à sua instabilidade térmica e sensibilidade a variações de pH (Almeida *et al.*, 2003; Bersanetti *et al.*, 2005). Aliado a sua baixa concentração em meio fermentado, esta característica obriga a realização de estudos das etapas de extração e purificação, considerando-se a sua cinética de degradação.

Atualmente diversos bioprodutos de alto valor agregado são produzidos por via fermentativa, trazendo novos desafios para os processos de recuperação e purificação industrial. A ultrafiltração (UF) tem se mostrado um processo eficiente na separação de biomassa e ácido clavulânico originários do caldo fermentado, através da qual um permeado livre de proteína contendo ácido clavulânico é obtido. Faz-se então a concentração desses permeados (caldo clarificado) por nanofiltração (Brites Alves *et al*., 2002; Cavaco Morão *et al*., 2006a).

O transporte durante a nanofiltração é influenciado por diferentes mecanismos: convecção, devido à diferença de pressão aplicada sobre a membrana, difusão, devido ao gradiente de concentração através da membrana e, finalmente, efeitos de carga, devido à repulsão eletrostática entre a membrana carregada e um componente orgânico carregado (Szymczyk *et al*., 2003; Wang *et al.,* 1997; Szymczyk & Fievet, 2005). Verificam-se, ainda, efeitos nas interfaces da membrana, como o equilíbrio de Donnan, a exclusão dielétrica e efeitos estéricos. A retenção de compostos orgânicos é então determinada pela diferença de propriedades da membrana, pela massa molecular de corte (MWCO) e pela carga da membrana, além das propriedades dos componentes, sua massa molecular, hidrofobicidade e constante de ionização (Braeken *et al.*, 2006).

Estudos sobre a morfologia da superfície da membrana podem explicar os processos de separação nessas membranas pelas características da estrutura do poro (diâmetro, densidade e distribuição de tamanho de poros) e determinar suas propriedades filtrantes. A microscopia de força atômica permite a obtenção de imagens topográficas da superfície da membrana em uma resolução de nível atômico, o que torna a técnica atrativa aos pesquisadores interessados nas propriedades superficiais da membrana nanofiltrante (Hilal *et al.,* 2004).

O potencial zeta de materiais porosos é usualmente avaliado através de experimentos eletrocinéticos, como a medida do potencial elétrico, porque é uma técnica simples e muito sensível ao se variar a concentração de soluções diluídas (Martín *et al.,* 2003). Entre os dois métodos de medida de potencial elétrico que podem ser usados, ao longo e através das membranas, as medidas ao longo da superfície da membrana transpassam as dificuldades de interpretação dos dados eletrocinéticos devido aos pequenos tamanhos de poro e à anisotropia dessas membranas (Cavaco Morão *et al.*, 2006b).

Dentre os modelos existentes utilizados em processos de nanofiltração, destaca-se o modelo homogêneo SEDE-VCh (estérico, elétrico e exclusão dielétrica, abreviação em inglês). Esse modelo apresenta uma boa descrição das propriedades de transporte em membranas carregadas, como proposto inicialmente por Bowen & Welfoot (2002) e recentemente modificado considerando as variações de cargas dentro das membranas por Silva (2010), pois leva em conta também a exclusão dielétrica nas interfaces (Szymczyk & Fievet, 2005; Szymczyk *et al.*, 2006).

No presente trabalho foi proposta uma discussão mais aprofundada dos fenômenos envolvidos no processo de purificação e concentração de ácido clavulânico por nanofiltração, com um estudo mais completo que o disponível na literatura sobre a caracterização das membranas utilizadas. Para tanto a tese foi dividida em cinco capítulos, uma revisão sobre o tema, dois capítulos sobre caracterização das membranas, um sobre a seleção da membrana mais apropriada e um sobre a ampliação da escala do processo.

2. OBJETIVO

Desenvolver um protocolo que descreva a etapa de purificação e concentração de ácido clavulânico por nanofiltração. A solução resultante, contendo o ácido clavulânico, deverá ser suficientemente concentrada para permitir seu isolamento nas etapas posteriores do processo.

2.1. Objetivos específicos

- Selecionar a melhor membrana para concentrar o ácido clavulânico (AC), dentre as quatro avaliadas nesse estudo.
- Caracterizar as membranas morfologicamente antes e após seu uso em um microscópio de força atômica.
- Estudar os efeitos estéricos e eletrostáticos no transporte através da membrana para a caracterização eletrocinética da mesma.
- Definir os parâmetros envolvidos no modelo adequado ao processo e simular o processo a fim de ajustar o modelo e avaliar o desempenho deste.
- Ampliar a escala de estudo do processo da bancada para uma planta piloto.
- Otimizar o processo em relação à retenção de ácido clavulânico, sua produtividade e seletividade do ácido clavulânico em relação aos outros compostos obtidos durante a fermentação e etapas anteriores de separação.

3. REFERÊNCIAS BIBLIOGRÁFICAS

ALMEIDA, R. M. R. G.; BARBOZA, M.; HOKKA, C. O. (2003). Continuous clavulanic acid adsorption process. **Applied Bioch. and Biotechnol.,** v. 108, p.105-108.

BERSANETTI, P. A.; ALMEIDA, R. M. R. G.; BARBOZA, M.; ARAÚJO, M. L. G. C.; HOKKA, C. O. (2005). Kinetic studies on clavulanic acid degradation. **Bioch. Eng. J.,** v.23, p.31-36.

BRAEKEN, L.; BETTENS, B.; BOUSSU, K.; VAN DER MEEREN, P.; COCQUYT, J.; VERMANT, J.; VAN DER BRUGGEN, B. (2006). Transport mechanisms of dissolved organic compounds in aqueous solution during nanofiltration. **J. Membr. Sci.,** v.279, p.311-319.

BRITES ALVES, A. M.; MORÃO, A.; CARDOSO, J. P. (2002). Isolation of antibiotics from industrial fermentation broths using membrane technology. **Desalination,** v.148, p.181-186.

BOWEN, W. R. & WELFOOT, J. S. (2002). Predictive modeling of nanofiltration: membrane specification and process optimization. **Desalination,** v.147, p.197-203.

CAVACO MORÃO, A. I.; BRITES ALVES, A. M.; COSTA, M. C.; CARDOSO, J. P. (2006a). Nanofiltration of a clarified fermentation broth. **Chem. Eng. Sci.,** v.61, p.2418-2427.

CAVACO MORÃO, A. I.; BRITES ALVES, A. M.; AFONSO, M. D. (2006b). Concentration of clavulanic acid broths: influence of the membrane surface charge density on NF operation. **J. Membr. Sci.,** v.281, p.417-428.

HILAL, N.; AL-ZOUBI, H.; DARWISH, N. A.; MOHAMMAD, A. W.; ABU ARABI, M. (2004). A comprehensive review of nanofiltration membranes: treatment, pretreatment, modeling, and atomic force microscopy. **Desalination,** v.170, p.281-308.

MARTÍN, A.; MARTÍNEZ, F.; MALFEITO, J., PALACIO, L.; PRÁDANOS, P.; HERNANDEZ, A. (2003). Zeta potential of membranes as a function of pH: Optimization of isoelectric point evaluation. **J. Membr. Sci.**, v.213, p.225-230.

SILVA, V. (2010). Theoretical foundations and modelling in nanofiltration membrane systems. **Tese de Doutorado** – Facultad de Ciencias, Universidad de Valladolid, Valladolid, Spain.

SZYMCZYK, A.; LABBEZ, C.; FIEVET, P.; VIDONNE, A.; FOISSY, A.; PAGETTI, J. (2003). Contribution of convection, diffusion and migration to electrolyte transport through nanofiltration membranes. **Adv. Colloid Interface,** v.103, p.77-94.

SZYMCZYK, A. & FIEVET, P. (2005). Investigating transport properties of nanofiltration membranes by means of a steric, electric and dielectric exclusion model. **J. Membr. Sci.,** v.252, p.77-88.

SZYMCZYK, A.; SBAÏ, M.; FIEVET, P.; VIDONNE, A. (2006). Transport properties and electrokinetic characterization of an anphoteric nanofilter. **Langmuir,** v.22, p.3910-3919.

WANG, X. L.; TSURU, T.; NAKAO, S.; KIMURA, S. (1997). The electrostatic and steric-hindrance model for the transport of charged solutes through nanofiltration membranes. **J. Membr. Sci.,** v.135, p.19-32.

NANOFILTRATION PROCESS, ITS CHARACTERIZATION AND APPLICATION TO THE CONCENTRATION AND PURIFICATION OF CLAVULANIC ACID: A REVIEW

A. L. Carvalho*; F. Maugeri

Departament of Food Engineering, Faculty of Food Engineering, Rua Monteiro Lobato 80, Barão Geraldo, University of Campinas – UNICAMP, CEP: 13083-862, Campinas, SP, Brazil. E-mail: maugeri@fea.unicamp.br

*e-mail: limoeiro@fea.unicamp.br, telephone: +551935214052, fax: +551935214027

Abstract

In the present work is discussed the nanofiltration process, focusing its morphology, electrical and functional characterization, the use of the SEDE-VCh (steric, electric and dielectric exclusion) model to predict its performance, and the application to purify and concentrate clavulanic acid. The scale up of this process from a laboratorial scale to a pilot plant is also assessed. It is also the intention of this article to discuss the state-of-art of scientific research related to the nanofiltration process.

Keywords: nanofiltration, membrane, characterization, clavulanic acid, scale up

1. Introduction

Currently, several high-value bioproducts are being produced by fermentation, bringing new challenges for the recovery and purification processes. Ultrafiltration (UF) processes are an efficient way of separating the biomass from the CA fermentation broth, producing a free protein permeate containing CA, which can be subsequently concentrated using nanofiltration membranes [2,4,5].

The transport in the nanofiltration process is influenced by different mechanisms, such as convection, due to the transmembrane pressure, diffusion, because of the concentration gradient through the membrane and finally the charge effects, due to the electrostatic repulsion between the charged membrane and a charged organic compound [6-8]. Some effects in the membranes interface are also noticed, as the Donnan equilibrium, the dielectric exclusion and steric effects. Retention of organic compounds is therefore determined by different membrane properties, e.g. molecular weight cut-off (MWCO) and membrane charge, and compound properties, e.g. molecular weight, hydrophobicity and ionization constant [9].

Between the existent models used in nanofiltration process, the SEDE-VCh (steric, electric and dielectric exclusion) model can be noteworthy. This model presents a good description of transport properties in charged membranes proposed initially by Bowen & Welfoot [10] and recently modified in order to include a more realistic situation that includes the variation of the charge inside the membrane Silva [11]. The model also includes the dielectric effects in the interfaces proposed by Szymczyk *et al.* [8,12].

Clavulanic acid (CA) is a β-lactamase inhibitor, used in combination with β-lactamase sensitive penicillins, to protect the β-lactam ring of the antibiotic against hydrolysis [1,2]. CA is produced industrially by fermentation using *Streptomyces clavuligerus*, and presents low yields in the production process, particularly in the separation and purification step, due to its thermal instability and sensitivity to changes in pH [1,3]. Associated with its low concentration in the fermented broth, studies on its extraction and purification have to consider the kinetic degradation of CA, in order to minimize losses and maximize recovery yields and productivity.

2. β-lactam antibiotics

Nowadays, more and more high-value bioproducts are produced by fermentation bringing new challenges to industrial purification and recovery steps, which must count not only for the labile nature of most of these molecules but also for the economy of the process [13]. Some of these bioproducts of commercial interests are the antibiotics, such as the β-lactam antibiotics.

The use of antibiotics to control infectious diseases is greatly hindered by this kind of resistance. A variety of Gram-positive and Gram-negative pathogenic bacteria exhibit an antibiotic resistance mechanism based on their ability to produce β-lactamases, which deactivate penicillins and cephalosporins by hydrolyzing their β-lactam ring [13].

Likely the first antibiotic resistance mechanism reported in the literature was the production of penicillinase by pathogenic *Escherichia coli*. Since then, the study of the β-lactamases has been intense, and there are numerous reviews and monographs that confer the details of this broad family of enzymes [14]. Therefore, such kind of inhibitors is of a great clinical importance. Some β-lactams antibiotics are shown in the Table 1.

Those inhibitors, which are also β-lactams antibiotics, are produced through fermentation as secondary metabolites; or semi-synthetic, produced naturally with some radicals modified through induced chemical reactions, and are concomitantly used to the antibiotics sensible to β-lactamase, protecting their β-lactam ring against the action of the β-lactamases produced by the bacteria.

Table 1 – β-lactams antibiotics, its structure and producers microorganisms

Basic chemical structure	**Antibiotics**	**Mainly producers microorganisms**
Penam 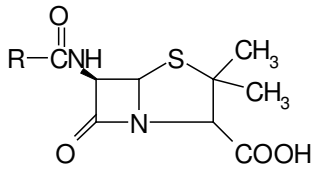	Penicillins	*Penicillium chrysogenum* *Aspergillus nidulans* *Cephalosporium acremonium* *Streptomyces clavuligerus*
Ceph-3-em 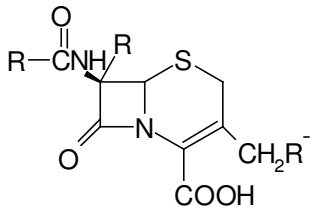	Cephalosporins	*Cephalosporium acremonium* *Norcadia lactamdurans*
Clavam 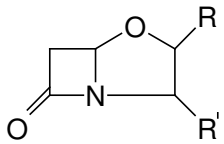	Clavulanic acid	*Streptomyces clavuligerus*
Carbapenem 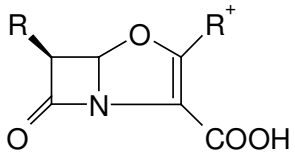	Thienamycins Olivanic acids	*Streptomyces cattleya* *Streptomyces olivaceus*
Monolactam 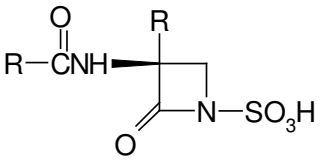	M onobactams	*Glunobacter sp.* *Pseudomonas acidophila* *Acetobacter sp.*
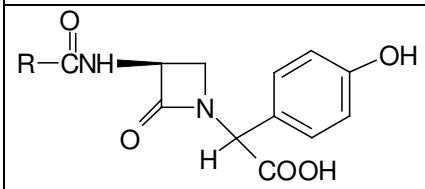	Norcadicins	*Norcadia uniformis*

Source: Almeida *et al.* [15]

2.1. Clavulanic acid

Clavulanic acid (CA) is a compound produced by *Streptomyces clavuligerus*, and it consists of a β-lactam ring fused to an oxozilidine ring [16]. It shows weak antibacterial activity against most bacteria, but is a potent inhibitor of a wide range of β-lactamase and is able to potentiate the antibacterial activity of penicillins and cephalosporins against many β-lactamase-producing resistant bacteria [17]. It is currently used in combination with amoxicillin or other semi-synthetic penicillins for the treatment of infections caused by β-lactamase-producing bacteria, in that way it increases the resistance of these antibiotics to the action of the β-lactamase over the β-lactam ring. It is known that the CA in its natural presentation is chemically instable to large pH and temperature variations and that it does not present any strongly hydrophobic group. This instability sharpens at temperatures superior to 30 ºC and pH values higher than 7.5 and lower than 4.5 [1,18].

The combination CA/amoxicillin presents a broad antibacterial spectrum, which have been used over 20 years and it is still commonly used nowadays [19]. The CA separation and purification process involves several steps, such as centrifugation and filtration, with recovery of the cell mass and techniques of extraction and adsorption to posterior antibiotic purification.

3. Purification of biotechnology products

The use of membranes in purification steps of biotechnological products surpasses the limitations of traditional techniques and their use in this field has shown a great increase in the last years [13]. This stage involves one, two or three operations in sequence, depending on the case.

The first operation, directed towards the solid-liquid separation of fermented broths is the clarification, which could be made by centrifugation, microfiltration (MF) or UF. In all cases, a concentrate containing all the biomass of the broths and a permeate containing the antibiotic, salts and water are obtained. The quality of the permeate thus obtained determines the subsequent operation(s) and, in some applications, a second filtration is necessary [4].

In a general manner, the permeate obtained after this stage is presented much diluted, becoming necessary a stage of concentration after the purification steps. One path to achieve the concentrated interest solute is the nanofiltration. This step can be carried out after the initial steps of

purification as well as in the end of the process, depending on the conditions of the permeate reached.

According to Cavaco Morão *et al.* [2], the isolation of CA through an integrated process involving UF and nanofiltration is economically and ecologically advantageous. After the bioproduct purification a refining stage is required that could be crystallization or dehydration, as, for instance, liofilization, used in the production of CA. In recent works the researches are concerned in evaluating the process of isolation and purification of CA obtained by fermentation of *Streptomyces clavuligerus*. Some routes are suggested by several authors.

Cook *et al.* [20] suggested the use of the organic solvent tertiary-butylamine for the CA isolation and consequent purification. The solvent would react with the CA forming a salt, so this salt of tertiary-butylamine would be converted in another salt of clavulanate pharmacologically acceptable through successive chemical reactions. Other authors, such as Yang *et al.* [21], Capuder [22], Cardoso [23] and Mosbach [24], also used solvent extraction to purify CA from fermentation broths.

An investigation about the use of the resin Amberlite XAD in the purification of CA was made by Mayer *et al.* [25]. Those authors achieved a better performance with the Amberlite XAD treated with quaternary ammonia than with Amberlite IRA 400. However, the system proposed by the authors unfeasible in an industrial scale.

The adsorption by ionic exchange was also evaluated by Barboza *et al.* [26]. Those authors concluded that the purification process of CA with the ionic exchange resin Amberlite IRA 400 pretreated with NaCl is a promising process, despite of the degradation of the former. The time needed to reach the adsorption equilibrium is small enough, allowing the use of this process.

Liquid-liquid extraction was also used for purification. In this process, the CA, present in an organic solution, was transformed into a salt and then put in contact with an aqueous phase, where the resulting salt is more stable [27].

Brites Alves *et al.* [4] suggested UF as a first step of purification, followed by a nanofiltration step prior to the solvent extraction. Those authors reached high fluxes of permeate, a high antibiotic production as well as a good phase separation when the retentates were submitted to the solvent extraction.

In their work, Cavaco Morão *et at.* [2] also used a step of nanofiltration between the UF and the solvent extraction. Commercial membranes Desal DK, Desal DL (both from Osmonics) and NFT50 (Alfa Laval) were used, achieving 99% - 100% of CA retention. However, a decline in the

flux of almost one order of magnitude was observed. This same process was proposed by Capuder [28].

Carvalho et al. [5,29] have found good results using nanofiltration to concentrate CA. They used four membranes NP010 and NP030 from Microdyn Nadir®, and NF and NF90 from Filmtec™. The membranes NP010 and NP030 showed rejections of 70% and 82% of mean rejection, respectively, while the membranes NF and NF90 showed rejections of 98.8% and 99.9% of rejection, respectively. In another study, Carvalho *et al.* [30] evaluated the scale up process using the membrane NF, and found a rejection of almost 100%.

Untill now few works were made about the use of nanofiltration to purify and concentrate CA, but some recent discoveries achieved with studies of membrane characteristics will contribute to the development of this process.

4. Nanofiltration

Considering its molecular weight and structure (Figure 1), nanofiltration seems fully adequate for the purification of CA and the potassium clavulanate (KCA). This raises some problems due to the high fouling levels appearing. In order to design an adequate process, nanofiltration with membranes with pores in the nanometer range with low fouling should be found.

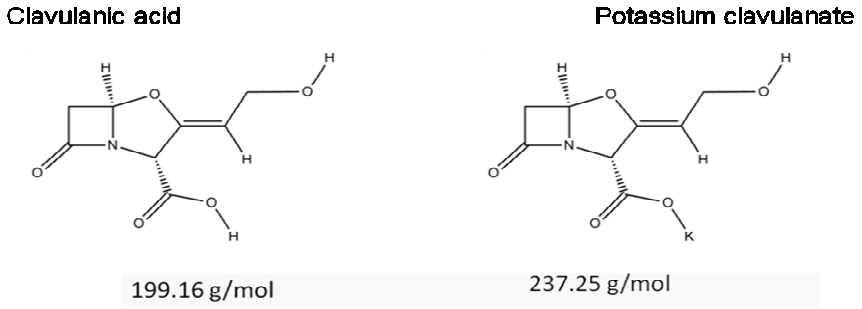

Figure 1 – Molecular structures of clavulanic acid and potassium clavulanate.

Nanofiltration is a relatively new pressure driven membrane process that has properties in between UF and reverse osmosis (RO). This process' main advantages are: operation at low pressures when compared to RO, high fluxes, considerable retention of multivalent anionic salts and

low molecular weight organic molecules, relatively low investment and low cost of operation and maintenance with a low energy consumption [31].

The nanofiltration performance can be identified as a sum of the convective, diffusive, steric and electrostatic effects through the membrane. In particular, in the interfaces the Donnan equilibrium, dielectric exclusion and steric effects take place. According to Hilal *et al.* [31], membranes that present smallest rejections of dissolved compounds and high water permeability has been of great improvement in the nanofiltration process, comparing to RO.

4.1. Membrane characterization

The characterization of nanofiltration membranes includes the use of predictive models, which help to understand the separation process. Because the morphological properties of the membranes have important consequences on performance and fouling, it is very important to characterize them by experimental techniques that could determine their structure and pore geometry [32-38].

Despite the efforts to minimize the fouling caused by the membrane-solute affinity, it occurs in many instances [39] and it is perhaps the most critical parameter in membrane filtration [39-42]. This is the reason why nanofiltration membranes, although having many applications [43-46], are still not totally implemented on an industrial scale. Fouling increases the operation and maintenance costs, it causes a decline in the permeate flux, and increments in the energy demands, turning down the membrane performance and ultimately reducing membranes life [40,47,48].

According to Yacubowicz & Yacubowicz [49] the crossflow nanofiltration process is characterized by a membrane pore size corresponding to Molecular Weight Cut-Off (MWCO) around 200-1000 Da, working at pressures of 150-500 psi (10-34 bar). Thus, retention of organic compounds is therefore determined by different membrane properties, such as MWCO, hydrophobicity and compound properties such as molecular weight and ionization constant [9]. In addition to these separation phenomena, in salt separation the membrane charge also causes an additional exclusion due to electric and dielectric effects.

4.1.1. Morphology characterization

An understanding of the relationship between membrane surface properties and separation characteristics can determine the choice of a membrane for a particular separation and can also lead

to the development of membrane technology [34]. Some of the most important surface characteristics are the mean pore size and the pore size distribution, the pore density and the surface roughness. The pore size plays an important role in the transport through the membrane, because it determines rejection and selectivity along with flux or permeability [34,39,50,51].

There are several well established techniques for the determination of the pore size distributions and porosity. They include the bubble point technique, mercury porosimetry, the microscopic technique, solute transport, permporometry and thermoporometry [34]. Many advances in the study of membrane structure have been made possible [52] by microscopy techniques such as: Scanning Electron Microscopy (SEM) [53], Transmission Electron Microscopy (TEM) [54], Atomic Force Microscopy (AFM) [33] and Scanning Tunneling Microscopy (STM) [55]. This is especially true for nanofiltration membranes that have nanopores in nature; i.e. they have pores in the nanometric range.

Among the microscopic techniques, AFM is the most recent technique. It gives topographical images of the membrane surface by scanning with a sharp tip over the surface without any previous sample preparation (Figure 2). Since its invention, AFM has been applied to study MF and UF membranes [36,55-59], and more recently nanofiltration membranes [33,34,37,60-65]. This technique allows characterizing membrane surfaces, including non-conducting surfaces, with a nanometer (or even atomic) resolution in wet and dry environments. AFM also allows the study of the adhesion of particles and the properties of the subsequent deposit during fouling.

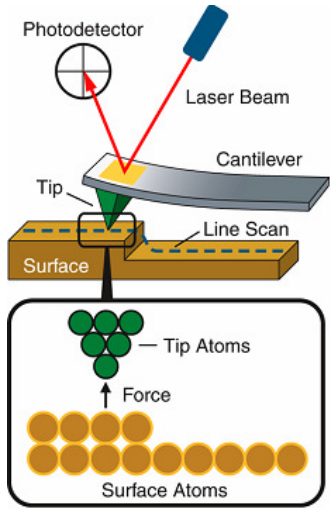

Figure 2 – Tip action over the membrane surface [66].

The pore size distribution alone does not describe completely the morphology of the membrane. In this sense, surface topology plays an important role in determining the fouling properties. Rough materials have more surface area and the fluid mechanics on them can also influence the resulting fouling rates. Very often, roughness is determined by using, for example, the average or the root-mean-square. Other complementary parameters are also interesting as skewness and kurtosis, which describe the peak asymmetry and flatness, respectively, of the height distribution on the surface. Moreover, most researchers appear to be unaware that several of these roughness measurements are scale dependent and dismiss the fractal dimension that is a key scale independent parameter reflecting the roughness [38,56].

4.1.2. Electric characterization

In electrokinetic characterization of solid-liquid interfaces the tangential streaming potential has been shown to be a reliable tool to obtain zeta potential and membrane charge [12].

The zeta potential of porous materials is usually evaluated from electrokinetic experiments, as streaming potential because it is a very simple technique and it is very sensitive to changes in concentration increase for low concentrations [67]. Between the two methods for measuring streaming potential that can be used, along and across the membrane, the first one is more appropriate for the nanofiltration membranes, once streaming potential measurements along the membrane bypass the hard interpretation of the electrokinetic data due to the small pore size and anisotropy of these membranes [68]. The system to measure the streaming potential in nanofiltration membranes is shown in the Figure 3.

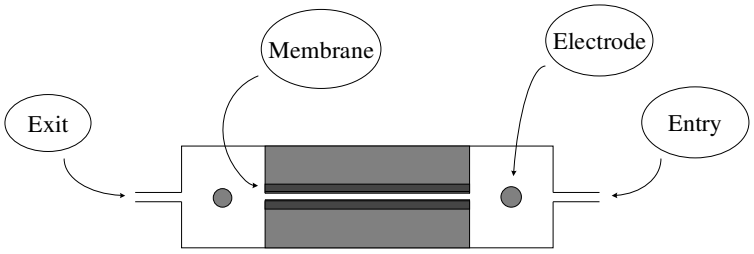

Figure 3 – Schematic representation of the streaming potential measurements cell.

In contact with solutions, the pH has a significant effect in membrane charge and in characteristics of the molecules in solution, because it protonates and deprotonates the functional

groups of membranes and molecules in solution, modifying the membrane charge and pore size and affecting hence the performance of nanofiltration and UF membranes [69-73].

From the plot of electric potential versus applied pressure the membrane streaming potential for each pH value can be obtained from the slope. The zeta potential for each concentration and pH value can be calculated through the Smoluchowsky equation as indicated below:

$$\zeta = \frac{\eta \lambda_0 \nu}{\varepsilon_0 \varepsilon_b} \tag{1}$$

where η is the streaming potential (V/Pa), λ_0 the solution average conductivity (S/m), ν the solution dynamic viscosity (Pa.s), ε_0 is the vacuum permittivity (F/m) and ε_b the dielectric constant of the bulk solution . With the zeta potential value (ζ) it is possible to calculate the surface charge density (σ_s) based on the Gouy-Chapman theory, as shown in Eq. 2:

$$\sigma_s = sign(\zeta)\sqrt{\left(2\varepsilon_0 \varepsilon_b RT \sum_i c_i(0^-)\left[\exp\left(-\frac{z_i F}{RT}\zeta\right)-1\right]\right)} \tag{2}$$

R is the ideal constant of gases, T is the temperature (K), c_i is the concentration of ion i (mol/m^3), z_i the charge of ion i and F is the Faraday constant (C). With the surface charge densities, it is finally possible, to calculate the membrane volume charge density (Eq. 3) considering a slit geometry:

$$X = \frac{\sigma_S}{F r_p} \tag{3}$$

where r_p is the average pore radius of the membrane (m).

4.1.3. Functional characterization

In order to determine the concentration polarization effect for the nanofiltration experiments, the mass transfer coefficient should be determined using the relation of Colton *et al.* [74], the method takes into account the appearance of the osmotic limit of flux and depends on the system geometry and others characteristics such as stirrer diameter and length, and from the membrane surface as indicated by the Eq. (4) [75]:

$$k = 0.0443\left(\frac{D}{r}\right)\left(\frac{\nu}{D}\right)^{0.33}\left(\frac{\omega r^2}{\nu}\right)^{0.8} \tag{4}$$

where D is the KCl diffusivity at infinite dilution, r is the membrane effective radius and ω is the rotation frequency.

Moreover, to find out the concentration at the external surface the gel layer theory can be used, which consider the volumetric flux by membrane area (J_V), the mass transference coefficient (k), and the KCl concentration on feed phase (c_0) and on the permeate (c_p) (Eq. 5) [76-78].

$$c_m = c_p + \left(c_0 - c_p\right)e^{\frac{J_V}{k}} \tag{5}$$

where k is obtained by the Eq. 4.

To predict the performance of the membranes it is necessary identify the different effects over the transport mechanisms. For that, several mathematical models has been developed.

4.2. SEDE model

Among the existent models used in nanofiltration process, the SEDE-VCh model can be noteworthy. This model presents a good description of transport properties in charged membranes proposed initially by Bowen & Welfoot [10] and recently modified to include a more realistic situation that considers the variation of the charge inside the membrane [11]. The model also includes the dielectric effects at the interfaces proposed by Szymczyk *et al.* [8,12]. Therefore, to determine the parameters involved in the process, the solute transport inside and at membrane surface has to be studied, since the charge distribution has different values in those different regions, usually modeled by thermodynamic equilibrium.

When the mean pore radius is obtained from an independent method [33] like AFM, the SEDE-VCh model is defined in terms of three independent parameters: the dielectric constant inside the pores (ε_p) and the two parameters of the Freundlich isotherm (a and b). The dielectric constant of the dry polymer of the membrane (ε_m) is usually taken from bibliography. The a and b parameters should be unique for a given solute and membrane system. The whole set of equations necessary to solve the system are summarized in Table 2 and a resolution algorithm can be found in Silva [11].

Table 2 – SEDE-VCh equations summarized

Transport equations

$$\frac{dc_i}{dx} = \frac{J_V}{D_{i,p}A_k}\left(K'_{i,c}c_i - c_{i,p}\right) - \frac{z_i F}{RT}\frac{d\psi}{dx} \quad \text{(I-1)}$$

where $D_{i,p} = K_{i,d}D_{i,\infty}$,

$$\sum_i c_i z_i + X_0 + ac_2^b = 0 \quad \text{(I-2)}$$

$$\frac{d\psi}{dx} = \frac{\sum_i\left(\frac{z_i J_V}{D_{i,p}A_k}\right)\left(K'_{i,c}c_i - c_{i,p}\right) + \left(\frac{J_V bac_2^{(b-1)}}{D_{2,p}A_k}\right)\left(K'_{2,c}c_2 - c_{2,p}\right)}{\frac{F}{RT}\left(\sum_i c_i z_i^2 + z_2 bac_2^b\right)} \quad \text{(I-3)}$$

Eqs. 2 and 4 can be numerically solved with the following boundary conditions,

$c_i(x = 0) = c_{i,0}$

$c_i(x = \Delta x) = c_{i,\Delta x}$ (I-4)

$$R_i = 1 - \frac{c_{i,p}}{c_{i,m}} \quad \text{(I-5)}$$

Partitioning equations

$$\frac{c_{i,0}}{c_{i,m}} = \phi_i \frac{\gamma_{i,m}}{\gamma_{i,0}}\exp(-z_i\Delta\Psi)\exp\left(-\Delta W'_{i,B}\right)\exp\left(-\Delta W'_{i,im}\right) \quad \text{(I-6)}$$

Where the dielectric effects are, Born energy:

$$\Delta W'_{i,B} = \frac{(z_i e)^2}{8\pi k_B \mathrm{T}\varepsilon_0 a_S}\left(\frac{1}{\varepsilon_p} - \frac{1}{\varepsilon_b}\right)$$ with a_S is defined by Rashin and Honig [79]. (I-7)

And the images force effect:

$$\Delta W'_{i,im} = -\alpha_i \ln\left[1 - \left(\frac{\varepsilon_p - \varepsilon_m}{\varepsilon_p + \varepsilon_m}\right)\exp(-2\mu)\right]$$ (Slit-like geometry) (I-8)

$$\alpha_i = \frac{(z_i F)^2}{8\pi\varepsilon_0\varepsilon_p RTN_A r_p} \quad \text{(I-9)}$$

$$v = \sqrt{k^2 + \mu^2} \quad \text{(I-10)}$$

$$\mu = Fr_p\sqrt{\frac{\sum_i z_i^2 c_{i,m}\phi_i\left(\gamma_{i,m}/\gamma_{i,0}\right)\exp\left(-z_i\Delta\Psi - \Delta W'_{i,B} - \Delta W'_{i,im}\right)}{RT\varepsilon_0\varepsilon_b}} \quad \text{(I-11)}$$

$$\beta = \frac{k}{\sqrt{k^2 + \mu^2}}\left(\frac{\varepsilon_m}{\varepsilon_p}\right) \quad \text{(I-12)}$$

The K_0, K_1, I_0, I_1 are the modified Bessel functions.

4.3. Scale up

The mass transfer through the membrane depends on several factors, such as the adsorption in the pores causing pore blockage and fouling on the membrane surfaces during the process [36,39,80], and the concentration polarization layer of the solutes on the high-pressure side of the membrane such as cake and gel layer formation [36,39,81]. Therefore, even with a large nanofiltration applications suggested [5,43-46], only few were implemented on an industrial scale, showing the need to investigate the scale up in membrane process.

Membrane test cells are extensively used for quality assurance, screening tests and in many research projects. However, many users will agree that test cell results may vary considerably and their accuracy can be inadequate for scale-up to larger membrane units [82]. The test cell (Figure 4) usually is carried out in dead-end process while the pilot plant (Figure 5) in a crossflow unit. In dead-end filtration the feed is presented to the membrane at right angles to its surface. As separation progress the retained solids builds up into a layer which causes resistance to the liquid flow. In crossflow, on the other hand, the mixture flows across the surface of the membrane. The liquid permeates through the membrane at right angles to the direction of flow of the feed and cake formation can be reduced by a transmembrane sheer stress [83,84]. In their work Lawrence *et al.* [85] have found that all results using the laboratory scale membrane unit under conditions of constant concentration gave flux curves indicative of fouling cake formation, with slight declines in value over the experimental period.

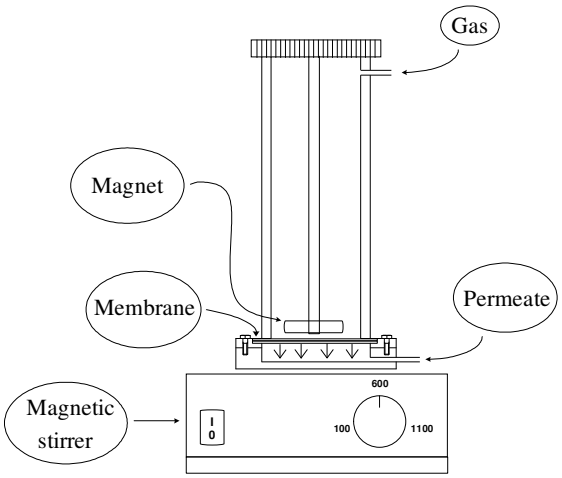

Figure 4 – Schematic representation of the bench-scale stirred cell.

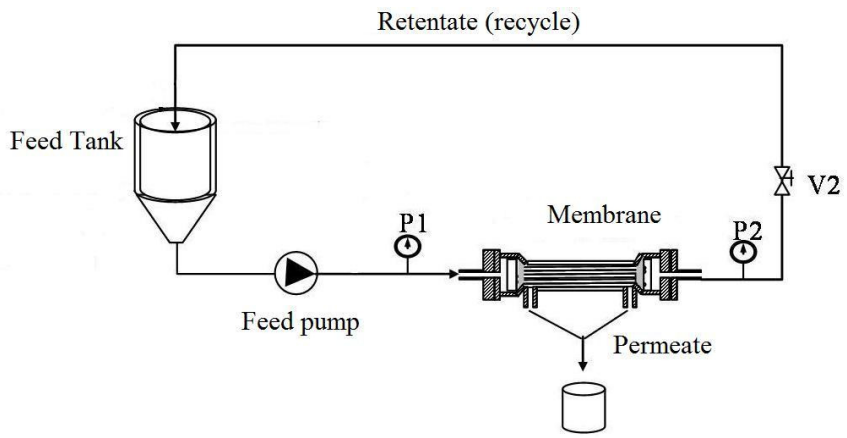

Figure 5 – Schematic representation of the pilot plant.

The cake structure otherwise has been predicted to vary as a function of particle transport and surface potential. Moreover, this structure may be modified as a function of the relative balance between applied pressure and surface forces. Thus, the propensity of membrane cakes for reorganization and collapse is determined by a balance of forces acting on the particles in the cake [48].

The crossflow configuration shows a better performance, since its characteristics allow the particles to remain in a suspended state above the outer surface instead of being deposited, due to the tangential flow to on the membrane surface, leading to higher permeate ratios, due to the enhanced control over the fouling and the membrane concentration polarization [83,86,87]. In their work Chun *et al.* [87] demonstrated that both the cake layer thickness and the particle concentration in the cake layer, for dead-end case, showed higher values than those of cross-flow one. The use of the best operational conditions such as temperature, pressure and tangential flow should also be considered. Those conditions should be sought to optimize the process, especially in the case of a large scale application [23,88].

Carvalho *et al.* [30] concluded in their work that the variations predicted during the scale-up procedure can be bypassed and that the use of a stirred dead-end process, in which is promoted the convection movement in the process, can be used to evaluate other processes aiming their use in an industrial scale.

In fact, moving from laboratory experiment to pilot plant operations and finally to a demonstration unit becomes progressively more complicated. Each step brings an increase in membrane area requirement, equipment, quantity of required feedstocks, time for execution, analytical facilities, technical issues, and operating personnel. Design advantages for the pilot plant

over lab-scale operations included continuous monitoring of process conditions with a data collection system [89]. Those steps, however, can work as an indication of the economical feasibility of the implementation on full industrial scale [90].

5. Conclusions

A comprehensive review is given on the β-lactam antibiotics, especially on the clavulanic acid, the purification of bioproducts, nanofiltration process, its characterization and scale up. It was shown that the use of nanofiltration of clavulanic acid aiming its purification and concentration has been studied in different manners trying to lead this process to an industrial application. To achieve this goal, studies about the membrane characteristics were made and also scale up investigations.

The characterization of the membranes could provide information about their behavior, which can help to understand how the process works and predict its performance in the concentration and purification of the clavulanic acid. It is also useful to the process scale up, since the nanofiltration process act in different manners depending on the membrane presentation.

Acknowledgements

The authors acknowledge the financial support from the Coordenação de Aperfeiçoamento de Pessoal de Nível Superior (CAPES) and the State of São Paulo Research Foundation (FAPESP). The authors are also grateful for the membranes supplied by Mycrodin Nadir® and Dow Filmtec™.

References

[1] P.A. Bersanetti, R.M.R.G. Almeida, M. Barboza, M.L.G.C.Araújo, C.O. Hokka, *Bioch. Eng. J.* 23 (2005) 31-36.

[2] A.I. Cavaco Morão, A.M. Brites Alves, M.C. Costa, J.P. Cardoso, *Chem. Eng. Sci.* 61 (2006) 2418-2427.

[3] R.M.R.G. Almeida, M. Barboza, C.O. Hokka, *Applied Bioch. and Biotechnol.* 108 (2003) 867-879.

[4] A.M. Brites Alves, A. Morão, J.P. Cardoso, *Desalination* 148 (2002) 181-186.

[5] A.L. Carvalho, M.I. Rodrigues, F. Maugeri, Sep. Sci. Technol. (2010) Submitted.

[6] A. Szymczyk, C. Labbez, P. Fievet, A. Vidonne, A. Foissy, J. Pagetti, *Adv. Colloid Interface* 103 (2003) 77-94.

[7] X.L. Wang, T. Tsuru, S. Nakao, S. Kimura, *J. Membr. Sci.* 135 (1997) 19-32.

[8] A. Szymczyk & P. Fievet, *J. Membr. Sci.* 252 (2005) 77-88.

[9] L. Braeken, B. Bettens, K. Boussu, P. Van Der Meeren, J. Cocquyt, J. Vermant, B. Van Der Bruggen, *J. Membr. Sci.* 279 (2006) 311-319.

[10] W.R. Bowen & J.S. Welfoot, *Desalination* 147 (2002) 197-203.

[11] V. Silva (2010) Doctoral Thesis in: Facultad de Ciencias, Universidad de Valladolid, Valladolid, Spain.

[12] A. Szymczyk, M. Sbaï, P. Fievet, A. Vidonne, *Langmuir* 22 (2006) 3910-3919.

[13] J.C. Rosa, A. Baptista Neto, C.O. Hokka, A.C. Badino Júnior, *Bioprocess and Biosys. Eng.* 27 (2005) 99-104.

[14] G.D. Wright, *Adv. Drug Deliv. Rev.* 57 (2005) 1451-1470.

[15] R. M. R. G. Almeida (2003) Doctoral Thesis in: Universidade Federal de São Carlos.

[16] T.T. Howarth, A.G. Brown, T.J. King, *J. Chem. Soc., Chem. Commun.* (1976) 266-267.

[17] E.J. Vandamme, *Biorechnology of Industrial Antibiotics* 22 (1984) Marcel Dekker, New York.

[18] R. M. R. G. Almeida, M. Barboza, C. O. Hokka, *Applied Bioch. and Biotechnol.* 108 (2003) 867-879.

[19] A.G. Brown, D. Butterworth, M. Cole, G. Hanscomb, J.D. Hood, C. Reading, G.N. Rolinson, *J. Antibiotics* 29 (1976) 668-669.

[20] M.A. Cook, A.D. Curzons, R.B. Wilkins, *Espacenet (0 026 044 B1)* (1983).

[21] H.S. Yang, N.H. Choi, S.C. Lee, Y.B. Ham, K.B. Min, *Espacenet (0 594 099 A1)* (1994).

[22] E. Capuder, *Espacenet (WO 96/33197)* (1996).

[23] J.P. Cardoso, *Espacenet (US 6,417,352 B1)* (2002).

[24] K. Mosbach, *Espacenet (WO 2002/022846)* (2004).

[25] A.F. Mayer, F.B. Anspach, W.D. Deckwer, *Bioseparation* 6 (1996) 25-39.

[26] M. Barboza, R.M.R.G. Almeida, C.O. Hokka, *Bioseparation* 10 (2002) 221-227.

[27] S. Ruddick, *Espacenet (WO 1996/022296)* (2004).

[28] E. Capuder, *Espacenet (US 6,274,575 B1)* (2001).

[29] A.L. Carvalho, F. Maugeri, V. Silva, P. Prádanos, A. Hernández, (2011) Not submitted yet.

[30] A.L. Carvalho & F. Maugeri, (2011) Not submitted yet.

[31] N. Hilal, H. Al-Zoubi, N.A. Darwish, A.W. Mohammad, M. Abu Arabi, *Desalination* 170 (2004) 281-308.

[32] W.R. Bowen, A.W. Mohammad, N. Hilal, *J. Membr. Sci.* 126 (1997) 91-105.

[33] J.A. Otero, O. Mazarrasa, J. Villasante, V. Silva, P. Prádanos, J.I. Calvo, A. Hernández, *J. Membr. Sci.* 309 (2008) 17–27.

[34] S. Singh, K.C. Khulbe, T. Matsuura, P. Ramamurthy, *J. Membr. Sci.* 142 (1998) 111-127

[35] P. Prádanos, M.L. Rodriguez, J.I. Calvo, A. Hernández, F. Tejerina, J.A. de Saja, *J. Membr. Sci.* 117 (1996) 291-302.

[36] N.A. Ochoa, P. Prádanos, L. Palacio, C. Pagliero, J. Marchese, A. Hernández, *J. Membr. Sci.* 187 (2001) 227-237.

[37] I. Koyuncu, J. Brant, A. Lüttge, M.R. Wiesner, *J. Membr. Sci.* 278 (2006) 410-417.

[38] P.C.Y. Wong, Y.-N. Kwon, C.S. Criddle, *J. Memb. Sci.* 340 (2009) 117-132.

[39] A.I. Schäfer, A.G.; Fane, T.D. Waite, *Desalination* 131 (2000) 215-224.

[40] E.M. Vrijenhoek, S. Hong, M. Elimelech, *J. Membr. Sci.* 188 (2001) 115-128.

[41] W.J. Koros, Y.H. Ma, T. Shimidzu, Reprinted from Pure and Applied Chemistry 68:1479-1489. *J. Membr. Sci.* 120 (1996) 149-159.

[42] L.D. Nghiem, D. Vogel, S. Khan, *Water Research* 42 (2008) 4049-4058.

[43] D. Bhattacharyya, J. Hestekin, D. Shan, S. Ritchie, *J. Chin. Inst. Chem. Eng.* 33 (2002) 61-66.

[44] B. Van der Bruggen, C. Vandecasteele, T. Van Gestel, W. Doyen, R. Leysen, *Environ. Progress* 22 (2003) 46-56.

[45] I. Koyuncu, M. Turan, D. Topacik, A. Ates, *Water Sci. Technol.* 41 (2000) 213-221.

[46] B. Van der Bruggen, J.H. Kim, F.A. DiGiano, J. Geens, C. Vandecasteele, *Sep. Purif. Technol.* 36 (2004) 203-213.

[47] J.S. Vrouwenvelder, J.W.N.M. Kappelhof, S.G.J. Heijman, J.C. Schippers, D. Van der Kooij, *Desalination* 157 (2003) 361-365.

[48] V.V. Tarabara, I. Koyuncu, M.R. Wiesner, *J. Membr. Sci.* 241 (2004) 65-78.

[49] H. Yacubowicz & J. Yacubowicz, *Filt. Sep.* sept. (2005).

[50] B. Van der Bruggen & C. Vandecasteele, *Environ. Sci. Technol.* 35 (2001) 3535-3540.

[51] B. Van der Bruggen, L. Braeken, C. Vandecasteele, *Desalination* 147 (2002) 281-288.

[52] Y. Wyart, G. Georges, C. Deumié, C. Amra, P. Moulin, *J. Memb. Sci.* 315 (2008) 82-92.

[53] M. Elimelech, X. Zhu, A.E. Childress, S. Hong, *J. Membr, Sci.* 127 (1997) 101-109.

[54] J.M. Sheldon, *J. Membr. Sci.* 62 (1991) 75-86.

[55] A. Bessières, M. Meireles, R. Coratger, J. Beauvillain, V. Sanchez, *J. Membr. Sci.* 109 (1996) 271-284.

[56] Q. Wei & D. Wang, *Materials Letters* 57 (2003) 2015-2020.

[57] W.R. Bowen, N. Hilal, R.W. Lovitt, P.M. Willians, *J. Membr. Sci.* 110 (1996) 229-232.

[58] W.R. Bowen, N. Hilal, R.W. Lovitt, P.M. Willians, *J. Membr. Sci.* 110 (1996) 233-238.

[59] N. Hilal & W.R. Bowen, *Desalination* 150 (2002) 289-295.

[60] A.W. Mohammad, N. Hilal, M.N.A. Seman, *J. App. Polym. Sci.* 96 (2005) 605-612.

[61] N. Hilal, H. Al-Zoubi, N.A. Darwish, A.W. Mohammad, *Desalination* 177 (2005) 187-199.

[62] K. Boussu, B. Van der Bruggen, A. Volodin, J. Snauwaert, C. Van Haesendock, C. Vancasteele, *J. Colloid Int. Sci.* 286 (2005) 632-638.

[63] K. Boussu, B. Van der Bruggen, A. Volodin, C. Van Haesendonck, J.A. Delcour, P. Van der Meeren, C. Vandecasteele, *Desalination* 191 (2006) 245-253.

[64] Y. Lu, T. Suzuki, W. Zhang, J.S. Moore, B.J. Mariñas, *Chem. Mater.* 19 (2007) 3194-3204.

[65] K. Boussu, C. Vandecasteele, B. Van der Bruggen, *J. Membr. Sci.* 310 (2008) 51–65.

[66] Agilent Technologies. What is an atomic force microscope? In: <http://nano.tm.agilent.com/blog/page/3/?s>. Accessed in: August 20th, 2009.

[67] A. Martín, F. Martínez, J. Malfeito, L. Palacio, P. Prádanos, A. Hernandez, *J. Membr. Sci.* 213 (2003) 225-230.

[68] A.I. Cavaco Morão, A.M. Brites Alves, M.D. Afonso, *J. Membr. Sci.* 281 (2006) 417-428.

[69] M.S. Oak, T. Kobayashi, Y.H. Wang, T. Fukaya, N. Fujji, *J. Membr. Sci.* 123 (1997) 185-195.

[70] A. E. Childress & M. Elimelech, *Environ. Sci. Technol.* 34 (2000) 3710-3716.

[71] J. Schaep & C. Vandecasteele, *J. Membr. Sci.* 188 (2001) 129-136.

[72] M. Ribau Teixeira & M. J. Rosa, *Desalination* 151 (2002) 165-175.

[73] M. Ribau Teixeira, M. J. Rosa, M. Nyström, *J. Membr. Sci.* 265 (2005) 160-166.

[74] C.K. Colton, S. Friedman, D.E. Wilson, R.S. Lees, *J. Clin. Invest.* 51 (1972) 2472-2481.

[75] S. Sridhar & P.K. Bhattacharya, *J. Membr. Sci.* 57 (1991) 187-206.

[76] S. Kimura & S. Nakao, *Desalination* 17 (1975) 267-288.

[77] G. Jonsson & C.E. Boesen, *Desalination* 21 (1977) 1-10.

[78] F. Martínez, A. Martín, J. Malfeito, L. Palacio, P. Prádanos, F. Tejerina, A. Hernández, *J. Membr. Sci.* 206 (2002) 431-441.

[79] A.A. Rashin & B. Honig, *J. Phys. Chem.* 89 (1985) 5588-5593.

[80] E. Mathiason, *J. Membr. Sci.* 16 (1983) 23-36.

[81] V. Gekas & B. Hallström, *J. Membr. Sci.* 30 (1987) 153-170.

[82] T. Schipolowski, A. Jeżowska, G. Wozny, *Desalination* 189 (2006) 71-80.

[83] M.S. Le & T. Atkinson, *Process Biochem.* 20 (1985) 26-31.

[84] S. Eberhard, *Kluwer Academic/Plenum Publishers, New York* (2000) 19-40.

[85] N.D. Lawrence, S.E. Kentish, A.J. O'Connor, A.R. Barber, G.W. Stevens, *Sep. Purif. Technol.* 60 (2008) 237-244.

[86] H. Strathmann, *Trends Biotechnol.* 3 (1985) 112-118.

[87] M.-S. Chun & W.C. Park, *J. Membr. Sci.* 243 (2004) 417-424.

[88] M.V. Tres, S. Mohr, M.L. Corazza, M. di Luccio, J.V. Oliveira, J. Membr. Sci. 333 (2009) 141-146.

[89] L.S. White, *J. Membr. Sci.* 286 (2006) 26-35.

[90] W.-J. Lau & A.F. Ismail, *Desalination* 245 (2009) 321-348.

AFM ANALYSIS OF THE SURFACE OF NANOPOROUS MEMBRANES: APPLICATION TO THE NANOFILTRATION OF POTASSIUM CLAVULANATE

A. L. Carvalho[1]; F. Maugeri[1]; V. Silva[2], A. Hernández[2*]; L. Palacio[2]; P. Pradanos[2]

[1]Departament of Food Engineering, Faculty of Food Engineering, Rua Monteiro Lobato 80, Barão Geraldo, University of Campinas – UNICAMP, CEP: 13083-862, Campinas, SP, Brazil

[2]Depto. de Física Aplicada, Fac. de Ciencias, Universidad de Valladolid, Real de Burgos s/n, 47071 Valladolid, Spain

[*]e-mail: tonhg@termo.uva.es

Abstract

This study presents the structural characterization of the surface of four commercial nanofiltration membranes: NF90 (polyamide) and NF (polypiperazine amide) from Filmtec™ and NP010 and NP030 (polysulfone) from Microdyn Nadir®, by Atomic Force Microscopy (AFM). These membranes have been studied before and after undergoing a filtration process with potassium clavulanate. The fast Fourier filtering of AFM images with very high magnification (40 x 40 nm) has allowed identifying the pore size distribution and geometry of the pores on the surface of the membrane before their use. Images between 0.5 x 0.5 and 10 x 10 μm^2 have allowed the study of the surface roughness of the samples before and after being used to filtrate potassium clavulanate solutions. The results of roughness and power spectral fractal dimension along with the skewness and kurtosis of the height distribution have been analyzed in terms of pore size, hydraulic permeability and the adsorption of clavulanate for the different samples.

Keywords: Nanofiltration membranes, AFM, Roughness, Fractal dimension, Clavulanic acid.

1. Introduction

Nanofiltration is a relatively new pressure driven membrane process that has properties in between ultrafiltration and reverse osmosis. The main advantages of this process are: operation at low pressures when compared to reverse osmosis, high fluxes, considerable retention of multivalent anionic salts and low molecular weight organic molecules, relatively low investment and low cost of operation and maintenance with a low energy consumption [1]. It has applications in a wide range of fields that include fractionation and selective removal of solutes from complex process streams with rejection of ions and charged organic pollutants [2, 3]. In the food industry it has been used for the demineralization and the fractionation of whey [4], etc. It is considered the most important recent development in process engineering and environmental protection [2, 5, 6].

The characterization of nanofiltration membranes includes the use of predictive models, which help to understand the separation process. Because the morphological properties of the membranes have important consequences on performance and fouling, it is very important to characterize them by experimental techniques that could determine their structure and pore distribution [2, 6-11].

Despite the efforts that could be made to minimize the fouling caused by the membrane-solute affinity, it occurs in many instances [12] and it is perhaps the most critical parameter in membrane filtration [12-15]. This is the reason why nanofiltration membranes, although having many applications [16-19], did not still reach their potential on an industrial scale. Fouling increases the operation and maintenance costs, it causes a decline in the permeate flux, and increments in the energy demands, turning down the membrane performance and ultimately reducing membranes life [13, 20, 21].

An understanding of the relationship between membrane surface properties and separation characteristics can determine the choice of a membrane for a particular separation and can also lead to the development of membrane technology [7]. Some of the most important surface characteristics are the mean pore size and the pore size distribution, the pore density and the surface roughness. The pore size plays an important role in the transport through the membrane, because it determines rejection and selectivity along with flux or permeability [7, 12, 22, 23].

There are several well established techniques for the determination of the pore size distributions and porosity. They include the bubble point technique, mercury porosimetry, the microscopic technique, solute transport, permporometry and thermoporometry [7]. Many advances

in the study of membrane structure have been made possible [24] by microscopic techniques such as: Scanning Electron Microscopy, SEM, [25], Transmission Electron Microcopy, TEM, [26], Atomic Force Microscopy, AFM, [6] and Scanning Tunneling Microscopy, STM, [27]. This is especially true for nanofiltration membranes that are nanoporous in nature; i.e. they have pores in the nanometric range.

Among the microscopic techniques, AFM is a relatively recent technique. It gives topographical images of the membrane surface by scanning with a sharp tip over the surface without any previous sample preparation. Since its invention, AFM has been applied to study microfiltration, ultrafiltration membranes [9, 27-31], and more recently nanofiltration membranes [3, 6, 7, 10, 32-36] and other nanoporous materials [37-40]. This technique allows characterizing membranes surfaces, including non-conducting surfaces, with a nanometer (or even atomic) resolution in wet and dry environments. AFM also allows the study of the adhesion of particles and the properties of the subsequent deposit during fouling.

Most investigations have focused on the pore structure disregarding other important parameters that might be taken into account. Nevertheless, it is obvious that the pore size distribution alone do not describe completely the morphology of the membrane. In this the sense surface topography plays an important role in determining the fouling properties. Rough materials have more surface area and the fluid mechanics on them can also influence the resulting fouling rates. Very often, roughness is determined by using, for example, the average or the root-mean-square. Other complementary parameters are also interesting as skewness and kurtosis which describe the peak asymmetry and flatness, respectively, of the height distribution on the surface. Moreover, most researchers appear to be unaware that several of these roughness measurements are scale dependent and dismiss the fractal dimension that is a key scale independent parameter reflecting the roughness [11, 28].

Clavulanic acid, CA, is a compound produced by *Streptomyces clavuligerus*, and it consists of a β-lactam ring fused to an oxozilidine ring [41]. It shows weak antibacterial activity against most bacteria, but is a potent inhibitor of a wide range of β-lactamase and is able to potentiate the antibacterial activity of penicillins and cephalosporins against many β-lactamase-producing resistant bacteria [42]. It is currently used in combination with amoxicillin or other semi-synthetic penicillins for the treatment of infections caused by β-lactamase-producing bacteria. Clavulanic acid is produced industrially by fermentation and is isolated and purified from the fermentation medium in several steps. The first step involves clarification of the medium by filtration or

centrifugation followed by either adsorption or liquid-liquid extraction with an organic solvent, normally butanol. Further purification is achieved by anion-exchange chromatography.

It is known that the clavulanic acid is chemically unstable to temperatures over 30 ºC and pH over 7.5 or below 4.5 [43, 44]. Owing to this unstable nature of the free acid, clavulanic acid is isolated as the lithium, potassium or sodium salt. The molecular structures of both the clavulanic acid and the potassium clavulanate, KCA, are shown in Figure 1.

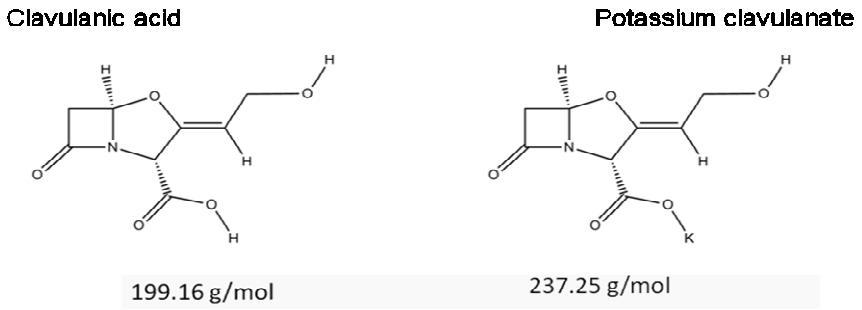

Figure 1 – Molecular structures of clavulanic acid and potassium clavulanate.

Concerning its molecular weight, see Figure 1, nanofiltration seems fully adequate for the purification of KCA. This raises some problems due to the high fouling levels appearing. In order to design an adequate process, nanofiltration with membranes with pores in the nanometer range with low fouling should be sought. Furthermore, the characterization of some potentially appropriate membranes can be profited to test how AFM techniques can help in this process.

By using AFM, the pore size of four commercially available membranes, with appropriate characteristics, will be studied. AFM is also uniquely qualified to investigate the dominant factors associated in the adsorption of solutes on surfaces, with variation of surface topography at nanoscale resolution [45, 46]. Thus the morphology of these membranes will be studied, before and after their use to concentrate KCA, by analysing their surface roughness and fractal dimension. This will be done in order to analyse how KCA is deposited on the membranes and trying to correlate these parameters with the reduction in flux.

2. Methodology

2.1. Membranes and chemicals

Four commercial membranes have been selected and studied here. Two of them are made from polyamides: NF (polypiperazine amide) and NF90 (fully aromatic polyamide [15, 47]) membranes, from Filmtec™. Another two membranes, NP010 and NP030, are made from polyethersulfone and manufactured by Microdyn Nadir®. Table 1 shows the main characteristics of these membranes according to their manufacturers.

Table 1 – Characteristics of the membranes used here as given by their manufacturers

Membrane	NF90	NF	NP030	NP010
MWCO (Da)	180[a]	>200	400	1000
Max. pressure (bar)	41	41	40	40
Max. temperature (ºC)	45	45	95	95
pH range	2-11	3-10	0-14	0-14
Rejection (%)	>97[b]	>99[c]	80-95[d]	25-55[d]

[a] Molecular weight cut off according to Lopez Muñoz *et al.* [48] in Da (g/mol)

[b] Rejection of $MgSO_4$ (25ºC, 4.8 bar)

[c] Rejection of $MgSO_4$ (25ºC, 8.9 bar)

[d] Rejection of Na_2SO_4 (20ºC, 40 bar)

Milli-Q quality water has been used both for water permeability measurements and for the aqueous solution filtration experiments. These solutions were prepared with potassium clavulanate salt (KCA), from the medicine Clavulin® (revested pills with 125 mg of potassium clavulanate and 500 mg of amoxicillin). They were vacuum filtered and micro-filtered in 14 µm and 0.45 µm pore membranes, respectively. The pH of the potassium clavulanate solutions was adjusted to 6.2 with HCl 0.2 M and KOH 1M solutions prepared from analytical grade reagents from Probus and Panreac, respectively.

2.2. Nanofiltration experiments

Nanofiltration of KCA has been performed in a stainless steel stirred dead-end process that simulates a crossflow process. The system consists in a cylindrical container with a membrane located at its bottom, whose area was 1.52 x 10^{-3} m^2, and provided with a magnetic stirrer that simulates the convection in a crossflow process. Pressure differences have been applied by application of pressurized nitrogen, as shown in Figure 2. The operational conditions consisted in: a stirring frequency of 600 rpm, an applied transmembrane pressure of $2x10^6$ Pa, a volume of the feed phase of 200 mL, a process temperature of 25 ºC, a pH of 6.2 and a potassium clavulanate concentration on the feed phase of 750 mg/L. The process was stopped when the volume permeated reached 100 mL.

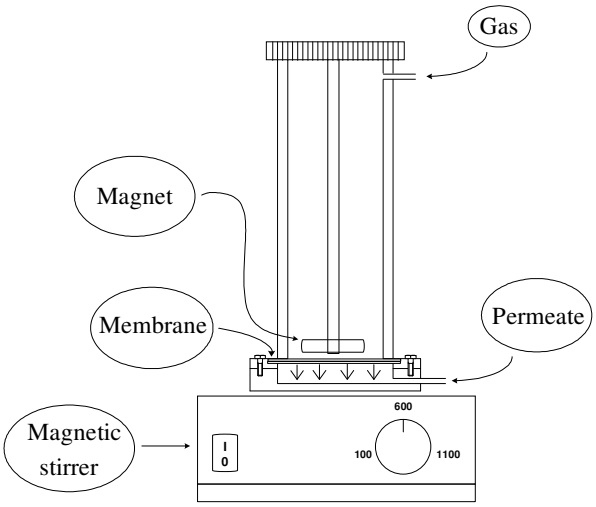

Figure 2 – Schematic representation of a crossflow nanofiltration experimental setup at laboratory scale.

The water permeability has been determined from the variation of the flux with increasing pressure differences up to $4x10^6$ Pa across the membrane at 25 ºC. Water was permeateded under a $2x10^6$ Pa pressure gradient through each membrane before and after its use with clavulanate, KCA until the resulting pure water flux remained constant.

2.3. Atomic Force Microscopy

With Atomic Force Microscopy, AFM, images, we can study the topography of the surface of clean membranes as well as of the fouled ones. Atomic Force Microscopy has been performed with a Nanoscope Multimode IIIa scanning probe microscope from Digital Instruments (Veeco Metrology Inc., Santa Barbara, CA). Two scanners have been used: the J scanner with a maximum lateral (x, y) scan range of 115 μm and a maximum vertical (z) range of 5.5 μm for the biggest images; and the E scanner for the smallest areas analyzed (horizontal and vertical ranges of 10 μm and 2.5 μm respectively). The scanned areas have gone from 40 × 40 nm to 100 × 100 μm. The smallest areas of 40 x 40 nm have only been used to get the optimal resolution allowing an accurate detection of the pore edges. For scanned areas over 10 x 10 μm scratches and other surface damages are shown. Roughness has been measured for images from 0.5 x 0.5 μm to 10 x 10 μm.

For the images used to measure roughness the resolution in the x-y scale decreases for increasing scanned areas because the size of the detectable details is L /512, L being the length of each side of the scanned square, this means that it goes from 1 nm to 20 nm. Referring to the z resolution, the corresponding set range has been appropriately reduced depending on the surface roughness to increase the z resolution. As a result, this zeta resolution is approximately of 0.2 nm in the worst case.

The contact mode of operation has been used for the most detailed pictures (40 x 40 nm images of clean membranes) while tapping (or intermittent contact) mode analysis has been used for the rest of the images.

In the intermittent contact operation mode, the tip and the supporting cantilever are made to oscillate close to their resonance frequency. In this case, it is not the cantilever deflection which is measured (as in conventional AFM techniques: both contact and non-contact methods), but the root mean square of the oscillation amplitude of the cantilever once it has been excited into resonance with a piezo-electric driver. The phase shift appearing at the resonance can be detected to give the so called phase contrast images where the dominions with different viscoelastic properties can be easily detected. In any case the tapping mode is an especially useful technique because it limits the possibility to damage both tip and sample due to their contact because it is only intermittent.

In both the techniques used here (tapping and contact mode), the measurements have been performed in open atmosphere conditions and in the repulsive mode. Moreover the tip always enters the condensation (contamination, humidity etc) layer because the required strength is set adequately

to overcome the capillary forces appearing in such a layer. The state of the tip has been tested before and after each kind of experiment, and no significant variations have been detected. The test has been done by measuring standard calibration samples.

The tapping mode gives better-quality pictures than the non-contact mode but it is also free from the very typical artefacts obtained with the conventional contact method. Nevertheless, for the smallest images, used to determine the pore size distribution, the contact mode of operation has been used with a very low feed-back in order to measure heights by the cantilever deflection rather than by the vertical motion of the scanner that supports the sample. This method allows an increase in the scanning speed (without damages in tip and/or surface) that reduces noise and improves real resolution to reach even the atomic range [49]. This procedure can only be used for relatively flat surfaces. For larger scanned areas, due to the high roughness the feed-back system should act to avoid surface-tip crashing and consequently the tapping mode should be preferable due to the friction forces that would decrease resolution in the contact mode drastically.

The tapping mode has been performed using the Olympus™ probes OMCL-AC160TS-W with a spring constant of 40 N/m. Drive frequency was determined by automatic tuning around 350 kHz at a target amplitude of 2V. Tip velocities were adjusted according to the roughness of the sample and the size of the image. The curvature radius of this tip is below 10 nm. For the contact mode operation Nanosensor® silicon tips of the CONTR#19809 type have been used. Their force constant is 0.12 N/m with a curvature radius below 10 nm. In both cases the state of the tip has been tested before and after each experiment and no significant variations have been detected. The test has been done by measuring the corresponding recommended standard calibration samples.

Tapping mode pictures (topographical images and phase contrast ones) have been acquired for each sample and focusing in areas randomly distributed on them. All images have been acquired with 512 points per scan line and with 512 lines. Images of 40 nm × 40 nm have been analyzed by using the command *Spectrum 2D*, function which transforms images by applying a 2D fast Fourier transform (FFT), to pass or remove specific frequencies from the images. This modification is necessary to eliminate the electrical noise and some other parasite vibrations (that affect specially the high resolution images). The image acquisition and treatment has been done with Nanoscope Software, version 5.12 rev. B.

2.4. Surface analysis

A quantitative analysis of the roughness of the membrane has been performed, by using the Nanoscope Software functions. The surface roughness has been studied by statistical analysis of images with areas between (0.05 × 0.05) μm^2 to (10 × 10) μm^2.

A common quantification of surface roughness is the root-mean-square roughness RMS or S_q:

$$S_q = \sqrt{\frac{\sum_{i=1}^{N_t}(z-\bar{z})^2}{N_t}} \tag{1}$$

referred to the average height,

$$\bar{z} = \frac{\sum_{i=1}^{N_t} z_i}{N_t} \tag{2}$$

where z_i is the deviation in height at the (x_i ,y_i) point from the mean after baseline subtraction, and N_t is the total number of data points in the surface (N_t= mN_l being m the number of lines and N_l the number of points per line) where z_i is collected. However this parameter strongly depends on the instrument and the tip used and on the measurement procedure. In this sense [50], there is another parameter less dependent and based on a Fourier transform: the Power Spectra Density which analyses the two dimensional roughness spectra of the surface [51]. This spectrum can be evaluated as [24, 52]:

$$\gamma(p,q) = \gamma(p\Delta\sigma_x, q\Delta\sigma_y) = \left(\frac{2\pi}{L}\right)^2 \left|\hat{z}(p\Delta\sigma_x, q\Delta\sigma_x)\right|^2 \tag{3}$$

where

$$\Delta\sigma_x = \Delta\sigma_y = \frac{\pi}{N\Delta x} = \frac{\pi}{N\Delta y} = \frac{\pi}{L} \tag{4}$$

L being the length of each side of the scanned square, N is the number of points along each side of the square, Δx and Δy are the distance between neighbour points along each direction on the scanned area. $\hat{z}$ is the discrete bi-dimensional Fourier transform of the height:

$$\hat{z}(p,q) = \frac{1}{4\pi^2}\left[\frac{L}{N}\right]^2 \sum_{m,n} z\left(m^L/N, n^L/N\right)\exp\left[-j\frac{2\pi}{N}[mp+nq]\right] \tag{5}$$

where $j = \sqrt{-1}$. Therefore

$$\gamma(\vec{\sigma}) = \gamma(p,q) = \frac{L^2}{4\pi^2 N^4}\left|\sum_{m,n} z\left(m^L/N, n^L/N\right)\exp\left[-j\frac{2\pi}{N}[mp+nq]\right]\right|^2 \tag{6}$$

The bi-dimensional spectrum $\gamma(\vec{\sigma})$, or even better its average on the polar angle $\gamma(\sigma)$ where $\sigma = |\vec{\sigma}|$ can be represented and allows to calculate the RMS roughness, S_q, as

$$S_q = \int_{\vec{\sigma}} \gamma(\vec{\sigma})\, d\vec{\sigma} = 2\pi \int_{\sigma} \gamma(\sigma)\, d\sigma \tag{7}$$

The spatial pulsation σ has to be included in the interval:

$$\sigma \in \left[\frac{\pi}{L}, N\frac{\pi}{L}\right] \tag{8}$$

This methodology provides valuable information not only on the height deviation of the roughness profile, but also on its lateral distribution [53].

In a logarithmic scale, this spectrum has a linear behaviour in very large ranges, according with the equation:

$$\gamma = \beta/\sigma^{\alpha} \tag{9}$$

β being a constant and α the spectrum slope. This power law is typical of fractal behaviour of roughness (self-affine behaviour). In this situation the corresponding fractal dimension D can be evaluated as a function of the spectrum slope [24, 52]:

$$D = (8-\alpha)/2 \tag{10}$$

There are other useful parameters, two of them are especially significant and have been analyzed here:

- The surface skewness, S_{sk}, related to the third moment of the height of the distribution, which informs about the asymmetry relative to Gaussian distribution. For a set of discrete data can be calculated as [54]:

$$S_{sk} = \frac{1}{N_t S_q^3} \sum_{i=1}^{N_t} \left(z_i - \overline{z} \right)^3 \tag{11}$$

- The surface kurtosis, S_{ku}, is a measure of how sharp the distribution is as compared to the Gaussian, and it is related to the fourth moment of the height of the distribution. It is calculated as:

$$S_{ku} = \frac{1}{N_t S_q^4} \sum_{i=1}^{N_t} \left(z_i - \overline{z} \right)^4 \tag{12}$$

The pores size distributions have been obtained by computered image analysis (CIA) from the same images. Image Analysis was carried out by means of Jandel® ScanPro software (version 3.00.0030), in order to study the pore size distribution. Each photograph was digitized with a resolution of 1024 x 768 pixels, assigning to each one a grey level ranging from 0 (black) to 255 (white). Then, a clear-field equalization was applied to each image field to eliminate parasite changes in grey levels due to uneven bending. Once the bending effects were eliminated, the image grey spectrum was spanned to get the maximum contrast and definition. Then the images were redefined according to an assigned grey threshold level under which every pixel was assigned to 1 and the rest to 0. The resulting binary picture was improved by scraping isolated pixels, in such a way that all the remaining 1's in the matrix were assumed to belong to a pore. Finally the pore borders were smoothed in order to reduce the influence of the finite size of pixels and low definition. Of course a correct selection of threshold grey level is fundamental for correctly and accurately identifying pores. Customarily the grey spectrum is analyzed and the threshold centred in the peak to peak valley of the almost bimodal distributions obtained. Unfortunately sometimes the spectra are so flat that this technique is only of relative help in making a correct threshold selection. In any case, inspection by eye facilitates the process of selection of several reasonable threshold candidates whose outcomes are averaged.

3. Results and discussions

3.1. Filtration processes

The water permeability (L_p) of each membrane has been determined before and after their use with KCA. All membranes were conditioned at the highest pressure allowed for each one and the flows have been measured with time until becoming constant. This allows the hydration of the polymer material of the membrane and a correct measurement of the behaviour of the equilibrated membrane [27]. The permeabilities of each membrane are presented in Table 2.

Table 2 – Water permeability for each membrane evaluated, before and after KCA permeation

Lp (10^{-11}m/Pa.s)	NF90	NF	NP030	NP010
Before	1.53	3.39	4.36	6.47
After	1.10	2.46	1.96	1.38
Lp (used)/Lp (new) (%)	72%	73%	45%	21%

It is worth to note that the polyamide membranes (NF and NF90) have low initial permeabilities, but a quite small reduction in the flow after the filtering process, possibly due to a low affinity of the solute to the membrane surface. Polyethersulfone membranes (NP030 and NP010) have high initial permeabilities, nevertheless they suffer a more significant flux reduction, ending at low L_p, This behaviour might be related to the chemical nature of the membrane materials, their electrical charge and the morphological aspects of the membranes (pore size, porosity and surface roughness) as well as to the operation conditions.

3.2. AFM characterization

3.2.1 Pore size distributions for clean membranes

For the clean membranes, it has been possible to obtain images which processed by FFT to eliminate noise, allow a visualization of the pores on the surface of the membrane. Figures 3 (a-d) show representative images for sampled areas of 40 x 40 nm^2. This results impossible for the KCA

fouled membranes because they appear as covered by an almost totally dense layer of deposited KCA.

As Figure 3 reveals, the four membranes analyzed present clear differences at the nanometer scale. The membrane NF90 has pores with mostly circular surface sections, whereas for the other three membranes (NF, NP010 and NP030) it is impossible to detect a regular geometry of the surface sections for their pores. Referring to the z-axis range, it is clear that it is larger for the NF90 (6 nm) and NF (4 nm) than for the polyethersulfone membranes (/1 nm).

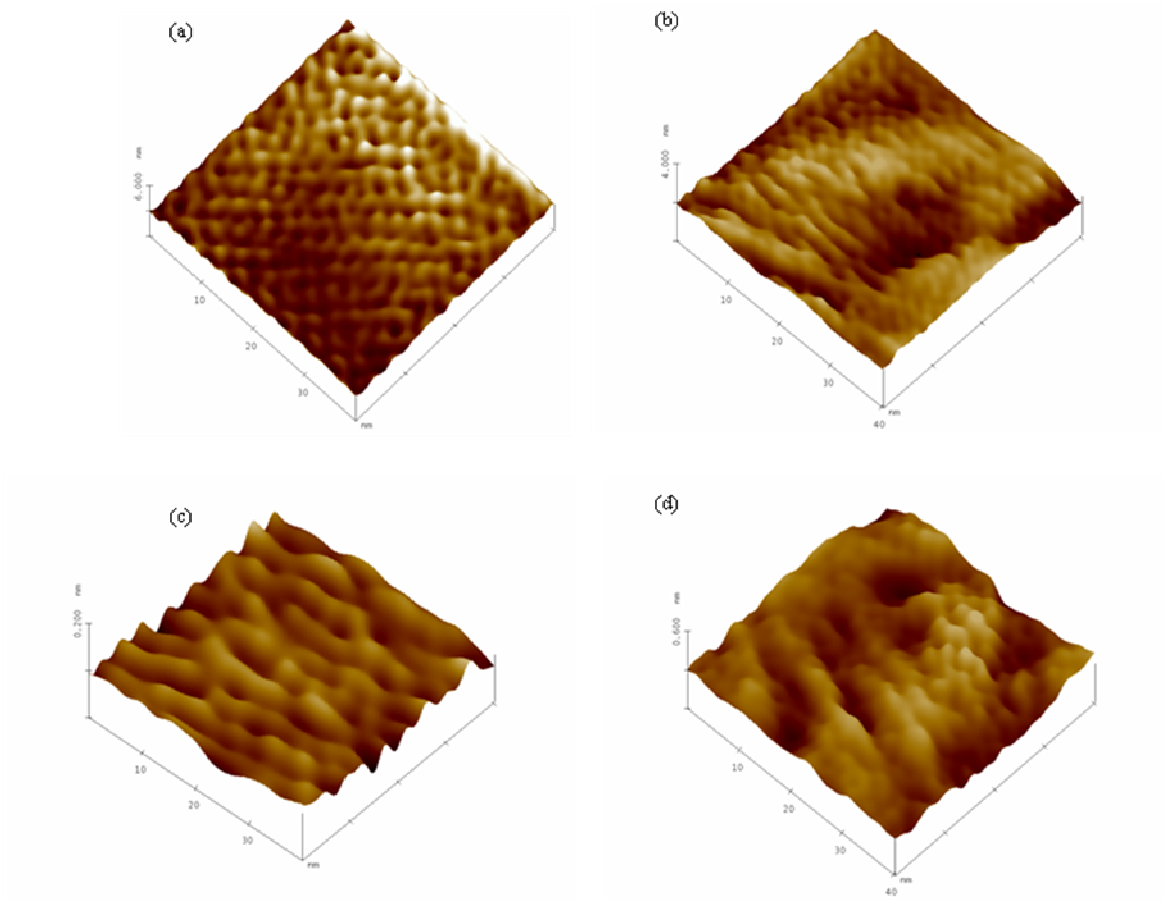

Figure 3 – Examples of the AFM images of the membranes with scanned areas of (40 × 40) nm^2 used to obtain the pore size distribution for: (a) NF90 (b) NF, (c) NP030 and (d) NP010.

The pore size distributions and the corresponding mean pore size for the membranes studied can be evaluated by computerized image analysis of the AFM images. Figures 4 (a-d) show the results obtained. It can be seen that the pore sizes follow Gaussian distributions. The mean pore size

refers to the diameter on the entrance of the pores where AFM generally gives a funnel structure due to the tip-sample convolution [27] what means that these pore sizes could be slightly overestimated [9]. All membranes present a mean pore size in the range of nanofiltration, with the sequence: NP010 > NP030 > NF > NF90, in the same order than their corresponding water permeability before being used with KCA and their nominal MWCO. The permeability-diameter relationship is not linear as shown in Figure 5. This behaviour is understandable, since the flow does not depend linearly on the pore size but on the squared diameter. The water permeability depends also on the density of pores per unit area according to the viscous flow regime.

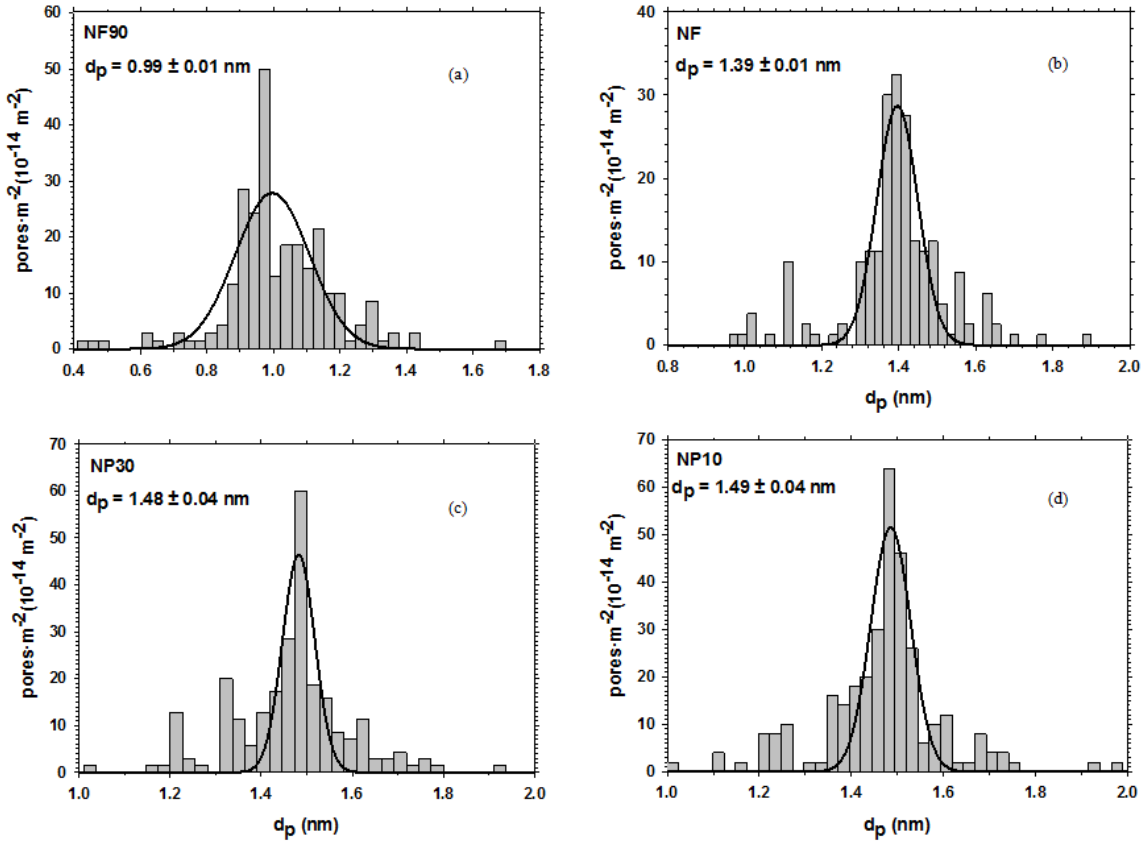

Figure 4 – Pore size distribution for the membranes NF90, NF, NP030 and NP010. They have been fitted to a Gaussian distribution showing the mean pore dimeter along with the standard deviation of the corresponding distribution.

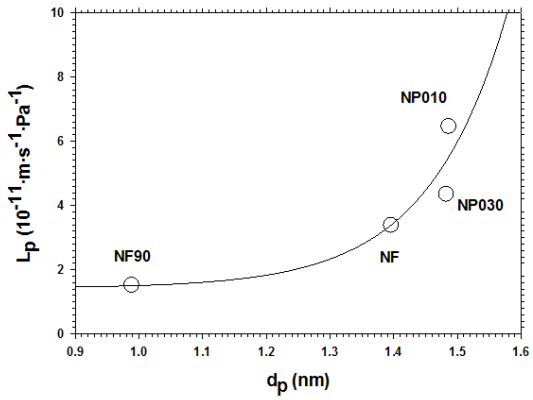

Figure 5 – Experimental water permeability versus mean pore diameters as obtained from AFM images.

To try to verify the validity of the distributions obtained, it is possible to compare the permeability obtained from the distribution (as predicted by the Hagen-Poisseuille law) with the experimental one. The Hagen-Poiseuille equation:

$$L_p = \sum_1^n \frac{\pi n_i r_i^4}{A \eta \Delta x} \tag{13}$$

where n_i is the number of pores per unit area of the membrane of the i-th class, r_i is the radius of these pores, η the water viscosity inside the pores, Δx thickness of the selective layer and A is 8 if the pores are assumed to have a cylindrical geometry or 3 if they are assumed to be slit-like.

Moreover, to evaluate L_p, with Eq. 13 we need to do a series of considerations:

- It has been proved that the viscosity of aqueous solutions inside nanometric pores is increased due to confinement effects. It was calculated by Wesolowska *et al.* [55] and for these membranes the value used is 6.3×10^{-3} Pa.s.
- It has to be taken into account that the active layer is the thickness that should be required. It is not always easy to detect, because very frequently there is a gradual transition from the tight active layer to the porous support layer. For some nanofiltration membranes this transition is sharp enough to be detected by using SEM images [56] giving values around 100 nm.

We compare the obtained results for the water permeability with the experimental values in Figure 6. The theoretical results for both the possible geometries (cylindrical or slit-like pores) are shown in this Figure. As mentioned, the NF90 membrane shows clear circular pore sections as shown in Figure 3. So we could assume that all of them contain actually cylindrical pores. Thus the

differences between the experimental permeabilities and those predicted on the basis of the measured pore size distributions could be attributed to the membrane thickness that could be slightly different from that assumed in the calculations (100 mm). When this is taken into account a fitted thickness could be evaluated to make coinciding experimental and theoretical values. This procedure gives the values shown in Table 3 for both the possible geometries. Note that these thicknesses are quite similar for the four membranes. This is why the lines in Fig. 6 resulted to be almost perfectly linear.

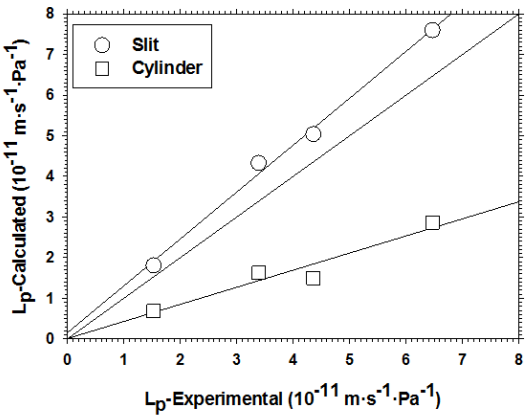

Figure 6 – Experimental permeability versus that calculated from the distributions shown in Fig. 4 and the Hagen-Poiseuille equation.

Table 3 – Membrane thickness in micrometer as obtained from the comparison of theoretical and experimental water permeabilities in Fig. 6

	NF90	NF	NP030	NP010
Cylindrical pores	118.3	127.7	115.6	117.5
Slit-like pores	44.4	47.8	34.4	42.4

Comparing with the results on pure water permeability after KCA filtration, it can be noted that the membranes which seem to have the largest pores, before being used, do not present the highest flux. It can be due to the other factors that have also influenced in the filtration process, as for example, the roughness or the hydrophobicity of the surface.

Comparing these results with those found in the literature, significant discrepancies are found. The NF membrane has only slightly larger pore sizes (between 3% and 13% depending on the conditions of measurement) than those found in the literature for neutral solute retention [4]. However, the NF90 presents pore sizes clearly larger than that found by Nghiem *et al.* [15] from

solute retention and Hilal *et al.* [32] from AFM, which showed a mean value of 0.68 nm and 0.55 nm, respectively. A huge discrepancy was found for the NP010 membrane with a pore size of 0.33 nm from AFM [32].

One of the sources of these discrepancies can be that the samples were coming from different batches, what should be caused by a poor reproducibility of the membrane. In any case, it is known the existence of differences in the results obtained by different techniques [6]. As mentioned, the AFM technique is strongly influenced by the convolution between the tip curvature and the pore borders. Other problems, such as white thermal noise, causing spurious unwanted oscillation of the cantilever, should have been overcome because Fast Fourier Transform filtering (FFT) [5, 32] has been used.

This could justify the huge discrepancy between the value of pore diameter of the membrane NP010 found by us (1.5 nm) and by other authors (0.33 nm). However, the value of 0.33 nm for the pore size given in the literature for this membrane; NP010, which has a retention between 25-55% of Na_2SO_4 (see Table 1) does not seem very realistic. An ion of sulfate has a Stokes radius of 0.23 nm, which one would expect to be almost totally retained (retentions over 90%) with a membrane with pore sizes of 0.33 nm.

3.2.2 Surface analysis

AFM has been used in order to study the morphology of the membranes and to evaluate the changes after the filtration of the synthetic solution of KCA described in the experimental section. In Figure 7, images of the membranes obtained before and after filtration can be compared. In all cases, phase contrast images have been taken (but not shown here) to confirm that the membranes are totally covered by the foulant.

The NF90 membrane presents a similar structure before and after its use (Figures 7.a and b). In both cases the surface is similarly highly rough. The lack of changes in this high roughness after filtration seems to indicate the appearance of a very thin layer of adsorption. In the case of NF membrane, (Figures 7.c and d), the surface is smoother than in the previous membrane, although it shows similar granular structures before and after the filtration of KCA. In this case, nothing can be concluded on the adsorption as far as it could be high but uniform, so it should lead to very slight changes in the morphology of the surface.

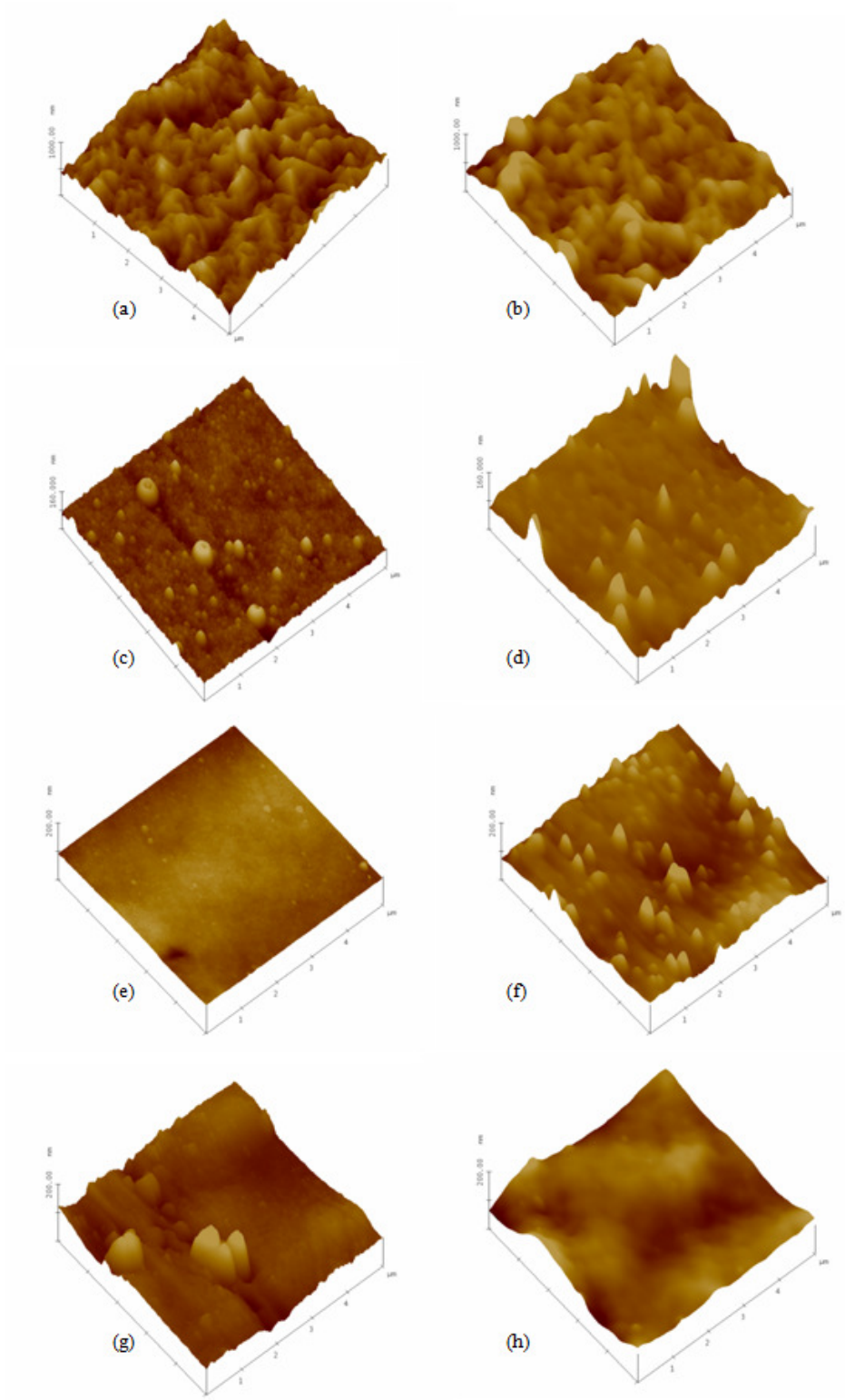

Figure 7 – 3D-AFM images corresponding to scanned areas of (5 × 5) μm^2 for: (a) NF90 clean and (b) used, (c) NF clean and (d) used, (e) NP030 clean and (f) used, and (g) NP010 clean and (h) used.

The NP030 membrane changed its structure from extremely smooth before the filtration to highly rough after its use, what indicates a high adsorption. This can be visualized in the Figures 7.e and f. Finally, the NP010 membrane presents a quite different structure after its use with a disappearance of the original topometry and the formation of a smooth morphology, as shown in the Figures 7.g and h.

From these results, it seems that the NF90 and possibly the NF membranes are less fouled by KCA. Probably the potassium clavulanate should interact less with the amide groups than with the sulfonic groups.

From the AFM images, the surface roughness was also analyzed. Figures 8 (a and b) show the variation of S_q with the length scale *L* for the membranes before and after KCA use, respectively. For non used membranes, S_q increases with *L* until reaching a pseudo-plateau as frequently happens in most surfaces [54, 57]. As was clearly seen in Figure 7, the NF90 membrane has an outstanding high roughness.

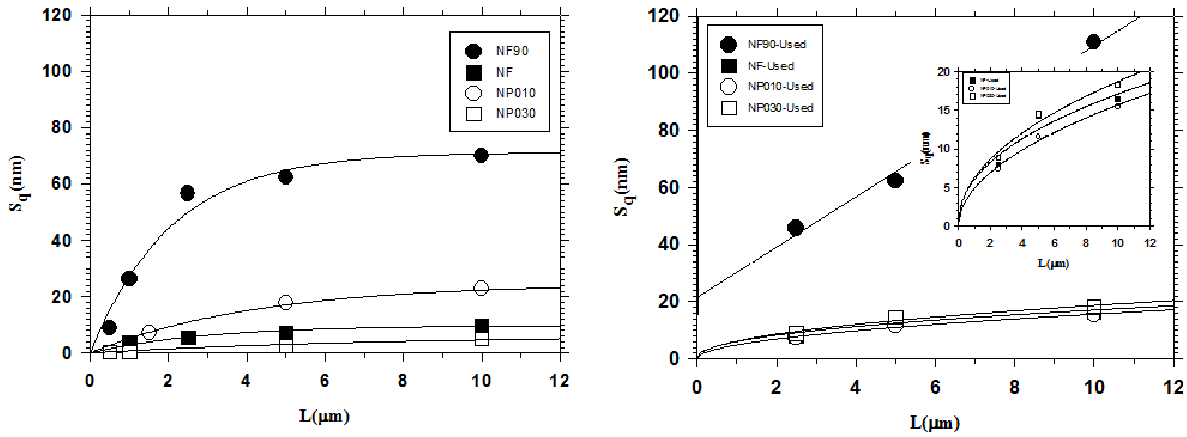

(a) (b)

Figure 8 – Roughness, S_q, as a function of the length scale, L, (side of the square scanned area) for all the membranes studied before (a) and after (b) fouling with KCA. The insert shows a detail of the three membranes with low and very similar roughness (NF90, NP030 and NP010).

After being used to filter KCA, the tendency is similar for the NF, NP030 and NP010, but this behaviour does not occur in the case of the NF90 membrane which in principle should have this plateau for higher values of *L*. This may be due to its high initial roughness. The three membranes with low roughness have different changes in their original roughness. While NP030 and the NF

increase their roughness, the NP010 one decreases as a result of the KCA adsorption. However, the three membranes tend to a similar roughness value which should correspond to a compact surface of potassium clavulanate. In these conditions, their roughness is between 15 and 20 nm after KCA use (amplified insert in Figure 8b).

The results reported on the roughness of fouled membranes are complicated to compare to each other due to the complex nature of foulants and particular interactions with each membrane type and composition that leads to a diversity of interpretations of the changes detected [57].

It seems clear that the NF90 membrane has a small adsorption of KCA, which can be confirmed by the small change in its high roughness and by the slight reduction of its permeability. According to Yangali-Quintanilla *et al.* [58] the NF90 membrane presents a quite different behaviour because they observed a reduction in the surface roughness which should be attributed to a higher adsorption of the fouling agent, sodium alginate, used by these authors. The value found for the NF90 roughness is very similar to that found by Xu *et al.* [59]. In their work they give for the NF90 surface roughness the value of 63.9 nm. On the other hand the value found by Nghiem *et al.* [15], 76.8 nm, is quite different. For the NP010 membrane the roughness found is very different from that found by Boussu *et al.* [36], which was of 2.4 nm for a 3 x 3 mm scanned area. On the other hand, the NP030 membrane presents a similar roughness to that also found in Boussu *et al.* [36], which was of 3.4 nm, also for the same scanned area. Nevertheless these values refer to membranes treated at pH 6.

It seems clear that rough surfaces present more adsorption surface area, than smooth surfaces [11, 13, 25, 34] made from the same material, especially when fouling is high as for the polyethersulfone membranes (NP030 and NP010). Therefore, in this case, particles are accumulated preferentially in the “valleys” than in the peaks, resulting in “valley clogging” that for membranes showing low affinity for the KAC (NF90 and NF) is avoided due to the sweeping effect of the retentate agitation. In Figure 9 we suggest a scheme that could explain how the roughness is modified after KCA filtration by taking into account the corresponding changes in permeability too. The gray lines represent the profile of a cross section of the membrane surface and the black balls the molecules or molecular aggregates of KCA. The polyamide membranes, NF90 and NF, have a lower reduction in permeability after contacting KCA and the roughness of the used membranes increases slightly as compared with those of the clean membrane. This behaviour is consistent with the scheme of Figure 9, where only a small amount of molecules are adsorbed on the surface. In contrast, the polyethersulfone membranes, NP030 and NP010, have a high reduction of

permeability while their roughness tends to a similar value. This suggests that there is a high affinity between the polyethersufone surface and the KCA molecules or aggregates and the high flows produce a multilayer of KCA which gives a roughness value mainly due to clavulanate, which mask the initial topography of the membrane surface.

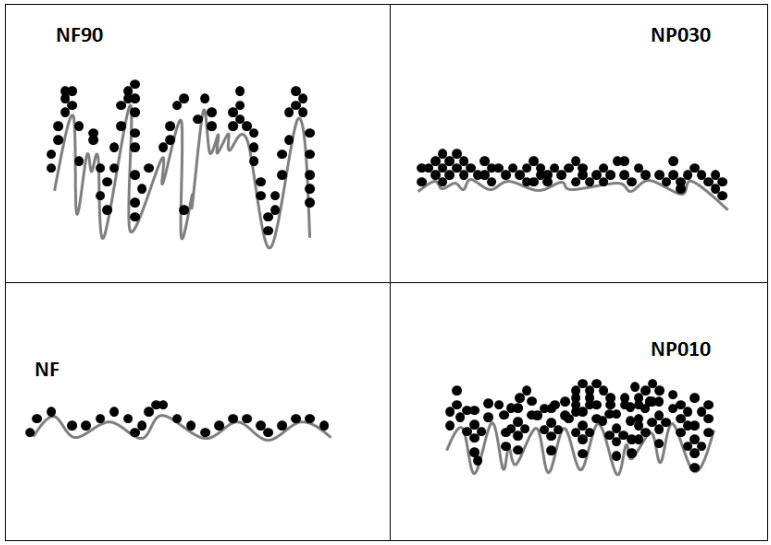

Figure 9 – Scheme of the cross section for the deposition of KCA (black balls) according to the fouling mechanism assumed on the surface (gray line) of each membrane studied.

The analysis of the roughness of these membranes shows that the NF90 membrane has a far greater roughness than the others, up to almost an order of magnitude. A high roughness in a nanofiltration membrane may be intentional to reduce the fouling process by creating micro or nanoturbulences on the membrane surface, thus increasing the coefficient of mass transfer [60]. For this reason when trying to correlate surface parameters of these membranes with flow and structural parameters, the NF90 membrane is out of the trend. As mentioned in the introduction, Hirose *et al.* [61] have found a linear relationship with positive slope between the roughness and the permeability for several reverse osmosis membranes made from the same crosslinked aromatic polyamide. These authors attributed the linear relationship they found to surface unevenness of the membranes, which should result in an enlargement of the effective membrane area. In our case NF, NP030 and NP010 membranes follow this tendency before their use with KCA as shown in Figure 10, for images of 2.5 x 2.5 μm in size. The NF90 membrane is placed far away from the trend with

the highest value of roughness and the lowest permeability. As expected the membranes used with KCA lost totally this correlation.

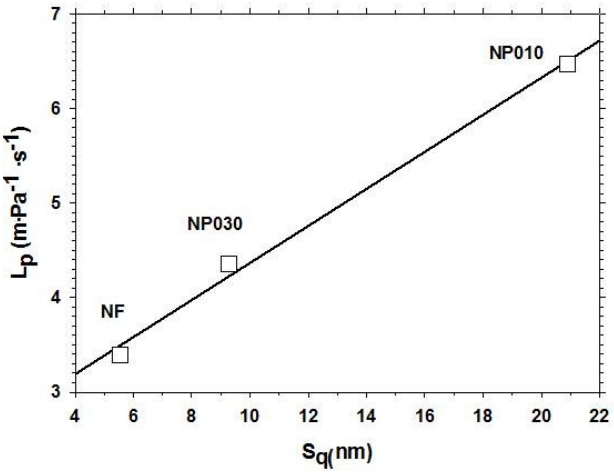

Figure 10 – Experimental water permeability versus roughness, S_q, as obtained from images with scanned areas of (2.5 x 2.5) μm^2 of the clean membranes.

All correlations of roughness with other functional parameters suffer the lack of definition of roughness that, as clearly shown in Figure 8, changes with the scanned area. One way to avoid this problem is to use the PSD of the surface according to Eq. 6 as discussed in section 2.4. Figure 11 shows an example of the spectrum for the clean NF membrane for three different scan sizes. One can see that in the central part of the spectrum, the slope is very similar for all scan sizes. This makes this technique clearly more powerful than the simple analysis of the roughness at given scanned areas. As mentioned, the slope of the spectrum allows evaluating the fractal dimension according to Eq. 10. When the slope decreases the fractal dimension increases, which corresponds to a surface that fills more the space, thus looking denser [24]. Table 4 shows the fractal dimension of the membranes studied before and after filtration of the KCA.

Table 4 – Fractal dimension for the clean and fouled membranes

Fractal dimension	NF90	NF	NP030	NP010
Clean	2.10 ± 0.02	2.14 ± 0.03	2.40 ± 0.04	2.50 ± 0.04
Fouled	2.45 ± 0.08	2.26 ± 0.05	2.72 ± 0.07	2.63 ± 0.05

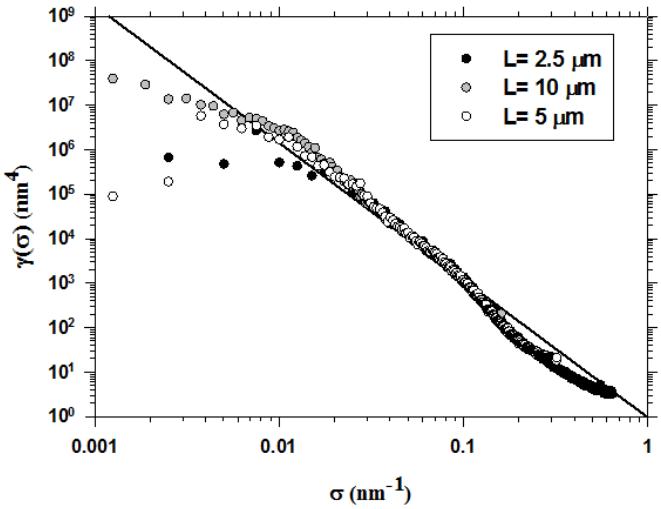

Figure 11 – 2D Power Spectra Density of NF clean membrane with several scan sizes. The fitted line (which slope determines the fractal dimension) corresponds to the best fitting to the three length scales (side of the square scanned area) shown.

It is noted that in this case there is always an increase in fractal dimension of the membrane (denser surface) due to the fouling process. This increase appears also for the NP010 membrane that shows a decrease in its surface roughness after being used (see Figure 8b). This difference in trend may be due to the highest error implicit in the method of analysis of the simple roughness. On the other hand, the fractal dimension is also connected with the lateral distribution of height deviations so is a more robust way to characterize the rough or flat nature of the surface. As a result, it can be concluded that the vertical profile of the surface of the NP010 membrane is flattened after interaction with KCA but the new surfaces fills more the space horizontally.

If the variation in fractal dimension, D, is related to the adsorption of KCA, which is correlated with variations in permeability, these two magnitudes should be correlated as well. Figure 12 shows the percentage of the initial (new membrane) permeability that remains after KCA filtration versus the difference in fractal dimension between the fouled membrane, D_f and the clean (unused one), D_i. It is noted that the membranes that have similar values of roughness before KCA use (NF, NP030 and NP010) can be fitted to an exponential decay. The NF90 membrane is clearly out of this relationship because, as mentioned above, it has a roughness three times greater than the other membranes.

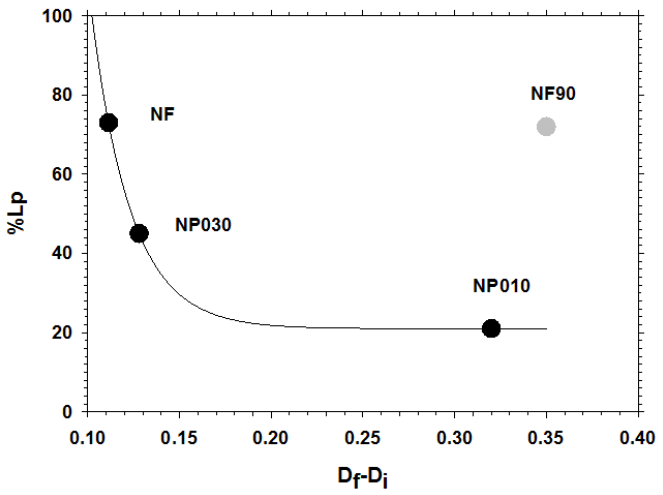

Figure 12 – Percent reduction of the permeability due to the KCA adsorption versus the difference of the fractal dimension of the clean membrane, D_i and the used one D_f.

Finally we have calculated the skewness of the height distribution on the surface of the membranes using Eq. 11. The values are positive in all cases, which indicate that these surfaces have high spikes that protrude over a flatter average [54]. Comparing the results of the membranes before and after filtration with KCA is observed that for the polyamide membranes, (NF and NF90) the value of the skewness increases, whereas those of polyethersulfone this trend is not so clear. Possibly, in this case, the highly coating layer of KCA molecules (on an initial relatively flat surface) does not follow a trend. The kurtosis has been computed using Eq. 12. For all membranes, except for NP010, it is observed an increase in kurtosis, indicating that the protuberances on the surface have more similar sizes after adsorption of the KCA. In contrast, for the NP010 it is observed a decreasing kurtosis, indicating a wider distribution of the heights of the surface. This must be the result of high accumulation of aggregates of KCA, such as all data have indicated.

4. Conclusions

The AFM technique allows a determination of the pore size distribution of membranes with pore sizes in the order of the nanometer when the surface roughness of the samples is low.

The results have been correlated with the permeability of the clean membrane and indicate that at least a proportion of the pores have slit type geometry.

The analysis of height difference in the surface images before and after the filtering process of potassium clavulanate has been studied by using: Root Mean Square roughness, S_q , Power Spectra Density, PSD, Fractal dimension, *D*, Skewness, S_{sk}, and Kurtosis, S_{ku}.

These parameters have been related to the permeability, the type of material, the amount of adsorbed solute on the surface and the pore size.

It is noted that for membranes with similar (here low) values of the initial roughness:

- The initial experimental permeability is linearly related to that evaluated from the pore size distributions.
- If the adsorption layers of potassium clavulanate are enough, the roughness tends to a similar value for all membranes.
- The fractal dimension increases in every case after the adsorption process, which is in agreement with the densification of the surface.
- The permeability reduction is higher the greater is the difference between the fractal dimension before and after the adsorption.

Acknowledgements

Brazilians authors acknowledge the financial support from the Coordenação de Aperfeiçoamento de Pessoal de Nível Superior (CAPES) and the State of São Paulo Research Foundation (FAPESP).
Spanish authors want to thank the "Ministerio de Ciencia e Innovación (MCINN)" for financing this work within the frame of the "Plan Nacional de I+D+I" and through the project CTQ2009-07666. Also the Spanish "Junta de Castilla y León" has contributed through the project Grupos de Excelencia-GR18.
The authors also acknowledge Filmtec™ and Microdyn Nadir® for the donation of the membranes.

References

[1] Hilal N, Al-Zoubi H, Darwish NA, Mohammad AW, Abu Arabi M (2004) A comprehensive review of nanofiltration membranes: Treatment, pretreatment, modelling, and atomic force microscopy. Desalination 170:281-308

[2] Bowen WR, Mohammad AW, Hilal N (1997) Characterisation of nanofiltration membranes for predictive purposes - Use of salts, uncharged solutes and atomic force microscopy. J. Membr. Sci. 126:91-105

[3] Mohammad AW, Hilal N, Seman MNA (2005) Interfacially polymerized nanofiltration membranes: atomic force microscopy and salt rejection studies. J. App. Polym. Sci. 96:605-612

[4] Bargeman G, Vollenbroek JM, Straatsma J, Schroën CGPH, Boom RM (2005) Nanofiltration of multi-component feeds. Interaction between neutral and charged components and their effect on retention. J. Membr. Sci. 247:11-20

[5] Bowen WR & Doneva TA (2000) Atomic Force Microscopy Studies of Membranes: Effect of Surface Roughness on Double-Layer Interactions and Particle Adhesion. J. Colloid Inter. Sci. 229:544-549

[6] Otero JA, Mazarrasa O, Villasante J, Silva V, Prádanos P, Calvo JI, Hernández A (2008) Three independent ways to obtain information on pore size distributions of nanofiltration membranes. J. Membr. Sci. 309:17–27

[7] Singh S, Khulbe KC, Matsuura T, Ramamurthy P (1998) Membrane characterization by solute transport and atomic force microscopy. J. Membr. Sci. 142:111-127

[8] Prádanos P, Rodriguez ML, Calvo JI, Hernández A, Tejerina F, de Saja JA (1996) Structural characterization of an UF membrane by gas adsorption-desorption and AFM measurements. J. Membr. Sci. 117:291-302

[9] Ochoa NA, Prádanos P, Palacio L, Pagliero C, Marchese J, Hernández A (2001) Pore size distributions based on AFM imaging and retention of multidisperse polymer solutes: Characterisation of polyethersulfone UF membranes with dopes containing different PVP. J. Membr. Sci. 187:227-237

[10] Koyuncu I, Brant J, Lüttge A, Wiesner MR (2006) A comparison of vertical scanning interferometry (VSI) and atomic force microscopy (AFM) for characterizing membrane surface topography. J. Membr. Sci. 278:410-417

[11] Wong PCY, Kwon Y-N, Criddle CS (2009) Use of atomic force microscopy and fractal geometry to characterize the roughness of nano-, micro-, and ultrafiltration membranes. J. Memb. Sci. 340:117-132

[12] Schäfer AI, Fane AG, Waite TD (2000) Fouling effects on rejection in the membrane filtration of natural waters. Desalination 131:215-224

[13] Vrijenhoek EM, Hong S, Elimelech M (2001) Influence of membrane surface properties on initial rate of colloidal fouling of reverse osmosis and nanofiltration membranes. J. Membr. Sci. 188:115-128

[14] Koros WJ, Ma YH, Shimidzu T (1996) Terminology for membranes and membranes processes. Reprinted from Pure and Applied Chemistry 68:1479-1489. J. Membr. Sci. 120:149-159

[15] Nghiem LD, Vogel D, Khan S (2008) Characterizing humic acid fouling of nanofiltration membranes using bisphenol A as a molecular indicator. Water Research 42:4049-4058

[16] D. Bhattacharyya, J. Hestekin, D. Shan, S. Ritchie, An overview of selected membrane techniques for environmental applications, J. Chin. Inst. Chem. Eng. 33 (2002) 61-66.

[17] Van der Bruggen B, Vandecasteele C, Van Gestel T, Doyen W, Leysen R (2003) A review of pressure-driven membrane processes in wastewater treatment and drinking water production. Environ. Progress 22: 46-56

[18] Koyuncu I, Turan M, Topacik D, Ates A (2000) Application of low pressure nanofiltration membranes for the recovery and reuse of dairy industry effluents. Water Sci. Technol. 41:213-221

[19] Van der Bruggen B, Kim JH, DiGiano FA, Geens J, Vandecasteele C (2004) Influence of MF pretreatment on NF performance for aqueous solutions containing particles and an organic foulant. Sep. Purif. Technol. 36:203-213

[20] Vrouwenvelder JS, Kappelhof JWNM, Heijman SGJ, Schippers JC, Van der Kooij D (2003) Tools for fouling diagnosis of NF and RO membranes and assessment of the fouling potential of feed water. Desalination 157:361-365

[21] Tarabara VV, Koyuncu I, Wiesner MR (2004) Effect of hydrodynamics and solution ionic strength on permeate flux in cross-flow filtration: direct experimental observation of filter cake cross-sections. J. Membr. Sci. 241:65-78

[22] Van der Bruggen B & Vandecasteele C (2001) Flux decline during nanofiltration of organic components in aqueous solution. Environ. Sci. Technol. 35:3535-3540

[23] Van der Bruggen B, Braeken L, Vandecasteele C (2002) Evaluation of parameters describing flux decline in nanofiltration of aqueous solutions containing organic compound. Desalination 147:281-288

[24] Wyart Y, Georges G, Deumié C, Amra C, Moulin P (2008) Membrane characterization by microscopic methods: multiscale structure. J. Memb. Sci. 315:82-92

[25] Elimelech M, Zhu X, Childress AE, Hong S (1997) Role of membrane surface morphology in colloidal fouling of cellulose acetate and composite aromatic polyamide reverse osmosis membranes. J. Membr, Sci. 127:101-109

[26] Sheldon JM (1991) The fine-structure of ultrafiltration membranes. I. Clean membranes. J. Membr. Sci. 62:75-86

[27] Bessières A, Meireles M, Coratger R, Beauvillain J, Sanchez V (1996) Investigations of surface properties of polymeric membranes by near field microscopy. J. Membr. Sci. 109:271-284

[28] Wei Q & Wang D (2003) Pore surface fractal dimension of sol-gel-derived Al_2O_3-SiO_2 membranes. Materials Letters 57:2015-2020

[29] Bowen WR, Hilal N, Lovitt RW, Willians PM (1996a) Visualisation of an ultrafiltration membrane by non-contact atomic force microscopy at single pore resolution. J. Membr. Sci. 110:229-232

[30] Bowen WR, Hilal N, Lovitt RW, Willians PM (1996b) Atomic force microscope studies of membranes: Surface pore structures of Cyclopore and Anopore membranes. J. Membr. Sci. 110:233-238

[31] Hilal N & Bowen WR (2002) Atomic force microscope study of the rejection of colloids by membrane pores. Desalination 150:289-295

[32] Hilal N, Al-Zoubi H, Darwish NA, Mohammad AW (2005) Characterisation of nanofiltratrion membranes using atomic force microscopy. Desalination 177:187-199

[33] Boussu K, Van der Bruggen B, Volodin A, Snauwaert J, Van Haesendock C, Vancasteele C (2005) Roughness and hydrophobicity studies of nanofiltration membranes using different modes of AFM. J. Colloid Int. Sci. 286:632-638

[34] Boussu K, Van der Bruggen B, Volodin A, Van Haesendonck C, Delcour JA, Van der Meeren P, Vandecasteele C (2006) Characterization of commercial nanofiltration membranes and comparison with self-made polyethersulfone membranes. Desalination 191:245-253

[35] Lu Y, Suzuki T, Zhang W, Moore JS, Mariñas BJ (2007) Nanofiltration Membranes based on Rigid Star Amphiphile. Chem. Mater. 12:3194-3204

[36] Boussu K, Vandecasteele C, Van der Bruggen B (2008) Relation between membrane characteristics and performance in nanofiltration. J. Membr. Sci. 310:51–65

[37] El-Said WH, Yea C-H, Jung M, Kim H, Choi J-W (2010) Analysis of effect of nanoporous alumina substrate coated with polypyrrole nanowire on cell morphology based on AFM topography, Ultramicroscopy, 110: 676-681

[38] Jaafar M, Navas D., Hernández-Vélez M, Balñdonedo JL, Vázquez M, Asenjo A (2009) Nanoporous alumina membrane prepared by nanoindentation and anodic oxidation. Surface Science 603: 3155-3159

[39] Popa AM, Angeloni S, Bürgi T, Hubbell JA, Heinzelmann H, Pugin R (2010) Dynamic Perspective on the function of thermoresponsive nanopores from in situ AFM and ATR-IR investigations, Langmuir 26:15356-15365

[40] De-Lima LC, De-Macedo MMG, De-Alburquerque M, De-Alburquerque M, Simvo RA (2009) Morphological characterization of the surface of nanoporous aluminium oxide by AFM and laws of scale, Nano 4:157-164

[41] Howarth TT, Brown AG, King TJ (1976) Clavulanic acid, a novel β-lactam isolated from Streptomyces clavuligerus: X-ray crystal structure analysis. J. Chem. Soc., Chem. Commun. 266b-267

[42] Vandamme EJ (1984) Clavulanic Acid: Properties, Biosynthesis and Fermentation (Biorechnology of Industrial Antibiotics 22). Marcel Dekker, New York

[43] Bersanetti PA, Almeida RMRG, Barboza M, Araújo MLGC, Hokka CO (2005) Kinetic studies on clavulanic acid degradation. Bioch. Eng. J. 23:31-36

[44] Almeida RMRG, Barboza M, Hokka CO (2003) Continuous clavulanic acid adsorption process. Applied Bioch. and Biotechnol. 108:867-879

[45] Bowen WR & Welfoot JS (2002) Predictive modelling of nanofiltration: membrane specification and process optimization. Desalination 147:197-203

[46] Calvimontes A, Stamm M, Dutschk V (2009) Effect of cellulose enzyme on cellulose nano- topography, Tenside Surfactants Detergents 46:368-372

[47] Nghiem LD, Shafer AI, Elimelech M (2005) Nanofiltration of hormone mimicking trace organic contaminants, Sep. Sci. Technol. 40:2633–2649

[48] López-Muñoz MJ, Sotto A, Arsuaga JM, Van der Bruggen B (2009) Influence of membrane, solute and solution properties on the retention of phenolic compounds in aqueous solution by nanofiltration membranes. Sep. Purif. Technol. 66:194–201

[49] Giessibl FJ (2003) Advances in Atomic Force Microscopy. Rev. Mod. Phys. 75: 949-983

[50] Walsh CJ, Leistner AJ, Oreb BF (1999) Power spectral density analysis of optical substrates for gravitational-wave interferometry. Appl. Opt. 38:4790-4801

[51] Church EL (1988) Fractal surface finish. Appl. Opt. 27:1518-1526

[52] Deumié C, Richier R, Dumas P, Amra C (1996) Multiscale roughness in optical multilayer: atomic force microscopy and light scattering. Appl. Optics 35:5583-5594

[53] Ruppe C, Duparré A (1996) Roughness analysis of optical films and substrates by atomic force microscopy. Thin Solid Films 288:8-13

[54] Mendez-Vilas A, Bruque JM, González-Martín ML (2007) Sensitivity of surface roughness parameters to changes in the density of scanning points in multi-scale AFM studies. Application to a biomaterial surface. Ultramicroscopy 1007:617-625

[55] Wesolowska K, Koter S, Bodzek M (2004) Modelling of nanofiltration in softening water. Desalination 162:137-151

[56] Montalvillo M, Silva V, Palacio L, Calvo JI, Hernández A and Prádanos P (2010) Electric and dielectric properties of nanofiltration membranes investigated by impedance spectroscopy. J Phys. Chem., Submitted

[57] Macanás J, Palacio L, Prádanos P, Hernández A, Muñoz M (2006) Microscopy as a suitable technique for surface characterization of Activated Composite Membranes for metal ion facilitated transport. Appl. Phys. A-Mater. Sci. & Process. 84:277-284

[58] Yagali-Quintanilla V, Sadmani A, McConville M, Kennedy M, Amy G (2009) Rejection of pharmaceuticlally active compounds and endocrine disrupting by clean and fouled nanafiltration membranes. Water Research 43:2349-2362

[59] Xu P, Drewes JE, Kim T-U, Bellona C, Amy G (2006) Effect of membrane fouling on transport of organic contaminants in NF/RO membrane applications. J. Membr. Sci. 279:165-175

[60] Izák P, Godinho MH, Brogueira P, Figueirinhas JL, Crespo JG (2008) 3D topography design of membranes for enhanced mass transport. J. Membr. Sci. 321:337-343

[61] Hirose M, Ito H, Kamiyama Y (1996) Effect of skin layer surface structures on the flux behavior of RO membranes. J. Membr. Sci, 121:209-215

NANOFILTRATION MEMBRANE SELECTION AND PROCESS MODELLING IN CLAVULANIC ACID SEPARATION

A. L. Carvalho[1*]; F. Maugeri[1]; V. Silva[2]; P. Prádanos[2]; A. Hernández[2]

[1]Departament of Food Engineering, Faculty of Food Engineering, Rua Monteiro Lobato 80, Barão Geraldo, University of Campinas – UNICAMP, CEP: 13083-862, Campinas, SP, Brazil

[2]Depto. de Termodinámica y Física Aplicada, Fac. de Ciencias, Universidad de Valladolid, Real de Burgos s/n, 47071 Valladolid, Spain

[*]e-mail: limoeiro@fea.unicamp.br, telephone: +551935214052, fax: +551935214027

Abstract

In this work, four commercial membranes were evaluated, NF and NF90 (Filmtec^{TM}), and NP010 and NP030 (Microdyn Nadir). The membranes were electrical and functional characterized by means of Tangential Streaming Potential (TSP) and rejection using different concentrations of KCl and pH values. Also, the concentration polarization effect was evaluated through the calculation of the mass transfer coefficient. The isoelectric point of the membranes was found to be between pH 5.0 and pH 6.0 and charges for the NF90 and NF membranes were negatives, whereas for the NP030, neutral and NP010 slightly negative. It was also detected that the NF90 membrane presented the highest KCl rejection among the evaluated membranes, followed by NF, NP030 and NP010 in sequence and they were considerably high retentive for clavulanic acid. The SEDE-VCh model satisfactorily modeled all the membranes for KCl rejection using dielectric constant inside the pores, ε_p, as fitting parameter. Finally, in order to determine the most suitable membrane for CA purification, the KCl/CA selectivity was evaluated and the NF membrane shows the best results.

Keywords: nanofiltration, characterization, zeta potential, membrane, SEDE model

1. Introduction

Clavulanic acid (CA) is a β-lactamase inhibitor, used in combination with β-lactamase sensitive penicillins, to protect the β-lactam ring of the antibiotic against hydrolysis [1,2]. CA is produced industrially by fermentation using *Streptomyces clavuligerus*, and presents low yields in the production process, particularly in the separation and purification step, due to its thermal instability and sensitivity to changes in pH [1,3]. Associated with its low concentration in the fermented broth, studies on its extraction and purification have to consider the kinetic degradation of CA, in order to minimize losses and maximize recovery yields and productivity.

Recent studies on the purification of CA were focused on the evaluation of procedures for its isolation and purification when produced by fermentation with *Streptomyces clavuligerus*. Some separation studies have used Amberlite XAD resin, Amberlite IRA 400 ion exchange resin pre-treated with NaCl, ultrafiltration (UF) followed by nanofiltration, and nanofiltration processes with different membranes and conditions [2,4-7]. Currently, several high-value bio-products are produced by fermentation, bringing new challenges for the recovery and purification processes. UF processes are an efficient way of separating the biomass from the CA fermentation broth, producing a protein free permeate containing CA, which can be subsequently concentrated using nanofiltration membranes [2,6].

Nanofiltration is a process that has as driving force the pressure difference through the membrane. This process offers as main advantages, the operation at low pressures when compared to reverse osmosis, high flow, considerable retention of multivalent anionic salts and organic molecules of molecular weight greater than 300 Da, relatively low investment and low cost of operation and maintenance [8]. According to Hilal *et al.* [8], membranes that present smallest rejections of dissolved compounds and high water permeability have been of great improvement in the nanofiltration process, comparing reverse osmosis.

According to Yacubowicz & Yacubowicz [9], a crossflow nanofiltration process is characterized by a membrane pore size corresponding to Molecular Weight Cut-Off (MWCO) around 200-1000Da, working at pressures of 150-500 psi (10-34 bar). Thus, retention of organic compounds is therefore determined by different membrane properties, such as MWCO, hydrophobicity and compounds properties such as molecular weight and ionization constant [10]. In addition to these separation phenomena, in salt separation the membrane charge also causes an additional exclusion due to electric and dielectric effects.

Summarizing, the nanofiltration performance can be identified as a sum of the convective, diffusive, steric and electrostatic effects through the membrane. In particular, in the interfaces the Donnan equilibrium, dielectric exclusion and steric effects take place. In electrokinetic characterization of solid-liquid interfaces, the tangential streaming potential has been shown to be a reliable tool to obtain zeta potential and membrane charge [11].

The zeta potential of porous materials is usually evaluated from electrokinetic experiments, as streaming potential because is a very simple technique and is very sensitive to changes in concentration increasing for low concentrations [12]. Between the two methods for measuring streaming potential that can be used, along and across the membrane, the first one is more appropriate for the nanofiltration membranes, once streaming potential measurements along the membrane bypass the hard interpretation of the electrokinetic data due to the small pore size and anisotropy of these membranes [13].

In contact with solutions, the pH has a significant effect in membrane charge and in characteristics of the molecules in solution, because it protonates and deprotonates the functional groups of membranes and molecules in solution, modifying the membrane charge and pore size and affecting hence the performance of nanofiltration and UF membranes [14-18].

Between the existent models used in nanofiltration process, the SEDE-VCh (steric, electric and dielectric exclusion) model can be noteworthy. This model presents a good description of transport properties in charged membranes proposed initially by Bowen & Welfoot [19] and recently modified in order to include a more realistic situation that includes the variation of the charge inside the membrane [20]. The model also includes the dielectric effects in the interfaces proposed by Szymczyk *et al.* [11,21]. Therefore, to determine the parameters involved in the process the solute transport inside and at membrane surface has to be studied, once the charge distribution has different values in those different regions, usually modeled by thermodynamic equilibrium.

The goal of this work is the selection of an appropriate membrane for separation of CA from a mixed salt solution based on the functionality of several membranes selected. To achieve this purpose, electrical and structural membrane characterization was carried on.

2. Methodology

2.1. Material

Four commercial membranes have been selected and studied here. Two of them are made from polyamides: NF (polypiperazine amide) and NF90 (fully aromatic polyamide [22,23]) membranes, from Filmtec™. Another two membranes, NP010 and NP030, are made from polyethersulfone and manufactured by Microdyn Nadir®. Table 1 shows the main characteristics of these membranes according to their manufacturers.

Table 1 – Characteristics of the membranes used.

Membrane	NF90	NF	NP030	NP010
MWCO (Da)	180[a]	>200	400	1000
Max. pressure (bar)	41	41	40	40
Max. temperature (ºC)	45	45	95	95
pH range	2-11	3-10	0-14	0-14
Pore size (nm)[b]	0.99	1.39	1.48	1.49
Lp (10^{-11}m/Pa.s)[b]	1.53	3.39	4.36	6.47
Rejection (%)	>97[c]	>99[d]	80-95[e]	25-55[e]

[a] Lopez Muñoz *et al.* [24]

[b] Carvalho *et al.* [25]

[c] Rejection of $MgSO_4$ (25ºC, 4.8 bar)

[d] Rejection of $MgSO_4$ (25ºC, 8.9 bar)

[e] Rejection of Na_2SO_4 (20ºC, 40 bar)

The determination of zeta potential and surface charge density was carried out through the measurement of electric potential produced when an electrolyte solution passes between two membranes facing their active layers at a given pressure gradient (Figure 1). The solution conductivities were measured in a GLP 32 condutimeter, from Crison.

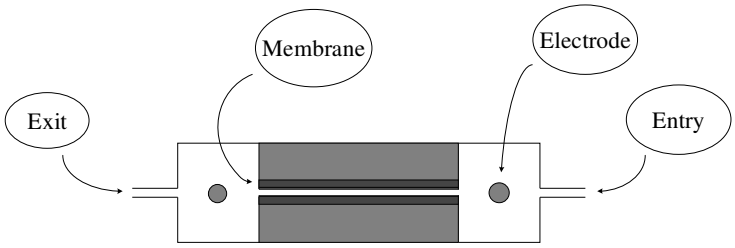

Figure 1 – Schematic representation of the streaming potential measurements cell.

To study the nanofiltration process a stainless steel stirred dead-end cell was used. The system consists of a cylindrical container jacketed, with a membrane located at the base, whose area was 1.52 x 10^{-3} m^2, and a magnetic stirrer that promotes the convection movement in the process. The pressure difference was applied by a change in the internal atmosphere with application of nitrogen gas, as shown in Figure 2.

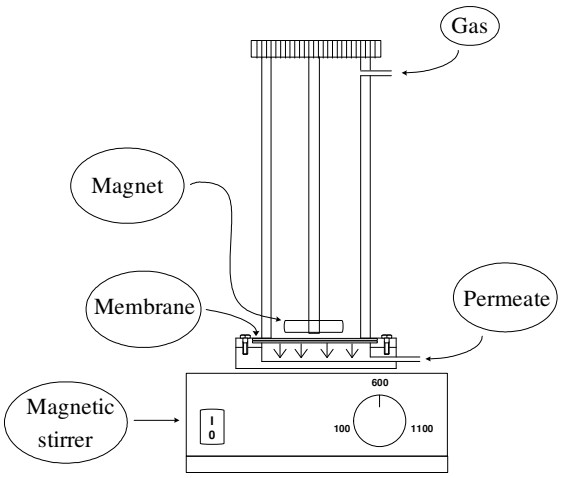

Figure 2 – Schematic representation of the bench-scale stirred dead-end cell.

The pH of the CA solutions was adjusted using 0.2 M hydrochloric acid and 1 M potassium hydroxide, prepared using analytical grade reagents. The solutions of KCl were prepared from KCl 36.5-38 % of purity. The concentrations of KCl in feed phase and in permeate were measured by a standard curve that correlates the solution conductivity with the salt concentration in solution.

The CA solutions were prepared from the medicine Clavulin® (revested pills with 125 mg of potassium clavulanate and 500 mg of amoxicilin, besides some salts, such as KCl [26]), from GlaxoSmithKline Brasil Ltda, which were vacuum filtered and microfiltered through 14 μm and

0.45 μm pore membranes, respectively. The concentration of CA was determined according to Bird *et al.* [27], using a Beckman Coulter™ model DU®640 spectrophotometer. The antibiotic was reacted with imidazole (60 g/L, pH 6.8) and the absorbance of the reaction product measured at 312 nm. The product of this reaction is more stable than CA and its formation is directly proportional to the CA concentration present in the reaction mixture. Potassium clavulanate, also from the medicine Clavulin®, was used as the standard.

2.2. Experimental procedure

For the electrical characterization, the TSP technique was evaluated and also the isoelectric point was determined. The measurements were carried out with KCl solutions at different concentrations, ranging from 10^{-5} to 2.10^{-3} M. Moreover experiments with KCl $1x10^{-4}$ M solutions were carried out, at pH values from 4.0 to 8.0.

The functional characterization was made by measurements of the rejection of KCl solution with the same concentrations and pH than in the electrical characterization. Different flow rates for each pH value were also performed, according to a change in the pressure applied to solution transport, from 1.10^{6} to 4.10^{6} Pa (or the maximum pressure suggested by the membrane manufacturer). The CA nanofiltrations were performed at concentrations between 250-750 mg/l, batch volume of 100 mL, agitation speed of 600 rpm, temperature of 25 ºC and at the same applied pressure than for KCl experiments.

3. Mathematical considerations

3.1. Electric Characterization

From the plot of electric potential versus applied pressure the membrane streaming potential for each pH value can be obtained from the slope. The zeta potential for each concentration and pH value was calculated through the Smoluchowsky equation as indicated below:

$$\zeta = \frac{\eta \lambda_0 \nu}{\varepsilon_0 \varepsilon_b} \tag{1}$$

where η is the streaming potential (V/Pa), λ_0 the solution average conductivity (S/m), ν the solution dynamic viscosity (Pa.s), ε_0 is the vacuum permittivity (F/m) and ε_b the dielectric constant of the bulk solution . With the zeta potential value (ζ) it was possible to calculate the surface charge density (σ_s) based on the Gouy-Chapman theory, as shown in Eq. 2:

$$\sigma_s = sign(\zeta)\sqrt{\left(2\varepsilon_0\varepsilon_b RT\sum_i c_i(0^-)\left[\exp\left(-\frac{z_i F}{RT}\zeta\right)-1\right]\right)} \quad (2)$$

R is the ideal constant of gases, T is the temperature (K), c_i is the concentration of ion i (mol/m^3), z_i the charge of ion i and F is the Faraday constant (C). With the surface charge densities, it was finally possible to calculate the membrane volume charge density (Eq. 3) considering a slit geometry:

$$X = \frac{\sigma_S}{Fr_p} \quad (3)$$

where r_p is the average pore radius of the membrane (m).

3.2. Structural and Functional Characterization

The pore size distribution of the membranes studied was obtained by Atomic Force Microscopy (AFM) in a previous work [25] and from these results the mean pore radius was determined from the maximum of the distribution been 0.494, 0.697, 0.741 and 0.743 nm for NF90, NF, NP030 and NP010, respectively.

In order to determine the concentration polarization effect for the nanofiltration experiments, the mass transfer coefficient was determined using the relation of Colton *et al.* [28], the method take in account the appearance of the osmotic limit of flux and depends on the system geometry and others characteristics such as stirrer diameter and length, and from the membrane surface as indicated by the Eq. (4) [29]:

$$k = 0.0443\left(\frac{D}{r}\right)\left(\frac{\nu}{D}\right)^{0.33}\left(\frac{\omega r^2}{\nu}\right)^{0.8} \quad (4)$$

where D is the KCl diffusivity at infinite dilution, r is the membrane effective radius and ω is the rotation frequency.

Moreover, to find out the concentration at the external surface the gel layer theory was used, which consider the volumetric flux per membrane area (J_V), the mass transfer coefficient (k), and the KCl concentration on feed phase (c_0) and on the permeate (c_p) (Eq. 5) [30-32].

$$c_m = c_p + \left(c_0 - c_p\right)e^{\frac{J_V}{k}} \tag{5}$$

where k is the mass transfer coefficient obtained by the Eq. 4.

3.3 Model Resolution

When the mean pore radius is obtained from an independent method [33] like in this work from AFM, the SEDE-VCh model is defined in terms of three independent parameters: the dielectric constant inside the pores (ε_p) and the two parameters of the Freundlich isotherm (a and b). The dielectric constant of the dry polymer of the membrane (ε_m) is usually taken from bibliography. The a and b parameters should be unique for a given solute and membrane system. The whole set of equations necessary to solve the system are summarized in Table 2 and a resolution algorithm can be found in Silva [20].

Table 2 – SEDE-VCh equations summarized

Transport equations	
$\frac{dc_i}{dx} = \frac{J_V}{D_{i,p}A_k}\left(K'_{i,c}c_i - c_{i,p}\right) - \frac{z_i F}{RT}\frac{d\psi}{dx}$	(I-1)
where $D_{i,p} = K_{i,d}D_{i,\infty}$,	
$\sum_i c_i z_i + X_0 + ac_2^b = 0$	(I-2)
$\frac{d\psi}{dx} = \frac{\sum_i\left(\frac{z_i J_V}{D_{i,p}A_k}\right)\left(K'_{i,c}c_i - c_{i,p}\right) + \left(\frac{J_V bac_2^{(b-1)}}{D_{2,p}A_k}\right)\left(K'_{2,c}c_2 - c_{2,p}\right)}{\frac{F}{RT}\left(\sum_i c_i z_i^2 + z_2 bac_2^b\right)}$	(I-3)
Eqs. 2 and 4 can be numerically solved with the following boundary conditions,	
$c_i(x = 0) = c_{i,0}$	

$c_i(x = \Delta x) = c_{i,\Delta x}$ (I-4)

$$R_i = 1 - \frac{c_{i,p}}{c_{i,m}} \quad \text{(I-5)}$$

Partitioning equations

$$\frac{c_{i,0}}{c_{i,m}} = \phi_i \frac{\gamma_{i,m}}{\gamma_{i,0}} \exp(-z_i \Delta\Psi) \exp(-\Delta W'_{i,B}) \exp(-\Delta W'_{i,im}) \quad \text{(I-6)}$$

Where the dielectric effects are, Born energy:

$$\Delta W'_{i,B} = \frac{(z_i e)^2}{8\pi k_B T \varepsilon_0 a_S} \left(\frac{1}{\varepsilon_p} - \frac{1}{\varepsilon_b} \right)$$ with a_S is defined by Rashin and Honig [80]. (I-7)

And the images force effect:

$$\Delta W'_{i,im} = -\alpha_i \ln\left[1 - \left(\frac{\varepsilon_p - \varepsilon_m}{\varepsilon_p + \varepsilon_m} \right) \exp(-2\mu) \right]$$ (Slit-like geometry) (I-8)

$$\alpha_i = \frac{(z_i F)^2}{8\pi \varepsilon_0 \varepsilon_p R T N_A r_p} \quad \text{(I-9)}$$

$$v = \sqrt{k^2 + \mu^2} \quad \text{(I-10)}$$

$$\mu = F r_p \sqrt{\frac{\sum_i z_i^2 c_{i,m} \phi_i (\gamma_{i,m} / \gamma_{i,0}) \exp(-z_i \Delta\Psi - \Delta W'_{i,B} - \Delta W'_{i,im})}{R T \varepsilon_0 \varepsilon_b}} \quad \text{(I-11)}$$

$$\beta = \frac{k}{\sqrt{k^2 + \mu^2}} \left(\frac{\varepsilon_m}{\varepsilon_p} \right) \quad \text{(I-12)}$$

The K_0, K_1, I_0, I_1 are the modified Bessel functions.

4. Results and discussions

4.1. Membrane charge results

Regarding the charge effects, membrane electric potential (ΔE) was carried out at pressures (P) in the module entrance ranging from $1x10^5$ to $5x10^5$ Pa. The solution conductivity was measured and used at the zeta potential calculations by the Smoluchowski equation (Eq. 1), which is suitable in situations where there is no overlap of electric double layer (high solute concentrations). The zeta potential should be equal in the surface and inside the membrane pores if the material is the same in all their faces. However, as the membranes have a multilayer structure,

and one of them is the support, none of the conventional techniques can provide direct information on charges density in the active layer of the pores, due to the contribution of the support in that [11].

The slope of the linearized data plotted on a graph of electric potential versus pressure difference between the entrance and exit of the cell is the membrane streaming potential in the respective pH. Along with data of the solution average conductivities, the concentration and average pore radius of the membranes, it was possible to obtain the zeta potential (ζ) (Eq. 1), the surface charge density (Eq. 2) and, finally, the volume charge density (X) (Eq. 3) of the four membranes, which is shown in the graph of the Figure 3. The results obtained also give the Freundlich isotherm for each membrane, which were represented by the continuous lines in the Figure 3 and by their corresponding equations in Eq. 6 to 9.

$$X_{NF90} = -11.4c^{0.69} \quad (6)$$

$$X_{NF} = -10.7c^{0.56} \quad (7)$$

$$X_{NP030} = -6.7c^{0.51} \quad (8)$$

$$X_{NP010} = -5.7c^{0.38} \quad (9)$$

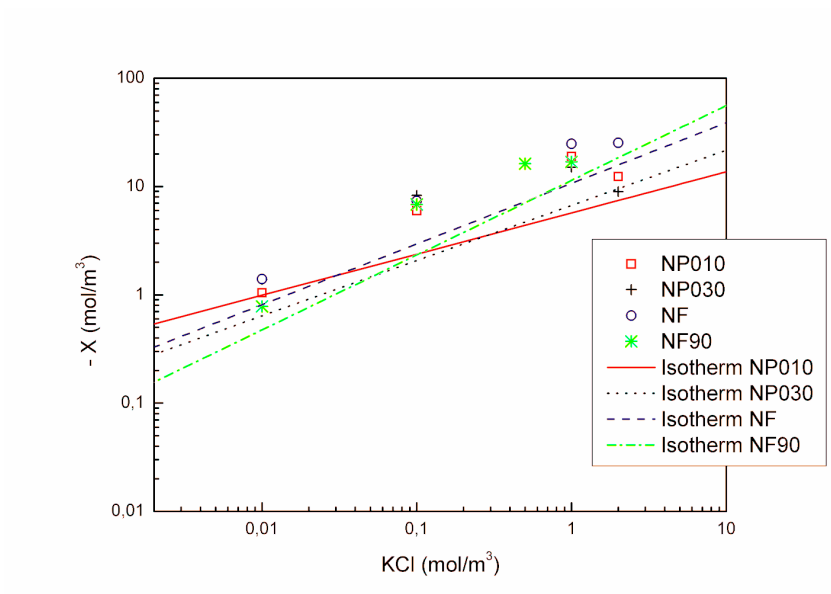

Figure 3 – Membrane charge versus KCl concentration for all evaluated membranes.

The charge density is a characteristic of the functional group of the membrane polymer and depends on the electrolyte concentration in solution. According to Bowen *et al.* [35], in some cases in which an increase in the charge density occurs it could be due to the co-ion adsorption. Thus, in low solute concentrations, the membrane would present more available adsorption sites than solutes in solution, so, all molecules would be adsorbed, which could explain the deep variation on the charge density in those conditions. Increasing the solution concentration, the co-ion adsorption would diminish due to the steric hindrance, leading to an ion concentration at the membrane surface and this would preserve the charge previously adsorbed by the membrane surface, and then retarding the increase in the membrane charge and facilitating the ion transport through the membrane.

4.2 pH characterization

The same evaluation was carried out varying the pH value and keeping the concentration constant. The representation of zeta potential versus the pH is shown in Figure 4 and 5. It can be observed that the volume charge densities change its signal with a change in pH, indicating that the membranes isoelectric points (IP) are among the values analyzed. The plots show that the IPs are between pH 5.0 and 6.0 for all membranes evaluated (5.7 for NF90, 5.3 for NF and NP010, and 5.5 for NP030). With charged membranes, as the case of membranes used in this work, the influence of charged solutions to be purified is noticeable in the process efficiency.

According to Ribau Teixeira *et al.* [18], if the overall membrane behavior is neutral, it presents a plateau in the region of their IP, being slightly positive charged before reaching the IP and slightly negative charged in values just above the IP. That behavior occurs with the NP030 membrane, as it can be observed in Figure 5, which shows the membranes charges in relation to pH values. In this plateau the membrane shows no net charge, behaving like a not charged membrane.

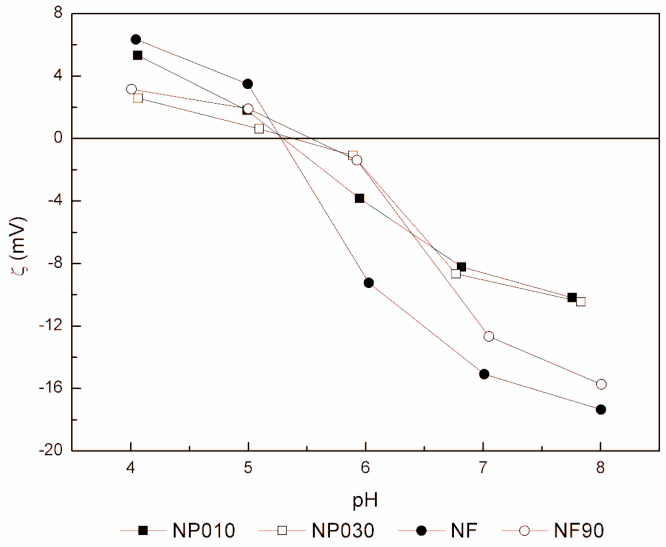

Figure 4 - Chart of zeta potential versus pH solution for the four membranes.

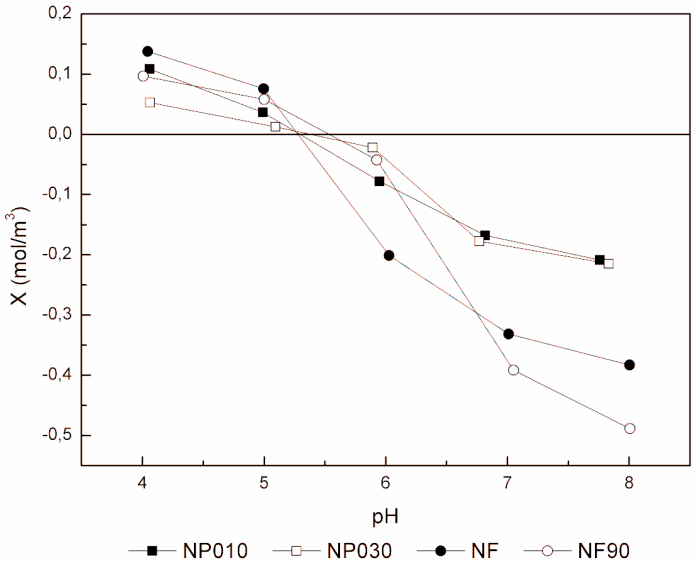

Figure 5 - Chart of membranes charges versus pH solution to the four membranes studied.

Also according to Ribau Teixeira *et al.* [18], if the overall behavior is acid, the membrane presents a positive charge at pH values very acidic, neutral in pH values acids, negative in pH values neutral to acids and very negative in basic pH values, as in the case of NF and NF90 membranes, thus the charge reduces in an acidic medium and increases, in module, from neutral to

basic medium. The NP010 membrane did not present the plateau as seen with the NP030 membrane, as well as with NF90 and NF membranes, nevertheless, the NP010 membrane is also considered neutral.

Bellona & Drewes [36] found that the zeta potential for the NF90 membrane did not present IP in the range of pH assessed (pH 3–9) by measures taken by electrophoresis neither an IP at pH 4.0 in measures of streaming potential, which differs from those found in this work. In that case, measurements of electrophoresis were performed in NaCl 10 mM solution and streaming potential in KCl 10 mM solution, whereas in this work a KCl 0.1 mM solution was used. Probably this variation in the IP is due to the differences in the solution ion concentration, as observed in the work of Cavaco Morão *et al.* [13].

4.3. Concentration polarization effect

Equally important is the study of the polarization effect, which allows determining mass transfer coefficient for each membrane, and also checking if the suggested model represents the process behavior. Besides, it helps to calculate the solute concentration in the external surface of the membranes, a necessary information to obtain the real rejection of the membrane and also to solve the SEDE-VCh model.

4.3.1. Mass transfer coefficient determination

To empirically determine the mass transfer coefficient the Velocity Variation Method (VVM) was used. In this method the solute concentration and transmembrane pressure (TMP) are kept constant in the higher values used during the permeation experiments, which were 2.5 MPa for the membrane NP010, 3 MPa for the membrane NP030, 3.5 MPa for the membrane NF and 4 MPa for the membrane NF90. It was also considered a correlation between the dimensionless number of Reynolds, Schmidt and Sherwood for stirred tanks, which provides the mass transfer coefficient through the Eq. 4.

For the VVM, the mass transfer coefficient can be considered as a function of Reynolds number, as shown the Eq.10.

$$k = b(\mathrm{Re})^{0.8} \tag{10}$$

where b is the inverse of the slope of the Eq. 11 plotted in a graph.

$$\ln\left(\frac{1-R_0}{R_0}\right) = \ln\left(\frac{1-R_r}{R_r}\right) + \frac{1}{b}\left(\frac{J_V}{\mathrm{Re}^{0.8}}\right) \tag{11}$$

where R_0 is the observed rejection (Eq. 12), R_r is the real rejection that take in account the permeate flux and the Reynolds number, J_V is the flux, and Re is the Reynolds number for each velocity evaluated [29,37].

$$R_0 = 1 - \frac{C_{PER}}{C_{REJ}} \tag{12}$$

Comparing the coefficients obtained experimentally with those obtained by the dimensionless numbers method (Eq. 4), was noticed the necessity of a better fit of the data to the model, since the membrane behavior is correlated with suction effects and membrane charges, and the membranes presented distinct permeability [25], related to mass transfer on the adjacent cover of the membranes. Thus, the equation for the membranes NF90, NF, NP030 and NP010 became, respectively:

$$k = 0.1782\left(\frac{D}{r}\right)\left(\frac{\nu}{D}\right)^{0.33}\left(\frac{\omega r^2}{\nu}\right)^{0.8} \tag{13}$$

$$k = 0.086\left(\frac{D}{r}\right)\left(\frac{\nu}{D}\right)^{0.33}\left(\frac{\omega r^2}{\nu}\right)^{0.8} \tag{14}$$

$$k = 0.0547\left(\frac{D}{r}\right)\left(\frac{\nu}{D}\right)^{0.33}\left(\frac{\omega r^2}{\nu}\right)^{0.8} \tag{15}$$

$$k = 0.0598\left(\frac{D}{r}\right)\left(\frac{\nu}{D}\right)^{0.33}\left(\frac{\omega r^2}{\nu}\right)^{0.8} \tag{16}$$

With those equations is possible to determine the mass transfer coefficient for the nanofiltration process using these membranes in different agitation velocities. As expected, as higher the permeability smaller the correction factor, mainly in charged membranes in the concentration evaluated, which were the larger used during the charge effects studies. Figure 6 presents the mass transfer coefficients (*k*) for each velocity for all membranes studied. The results for NP030 and NP010 were practically the same. The NF90 membrane showed the higher value, with a mass transfer coefficient three times higher than those obtained for NP030 and NP010 membranes.

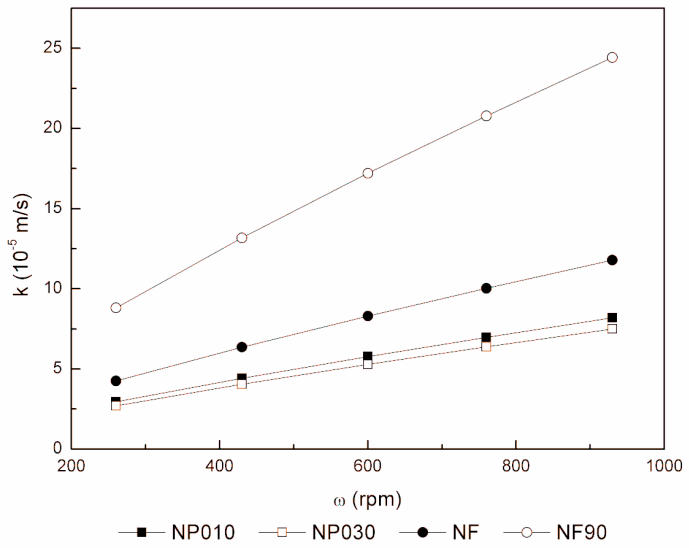

Figure 6 – Mass transfer coefficient for all membranes evaluated.

4.4. KCl and CA rejection results

The KCl rejections were obtained for all membranes using the same concentrations and pH values used in the electric characterization, in a crossflow system varying the TMP and keeping the initial concentration constant. Then, through the observed rejections, the real rejections were determined and used to build the graph in the Figure 7 which shows the real retention versus the permeate flux per unit area of membrane (J_V) for the membranes NF90, NF, NP030 and NP010, respectively. The KCl rejection for all concentration evaluated, in the highest TMP used for each

membrane (2.5 MPa for NP010, 3 MPa for NP030, 3.5 MPa for NF and 4 MPa for NF90), is also showed in the Table 3.

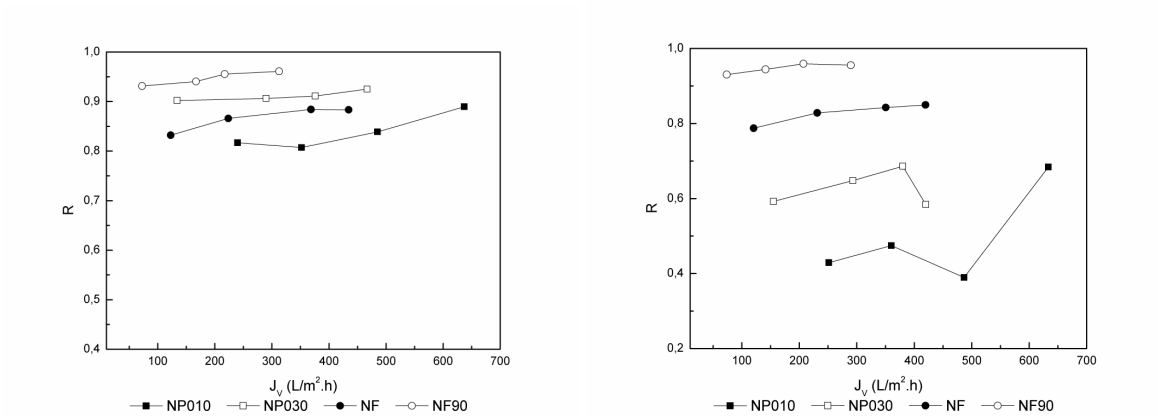

(a) (b)

Figure 7 – Real rejection versus permeate flux for all of the membrane at (a) $1x10^{-4}$ M and (b) $1x10^{-3}$ M KCl concentration.

Each permeate flux in the Figure 7 correspond to a TMP applied in the cell. Even with the membranes NP030 and NP010 working in the smaller TMP they presented the higher fluxes, due to their higher pore size. Analyzing the results of the NF90 membrane, it seems that it presented the highest rejections. For the NF membrane, as well as for the NF90, the rejection did not vary much with the permeate flux. This small variation with the permeate flux can be attributed to the smaller pore size of those membranes. Concerning the NP030 and NP010 membranes, the results show that the rejection is influenced by the initial KCl concentration (see Table 3), and that it vary with the permeate flux. These membranes are more succeptible to the effect of the membrane charge over the rejection at high permeate fluxes due its smaller volume density charge, which have the Cl^- rejection improved by an enhancing in their electrostatic repulsion with the permeate flux.

Table 3 – KCl real rejection for all membranes studied at the maximum TMP applied for each one

KCl Concentration (10^{-3} M)	NF	NP010	NP030	KCl Concentration (10^{-3} M)	NF90
0.01	0.83	0.89	0.92	0.01	0.78
0.1	0.88	0.89	0.93	0.1	0.96
1	0.85	0.68	0.58	0.5	0.96
2	0.84	0.48	0.74	1	0.93

The results in Table 3 show that the polyamide membranes had not a high variability in the rejections with the initial concentration used, whereas the polyethersulfone membranes presented a higher rejection in lower concentrations. According to Afonso [38] the rejection decreases when the salt concentration is increased, due to the shield effect of the cations on the membrane negatively charged groups, which became progressively stronger, leading to the decrease of the membrane forces on the anions. The same behavior was observed by Bowen & Welfoot [39] in a thin film composite membrane with an average pore size of 1.6 nm for permeation of NaCl. Likewise, the KCl rejections were also determined as a function of the pH of the solution, as shown in Figure 8.

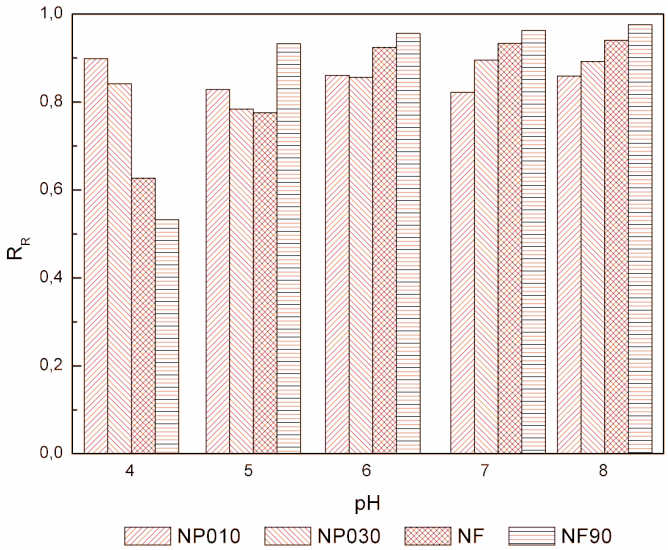

Figure 8 – KCl real rejection versus pH value for all membranes evaluated.

Alternatively, the real rejection varied more with the pH value for the membranes NF90 and NF, passing from 0.50 in pH 4.0 to 0.95 in pH 8.0. This behavior was not noticed for the membranes NP030 and NP010, which presented a rejection around 0.80. It occurred due to the difference in charge densities, which varied more for the NF90 and NF membranes, than for the NP030 and NP010 membranes. Moreover, the smaller rejections in the NF and NF90 membranes were at the pH's in which the membranes were positively charged and the KCl is dissociated, when the low electrostatic repulsion results in an improvement in the mass transfer.

Also, according to Ribau Teixeira *et al.* [18], the pore size of the membranes is reduced at high pH value because the negatively charged groups on the membrane pore surface adopt an

extended conformation due to electrostatic repulsion, causing a reduction on the pore size and, consequently, a decrease in flux and an increase in retention. For the membranes NP010 and NP030 the rejection did not change near the IP, confirming their neutral behavior, since nanofiltration selectivity is mainly controlled by electrostatic mechanisms and the IP corresponds to null electrical charge on the membrane, the rejection should bear a minimum at the IP indeed [38].

Using the same procedure the CA rejection was measured and for all concentrations the rejection values were considerably high, with mean observed rejection values of 99.9, 98.8, 82, 70 % for the NF90, NF, NP030 and NP010 membranes, respectively. The CA has a molecular radius of 0.28 nm [26], which is considerably higher than Cl^- (0.12 nm). These differences can explain the higher observed rejection.

4.4.1. SEDE-VCh model results

Through the real rejection it was possible to use the SEDE-VCh to fit the dielectric constant inside the pores (ε_p) considering a slit-like pore geometry. In Table 4, the ε_p values are presented for the different concentrations evaluated. They have a strong dependency on both the pore diameter and the solute concentration. Comparing the ε_p values, it is possible behold that the average values increased with the membranes pore size, as expected.

Table 4 – Dielectric constant inside the pores for all membranes studied

KCl Concentration (10^{-3} M)	NF	NP010	NP030	KCl Concentration (10^{-3} M)	NF90
0.01	90.6	76.4	84.9	0.01	80.9
0.1	58.4	57.0	53.9	0.1	48.4
1	50.9	67.6	61.0	0.5	44.9
2	52.3	67.4	54.3	1	42.4

The dielectric constants inside the pores and at solution are different, since the equilibrium and dynamic properties of a solvent inside the pores and in solution are also different, due to the smaller degree of spatial and orientation order in the bulk. Thus, the solvent molecules inside the pores respond to an external electric field in a different way, leading to a reduction in the dielectric constant [11].

4.4.2. Membrane selectivity for clavulanic acid

Since one of the aims of this work is the evaluation/selection a proper membrane for separation of CA from the salt concentration, a selectivity analysis based on observed rejection was made. Then, the selectivity of the salt in relation to the CA was obtained as:

$$\frac{S_{KCl}}{S_{CA}} = \frac{\left(1 - R_{O,KCl}\right)}{\left(1 - R_{O,CA}\right)} \tag{17}$$

In order to represent the closer situation compared with the fermentation broth, the 750 mg/L of CA rejection results were chosen and Eq. 17 was evaluated for KCl $1x10^{-3}$ M. These results are represented in Figure 9 for all membrane with a concentration ratio of $C_{KCl}/C_{CA} \approx 0.1$ as function of the applied pressure.

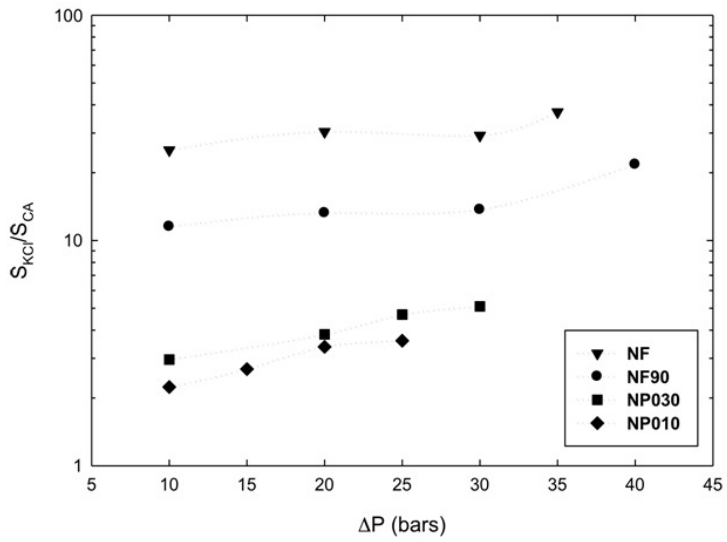

Figure 9 – KCl/CA selectivity as function of applied pressure, for $C_{KCl}/C_{CA} \approx 0.1$

In this figure it clear represented that the NF membrane are considerably more selective than NP030 and NP010 membranes. The higher the selectivity is, easier the separation of KCl from the CA should be. And according to that, NF membrane shows the best results.

5. Conclusions

The isoelectric point of the membranes studied was between the pH 5.0 and pH 6.0, with the NF90 and NF membranes presenting a negative behavior, and the NP030 and the NP010 membranes a neutral behavior.

The mass transfer coefficient of the membranes NP030 and NP010 are practically the same. The NF90 and NF membranes showed the highest mass transfer coefficient, especially the NF90 that presented a mass transfer coefficient three times higher than the NP030 and NP010 membranes.

It was also detected that the NF90 membrane presented the biggest KCl and CA rejection among the evaluated membranes, followed by NF, NP030 and NP010 in sequence, when the data for the higher KCl concentrations were compared.

The real rejection varied more with the pH value for the membranes NF90 and NF, increasing from 0.50 at pH 4.0 to 0.95 at pH 8.0. This behavior was not noticed for the membranes NP030 and NP010, which presented a rejection around 0.80.

An interesting comparison between the structural and electric parameters and the corresponding modeling result can be done if the sequence of membranes is compared:

- The and dielectric constant inside the pores decreases as the pore radius increases in the same membrane sequence than the mean pore radius obtained by AFM: NF90 < NF < NP030 < NP010 until the ε_p reaches the free water value when the pore radius is big enough. The experimental membrane permeability also shows the same trend.
- The membrane selectivity for KCl to CA shows a similar tendency than the volumetric charge density: NF > NF90 > NP030 ≈ NP010.

Acknowledgements

The authors acknowledge the financial support from State of São Paulo Research Foundation (FAPESP) and the Coordenação de Aperfeiçoamento de Pessoal de Nível Superior (CAPES). The authors also acknowledge the membranes donated by Mycrodin Nadir® and Dow Filmtec™.

References

[1] P. A. Bersanetti, R. M. R. G. Almeida, M. Barboza, M. L. G. C. Araújo, C. O. Hokka, Bioch. Eng. J. 23 (2005) 31-36.

[2] A. I. Cavaco Morão, A. M. Brites Alves, M. C. Costa, J. P. Cardoso, Chem. Eng. Sci. 61 (2006a) 2418-2427.

[3] R. M. R. G. Almeida, M. Barboza, C. O. Hokka, Applied Bioch. and Biotechnol. 108 (2003) 867-879.

[4] A. F. Mayer, F. B. Anspach, W. D. Deckwer, Bioseparation 15 (1996) 25-39.

[5] M. Barboza, R. M. R. G. Almeida, C. O. Hokka, Bioseparation 10 (2002) 221-227.

[6] A. M. Brites Alves, A. Morão, J. P. Cardoso, Desalination 148 (2002) 181-186.

[7] A. L. Carvalho, M. I. Rodrigues, F. Maugeri, Sep. Sci. Technol. (2010) Submitted.

[8] N. Hilal, H. Al-Zoubi, N. A. Darwish, A. W. Mohammad, M. Abu Arabi, Desalination 170 (2004) 281-308.

[9] H. Yacubowicz, & J. Yacubowicz, Filt. Sep. Sept (2005).

[10] L. Braeken, B. Bettens, K. Boussu, P. Van der Meeren, J. Cocquyt, J. Vermant, B. Van der Bruggen, J. Membr. Sci. 279 (2006) 311-319.

[11] A. Szymczyk, M. Sbaï, P. Fievet, A. Vidonne, Langmuir 22 (2006) 3910-3919.

[12] A. Martín, F. Martínez, J. Malfeito, L. Palacio, P. Prádanos, A. Hernandez, J. Membr. Sci. 213 (2003) 225-230.

[13] A. I. Cavaco Morão, A. M. Brites Alves, M. D. Afonso, J. Membr. Sci. 281 (2006b) 417-428.

[14] M. S. Oak, T. Kobayashi, Y. H. Wang, T. Fukaya, N. Fujji, J. Membr. Sci. 123 (1997) 185-195.

[15] A. E. Childress & M. Elimelech, Environ. Sci. Technol. 34 (2000) 3710-3716.

[16] J. Schaep & C. Vandecasteele, J. Membr. Sci. 188 (2001) 129-136.

[17] M. Ribau Teixeira & M. J. Rosa, Desalination 151 (2002) 165-175.

[18] M. Ribau Teixeira, M. J. Rosa, M. Nyström, J. Membr. Sci. 265 (2005) 160-166.

[19] W. R. Bowen, & J. S. Welfoot, Desalination 147 (2002a) 197-203.

[20] V. Silva (2010) Doctoral Thesis in: Facultad de Ciencias, Universidad de Valladolid, Valladolid, Spain.

[21] A. Szymczyk, & P. Fievet, J. Membr. Sci. 252 (2005) 77-88.

[22] L. D. Nghiem, A. I. Shafer, M. Elimelech, Sep. Sci. Technol. 40 (2005) 2633–2649.

[23] L. D. Nghiem, D. Vogel, S. Khan, Water Research 42 (2008) 4049-4058.

[24] M. J. López-Muñoz, A. Sotto, J. M. Arsuaga, B. Van der Bruggen, Sep. Purif. Technol. 66 (2009) 194–201.

[25] A. L. Carvalho, F. Maugeri, V. Silva, A. Hernández, L. Palacio, P. Pradános, J. Material Sci. (2010) Accepted.

[26] A. I. Cavaco Morão, A. Szymczyk, P. Fievet, A. M. Brites Alves, J. Membr. Sci. 322 (2008) 320-330.

[27] A. E. Bird, J. M. Bellis, B. C. Basson, Analyst 107 (1982) 1241-1245.

[28] C. K. Colton, S. Friedman, D. E. Wilson, R. S. Lees, J. Clin. Invest. 51 (1972) 2472-2481.

[29] S. Sridhar, & P. K. Bhattacharya, J. Membr. Sci. 57 (1991) 187-206.

[30] S. Kimura, & S. Nakao, Desalination 17 (1975) 267-288.

[31] G. Jonsson, & C. E. Boesen, Desalination 21 (1977) 1-10.

[32] F. Martínez, A. Martín, J. Malfeito, L. Palacio, P. Prádanos, F. Tejerina, A. Hernández, J. Membr. Sci. 206 (2002) 431-441.

[33] J. A. Otero, O. Mazarrasa, J. Villasante, V. Silva, P. Prádanos, J. I. Calvo, A. Hernández, J. Membr. Sci. 309 (2008) 17-27.

[34] A.A. Rashin & B. Honig, *J. Phys. Chem.* 89 (1985) 5588-5593.

[35] W. R. Bowen, A. W. Mohammad, N. Hilal, J. Membr. Sci. 126 (1997) 91-105.

[36] C. Bellona & J. E. Drewes, J. Membr. Sci. 249 (2005) 227-234.

[37] T. K. Poddar, R. P. Singh, P. K. Bhattacharya, Chem. Eng. Commun. 75 (1989) 39-56.

[38] M. D. Afonso, Desalination 191 (2006) 262-272.

[39] W. R. Bowen & J. S. Welfoot, Chem. Eng. Sci. 57 (2002b) 1393-1407.

Nomenclature

TSP – Tangential Streaming Potential

KCl – Potassium chloride

CA – Clavulanic acid

KCA – Potassium clavulanate

UF – Ultrafiltration

MWCO – Molecular Weight Cut-Off

SEDE-VCh – Steric, Electric and Dielectric Exclusion

η – Streaming potential

λ_0 – Solution conductivity

ν – Solution dynamic viscosity

ε_0 – Vacuum permittivity

ε_b – Dielectric constant of the bulk solution

ζ – Zeta potential value

σ_s – Surface charge density based on the Gouy-Chapman theory

R – Ideal constant of gases

T – Temperature

c_i – Concentration of ion i

z_i – Charge of ion i

F – Faraday constant

r_p – Average pore radius of the membrane

AFM – Atomic Force Microscopy

D – KCl diffusivity at infinite dilution

r – Membrane effective radius

ω – Rotation frequency

J_V – Volumetric flux by membrane area

k – Mass transference coefficient

c_0 – KCl concentration on feed phase

c_p – KCl concentration on the permeate

ε_p – Dielectric constant inside the pores

a and b – Parameters of the Freundlich isotherm

K_0, K_1, I_0, I_1 – Modified Bessel functions

ε_m – Dielectric constant of the dry polymer of the membrane

ΔE – Membrane electric potential

P – Pressures

X – Volume charge density

IP – Isoelectric points

NaCl – Sodium chloride

VVM – Velocity Variation Method

R_0 – Observed rejection

R_r – Real rejection

J_V – Flux

Re – Reynolds number

TMP – Transmembrane pressure

NANOFILTRATION MEMBRANE TECHNOLOGY APPLIED TO THE CONCENTRATION AND PURIFICATION OF CLAVULANIC ACID: EFFECT OF PORE SIZE AND PERMEABILITY

A. L. Carvalho*; M. I. Rodrigues; F. Maugeri

Departament of Food Engineering, Faculty of Food Engineering, Rua Monteiro Lobato 80, Barão Geraldo, University of Campinas – UNICAMP, CEP: 13083-862, Campinas, SP, Brazil. E-mail: maugeri@fea.unicamp.br, bel@fea.unicamp.br.

*e-mail: limoeiro@fea.unicamp.br, telephone: +551935214052, fax: +551935214027

Abstract

In the present work, studies on the nanofiltration of clavulanic acid are presented, aiming to select the most appropriate membrane and process conditions for the concentration and purification of the product. According to an evaluation of the results, the clavulanic acid retention depends on the membrane pore size. The trials were carried out taking into account the stability of clavulanic acid at different pH values and temperatures, as well as with different clavulanic acid concentrations in the feed phase. The permeability was decisive to determine the best membrane for this process and the NF membrane was chosen as the more appropriate one.

Keywords: nanofiltration, membrane, clavulanic acid, purification, permeability

1. Introduction

Clavulanic acid (CA) is a β-lactamase inhibitor, used in combination with β-lactamase sensitive penicillins, to protect the β-lactam ring of the antibiotic against hydrolysis [1,2]. CA is produced industrially by fermentation using *Streptomyces clavuligerus*, and presents low yields in the production process, particularly in the separation and purification step, due to its thermal instability and sensitivity to changes in pH [1,3]. Associated with its low concentration in the fermented broth, studies on its extraction and purification have to consider the kinetic degradation of CA, in order to minimize losses and maximize recovery yields and productivity.

Recent studies on the purification of CA were focused on the evaluation of procedures for its isolation and purification when produced by fermentation with *Streptomyces clavuligerus*. Some separation studies have used Amberlite XAD resin, Amberlite IRA 400 ion exchange resin pre-treated with NaCl, and ultrafiltration (UF) followed by nanofiltration [2,4-6]. Currently, several high-value bio-products are being produced by fermentation, bringing new challenges for the recovery and purification processes. UF processes are an efficient way of separating the biomass from the CA fermentation broth, producing a free protein permeate containing CA, which can be subsequently concentrated using nanofiltration membranes [2,6].

Nanofiltration is a process in which the driving force is the pressure difference between the two sides of the membrane. The main advantages of this process are the operation at low pressures when compared to reverse osmosis, high flow rate, considerable retention of multivalent anionic salts and organic molecules of molecular weight higher than 300 Da, and involves relatively low investment and low operational and maintenance costs [7]. The performance of nanofiltration depends on the sum of steric and electrostatic effects through the membrane, the Donnan equilibrium, dielectric exclusion, and a further steric effect at the membrane surface.

The mass transfer in the membrane depends on several factors, such as the adsorption in the inner of the pores causing pore blockage, and fouling on the membrane surfaces during the process [8-10], as the concentration polarization layer of the solutes on the high-pressure side of the membrane such as cake and gel layer formation [9-11], leading to an increase in the operation and maintenance costs, permeate flux decline, and energy demands, turning down the membrane performance and ultimately reducing membranes life [12-14].

Despite the efforts to minimize the fouling it occurs in many instances [10], becoming the mainly challenge for the nanofiltration process, since the extent of rejection of solutes by membranes is perhaps the most critical parameter in membrane filtration [10,12,15]. For a clean

(unfouled) membrane, the extent of rejection is influenced largely by the pore size or molecular weight cut-off (MWCO) [10].

Since the particles are accumulated preferentially in the "valleys" than in the peaks, a structural conformation that appears in rough membranes, it results in "valley clogging" and hence in a more severe flux decline in rough membranes in comparison with smooth membranes [16-18]. Hirose *et al.* [19] suggested an approximately linear relationship between membrane surface roughness and permeate flux for crosslinked aromatic polyamide RO membranes, where permeability increased with increasing surface roughness. However, for others researchers the hydrophobicity appears to be of fundamental importance to the cake formation, likewise the adsorption of hydrophobic compounds is major onto hydrophobic membranes [14, 17, 20, 21].

Another important membrane property is the permeability [17], since higher flux can bring more colloids to the membrane surface in a given time period, resulting in a faster growth of the cake layer [17]. However, reported results are complicated to follow due to the composite nature of foulants and particular interactions with each membrane type and composition that leads to a diversity of explanations for observed rejections [22].

Therefore, even with a large nanofiltration applications suggested [21,23-25], only few were implemented on an industrial scale. So, the main goals of this work were the selection of the most appropriate membrane and the optimization of the filtration conditions, taking into account the process conditions, the stability of the CA at different temperature and pH values, and different solute concentrations in the feed, evaluating the effect of the pore size and permeability over the process.

2. Methodology

2.1. Material

A stainless steel stirred dead-end cell was used to study the nanofiltration process. The system consists of a cylindrical container jacketed, with a membrane located at the base, whose area was 1.52 x 10^{-3} m^2, and a magnetic stirrer that promotes the convection movement in the process. The pressure difference was applied by a change in the internal atmosphere with the application of nitrogen gas, as shown in Figure 1.

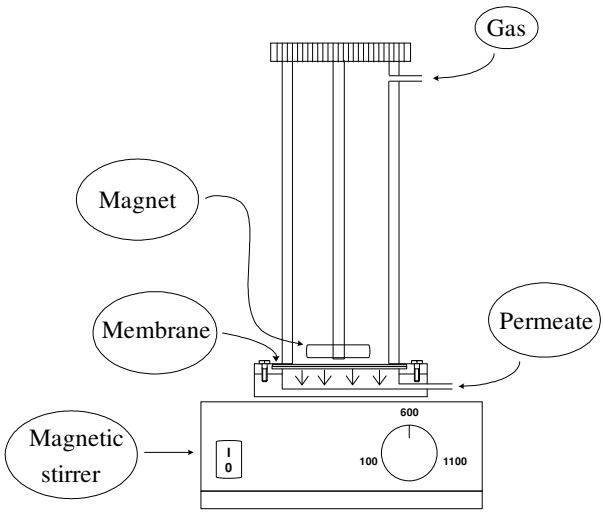

Figure 1 – Schematic representation of the bench-scale stirred dead-end cell.

The assays were performed with the NF (polypiperazine amide) and NF90 (fully aromatic polyamide [15,26]) membranes from Filmtec™, and the NP010 and NP030 membranes made from polyethersulfone and manufactured by Microdyn Nadir. Table 1 shows the characteristics of the membranes studied according to the manufacturers. The CA solutions were prepared from the medicine Clavulin® (revested pills with 125 mg of potassium clavulanate and 500 mg of amoxicilin), from GlaxoSmithKline Brasil Ltda. The pH of the CA solutions was adjusted using 0.2 M hydrochloric acid and 1 M potassium hydroxide, prepared using analytical grade reagents. The hydrochloric acid solutions were prepared using 36.5-38 % pure hydrochloric acid.

Table 1 – Characteristics of the membranes used

Membrane	NF90	NF	NP030	NP010
MWCO (Da)	180[a]	>200	400	1000
Max. pressure (bar)	41	41	40	40
Max. temperature (ºC)	45	45	95	95
pH range	2-11	3-10	0-14	0-14
Pore size (nm)[b]	0.99	1.39	1.48	1.49
Lp (10^{-11}m/Pa.s)[b]	1.53	3.39	4.36	6.47
Rejection (%)	>97[c]	>99[d]	80-95[e]	25-55[e]

[a] Lopez Muñoz *et al.* [27]

[b] Carvalho *et al.* [28]

[c] Rejection of $MgSO_4$ (25ºC, 4.8 bar)

[d] Rejection of $MgSO_4$ (25ºC, 8.9 bar)

[e] Rejection of Na_2SO_4 (20ºC, 40 bar)

The imidazole used in the analysis of the concentration of CA in the feed, permeate and rejection phases, was ultrapure. The results were analyzed using the statistical software Statistica 7.0® from StatSoft®.

2.2. Experimental procedure

The membrane selection step was carried out using a 2^3 rotational central composite experimental design, with 6 axial points and 3 central points, giving a total of 17 experiments for each membrane evaluated. It was expected that the applied pressure and the agitation speed influenced the process, so, to diminish the number of experiments they were kept constant during these experiments. Their values were: tangential flow velocity of 600 rpm and transmembrane pressure applied of $2x10^6$ Pa. The volume of the feed phase was also kept constant in 100 mL. Table 2 shows the levels of the independent variables (real and coded values).

Table 2 – Independent variables and their levels for membrane selection

Variable	Levels				
	-1.68	-1	0	1	1.68
Temperature [°C]	5	10	17.5	25	30
pH	4.5	5.11	6	6.89	7.5
C_{CA} [mg/L]	250	437.5	750	1062.5	1250

In these experiments, aqueous solutions of potassium clavulanate were used, which were vacuum filtered and microfiltered through 14 μm and 0.45 μm pore membranes, respectively. The retention coefficient and productivity were evaluated as responses.

The process was validated using experiments in triplicate under the optimal operating conditions as obtained for each membrane, and the Tukey test was applied to determine the best membrane for this process.

For the purification assays, an ultrafiltered fermentation broth was used, in which the concentration of CA varied according to the fermentation process. Only the NF and NF90 membranes were used in these assays, since they provided the best results in the first membrane selection step. In this case, two 2^{4-1} fractional factorial experimental designs were used, one for each membrane, each with 3 central points, as shown in Table 3.

Table 3 – Independent variables and levels for the purification assays

Variable	Levels					
	NF			NF90		
	-1	0	1	-1	0	1
Pressure applied [MPa]	1	2	3	1	2.5	4
Tangencial flow velocity [rpm]	260	600	930	260	600	930
Temperature [°C]	5	17.5	30	5	17.5	30
pH	4.5	6.0	7.5	4.5	6.0	7.5

2.3. Mathematical considerations

The retention coefficients were calculated from the CA mass found in the retentate and permeate phases of the process, since the concentration factor was kept constant for all experiments. The productivities were calculated according to the CA concentration in the retentate and feed phases, the feed tank volume and the time elapsed at the end of the process. The purification factor was determined by comparing the concentrations of CA and of the contaminants. Equations (1), (2) and (3) show these relationships.

$$R_C = 1 - \frac{M_{PER}}{M_{REJ}} \tag{1}$$

$$Productivity = \frac{[CA]_{REJ}}{[CA]_0 \times V_0 \times t} \tag{2}$$

$$PF = \frac{[CA]_{REJ} / [CA]_0}{[Cont]_{REJ} / [Cont]_0} \tag{3}$$

where R_C is the retention coefficient, M_{REJ} is the CA mass in the retentate, M_{PER} is the CA mass in the permeate, $[CA]_{REJ}$ is the clavulanic acid concentration in the retentate, $[CA]_0$ is the clavulanic acid concentration in the feed phase, V_0 is the initial volume in the feed phase, t is the process time

(h), $[Cont]_{REJ}$ is the concentration of contaminants in the retentate and $[Cont]_0$ is the concentration of contaminants in the feed phase.

2.4. Analytical methodology

The concentration of CA was determined according to Bird *et al.* [29], using a Beckman Coulter™ model DU®640 spectrophotometer. The antibiotic was reacted with imidazole (60 g/L, pH 6.8) and the absorbance of the reaction product measured at 312 nm. The product of this reaction is more stable than CA and its formation is directly proportional to the CA concentration present in the reaction mixture. Potassium clavulanate, also from the medicine Clavulin®, was used as the standard.

Additionally, in order to evaluate the contaminants, the reaction product was assayed at 280 nm, wavelength at which part of the amino acids can be detected, mainly the aromatic ones, since the contaminants are mainly amino acids [30].

3. Results and discussion

3.1. Membrane selection and process optimization

In the membrane selection assays the stability of the clavulanic acid was considered with respect to how it was affected by variations in the pH and temperature (T), and also the concentration at which it came from the previous phases of the process (C_0). The responses were the retention coefficient and process productivity ($[CA]_{RET}/[CA]_0$.L.h). Table 4 shows the data obtained in this preliminary phase.

Table 4 – Template for the planning and results obtained in the membrane selection experiments

				NP010		NP030		NF		NF90	
Exp.	T (°C)	pH	C_0 (mg/L)	R_C	Productivity ($[CA]_{RET}/[CA]_0$.L.h)	R_C	Productivity ($[CA]_{RET}/[CA]_0$.L.h)	R_C	Productivity ($[CA]_{RET}/[CA]_0$.L.h)	R_C	Productivity ($[CA]_{RET}/[CA]_0$.L.h)
1	-1 (10)	-1 (5.11)	-1 (437.5)	0.7361	48.85	0.8738	25.29	0.9675	40.98	0.9982	32.37
2	1 (25)	-1 (5.11)	-1 (437.5)	0.7492	68.24	0.8755	43.15	0.9860	65.12	0.9996	52.26
3	-1 (10)	1 (6.89)	-1 (437.5)	0.7319	46.24	0.8529	30.76	0.9730	49.11	0.9980	30.16
4	1 (25)	1 (6.89)	-1 (437.5)	0.7541	68.56	0.8481	49.08	0.9659	81.84	0.9981	47.37
5	-1 (10)	-1 (5.11)	1 (1062.5)	0.7055	34.01	0.8639	22.07	0.9873	38.61	0.9991	24.97
6	1 (25)	-1 (5.11)	1 (1062.5)	0.7623	44.88	0.8665	28.59	0.9853	51.80	0.9990	25.67
7	-1 (10)	1 (6.89)	1 (1062.5)	0.7027	34.25	0.8318	23.13	0.9886	32.46	0.9991	12.83
8	1 (25)	1 (6.89)	1 (1062.5)	0.7674	40.68	0.8498	29.41	0.9785	50.81	0.9992	29.47
9	-1.68	0 (6.0)	0 (750)	0.7522	29.36	0.8256	26.93	0.9911	20.61	0.9966	27.38
10	1.68	0 (6.0)	0 (750)	0.7982	60.58	0.8799	42.47	0.9892	57.37	0.9961	35.05
11	0 (17.5)	-1.68	0 (750)	0.7725	39.08	0.8743	24.10	0.9830	54.82	0.9985	37.71
12	0 (17.5)	1.68 (7.5)	0 (750)	0.6842	43.57	0.8193	30.81	0.9748	42.30	0.9974	39.78
13	0 (17.5)	0 (6.0)	-1.68 (250)	0.6904	66.18	0.8031	39.38	0.9866	74.22	0.9995	45.26
14	0 (17.5)	0 (6.0)	1.68 (1250)	0.7510	34.93	0.8529	24.34	0.9355	47.67	0.9991	26.89
15	0 (17.5)	0 (6.0)	0 (750)	0.7329	43.94	0.8849	28.44	0.9882	29.71	0.9987	17.85
16	0 (17.5)	0 (6.0)	0 (750)	0.6977	37.32	0.8410	38.20	0.9894	38.39	0.9994	32.74
17	0 (17.5)	0 (6.0)	0 (750)	0.7228	47.65	0.8611	32.50	0.9914	158.32	0.9984	40.44
Average ± standard deviation of central points				0.718[a] ± 0.018	42.97[a] ± 5.23	0.862[b] ± 0.022	33.05[b] ± 4.91	0.990[c] ± 0.002	34.05[b] ± 6.14	0.999[c] ± 0.001	30.34[c] ± 11.48

The results were statistically analyzed using the Tukey test at the central point, showing that the NF and NF90 membranes had higher average retention coefficients (R_C), with values of 0.990 and 0.999, respectively, as compared to the NP010 and NP030 membranes, with retention coefficients of 0.718 and 0.862, respectively, at a 10% significance level. Those results were expected when you compare the retention with the membranes pore size, which were NF90 < NF < NP030 < NP010, allied to their adsorption degree. According Carvalho *et al.* [28], the membranes NF and NF90 did not adsorb CA as the membranes NP010 and NP030, since the adsorption is related to the atraction of the CA molecules to the membrane surface, which is higher for the polyethersulfone membranes (NP010 and NP030) than for the polyamide membranes (NF and NF90).This smaller adsorption improves the rejection ability of the second two.

As the productivity is an important parameter when denaturing bioproducts are concerned, since the higher the productivity, the higher the chances of good product recovering. The average productivities for NF and NP030 membranes showed no significant differences, according to the test applied to the central point data, also at a 10% significance level, as can be seen in Table 4, where the same letters indicate that the responses are not statistically different for that parameter. The membranes NF90 and NP010 present different productivities by feed tank volume. This result is in accordance with the permeabilities found for these membranes by Carvalho *et al.* [28], including the similarity in the permeability of the membranes NF and NP030, as shown in the Table 1. For these Tukey test the last value for the productivity of the membrane NF and the first one for the membrane NF90 were discarded, since they were too much different than the other two and, probably, were an experimental error.

Since the NF and NF90 membranes presented the best results, for the retention coefficient, they were subjected to a more detailed treatment using the effect estimate analysis. This study was carried out considering both the responses and the results obtained for the retention coefficient showed that the determination coefficients of the statistical analysis were below 70%. This was certainly due to the low variability of the data for both membranes, as can be seen in Figure 2. In this figure, the membrane NF90 provided the best results for the retention coefficient with a small variability, with all results above 0.99. It can also be seen that the membrane NF presented a meaningful result, with a retention coefficient higher than 0.93. Again, the membrane with small pore showed better retention, reinforcing the idea that the CA retention strongly depends on the membrane pore size.

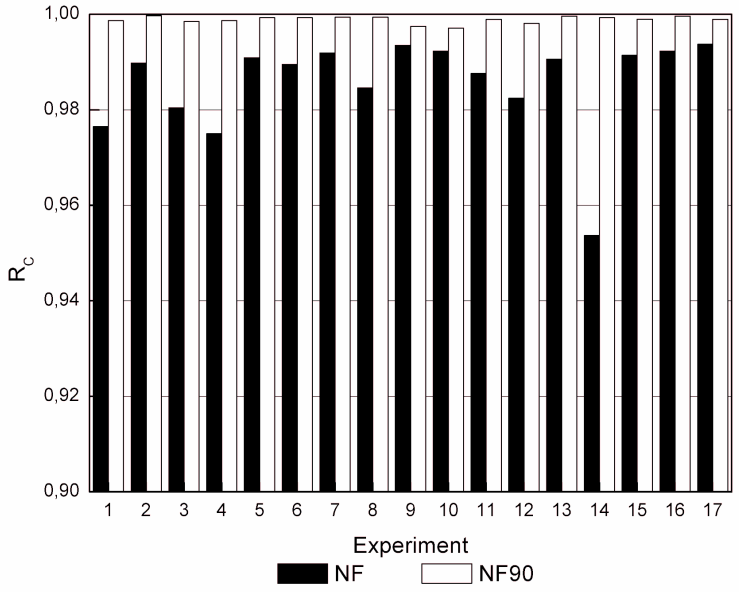

Figure 2 – Retention coefficients (R_C) for the NF and NF90 membranes.

For the membrane NF90 the determination coefficient was 84,13 % and for the membrane NF it was 95,91 %, at 10% significance, nevertheless, it is better to compare the results for both membranes using all the experiments results, since the overall behavior can show a general idea of the discrepancies between them. Therefore, it is possible to determine which membrane presented better productivity during the concentration of clavulanic acid in a given feed volume, as shown in Figure 3.

As can be seen above, the NF membrane showed the highest productivities, higher than those of the NF90 membrane, although the latter also presented good productivities, typically above 25 $[CA]_{RET}/[CA]_0$.L.h. When only these two membranes are analyzed it is possible to notice a greater difference in their productivities, which leads to a deeper study on their permeabilities. In our previous work [28] it was found that the permeability of the NF90 and NF membranes decreases after their use to concentrate CA in similar degrees, around 28%. However, when the absolute values are considered, they mean that the NF permeability is twice the NF90 permeability for both clean and used membranes, leading to a best productivity for the NF one.

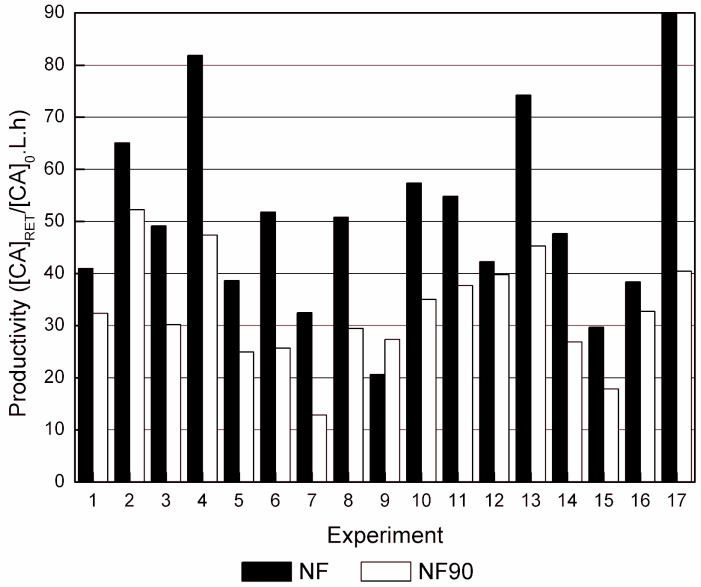

Figure 3 – Productivity ($[CA]_{RET}/[CA]_0$.L.h) for the NF and NF90 membranes.

According to the statistical analysis, it is evident that the higher the temperature and the higher the pH, the better the results. The CA concentration presented a negative effect over the productivity, however, it is interesting to produce a high quantity of CA, leading to the best operational conditions for the NF membrane being those of experiment 10: temperature of 30 ºC, pH 6.0, and a clavulanic acid concentration in the feed phase of 750 mg/L, since the production of CA improved.

On the other hand, for the NF90 membrane, it seems that the temperature is the limiting factor for the definition of the best operational conditions, even with the negative effect of the CA concentration over the productivity. Thus, the conditions at the central point were adopted for the system operation, which were temperature 17.5 ºC, pH 6.0 and a clavulanic acid concentration in the feed phase of 750 mg/L.

3.2. Validation

The validations of the best operational conditions were carried out for the NF and NF90 membranes using the following values: for NF90 - T = 17.5 ºC, pH = 6.0 and C_0 = 750 mg/L, and for NF - T = 30 ºC, pH = 5.11 and C_0 = 750 mg/L. A comparison between the average values for

both membranes was also carried out using a statistical test, to determine which of the two was more suitable for this process. The results are shown in Figure 4.

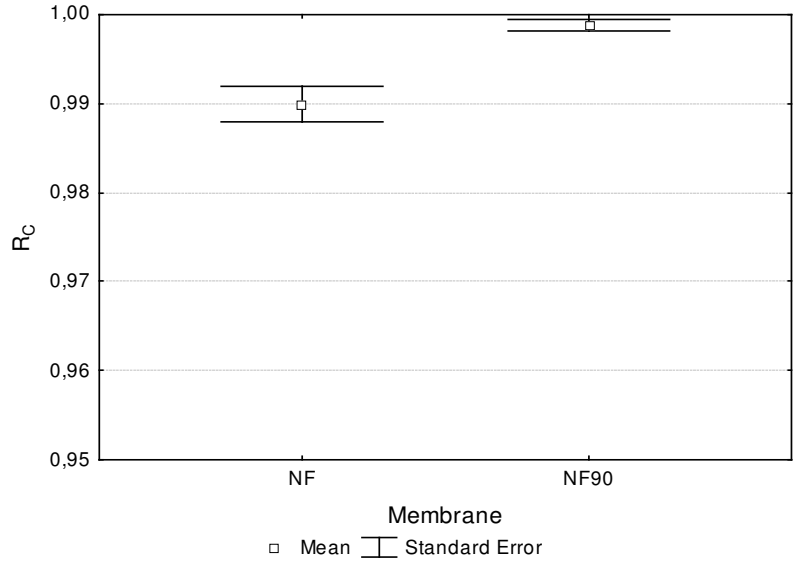

(a)

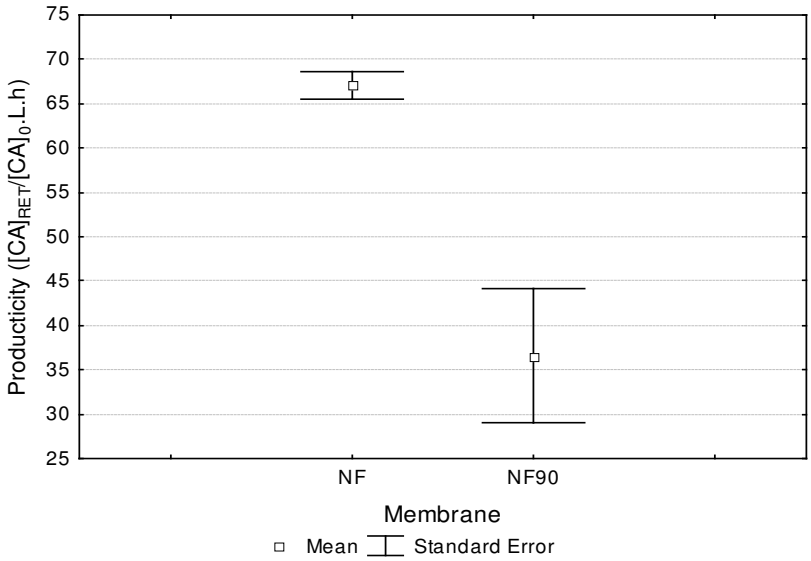

(b)

Figure 4 – Responses for NF and NF90 membranes, with their respective repetitions and averages: (a) retention coefficient and (b) productivity ($[CA]_{RET}/[CA]_0$.L.h).

As shown in Figure 4a, the average retention coefficient was higher than 0.98 for both membranes, showing good reproducibility as well when considering the best operational conditions.

It can be seen in Figure 4b that the NF membrane showed productivity higher than 65 $[CA]_{RET}/[CA]_0$.L.h, whereas that for the NF90 membrane was around 37 $[CA]_{RET}/[CA]_0$.L.h. It can also be concluded that the process allowed for good reproduction of these results, especially for the NF membrane, which showed the best performance.

A Tukey test was carried out to compare the averages for each response, in order to better compare the membranes. The results can be seen in Table 5, where the averages for all the responses and the relationship between them are shown, at a 10% level of significance. The averages denoted with different letters differ statistically, whereas those denoted with the same letters are statistically equivalent.

Table 5 – Results of the Tukey test for both membranes

	R_C	Productivity ($[CA]_{RET}/[CA]_0$.L.h)
NF	$0.992^a \pm 0.0015$	$67.10^a \pm 1.33$
NF90	$0.999^b \pm 0.0004$	$36.59^b \pm 5.45$

The results in Table 5 show that the retention coefficients and the productivity, for the NF and NF90 membranes, differed statistically at a 10% level of significance. The NF membrane showed the best performance concerning the productivity.

When these results are compared with those found in the literature, the recoveries of clavulanic acid obtained with both these membranes, working under the optimized conditions, were better than those found by Barboza *et al.* [5] and Hirata *et al.* [31], who obtained a maximum recovery of 70%, and similar to those found by Cavaco Morão *et al.* [32], with values of 99.1%, 92.8% and 98.1% of rejection for the membranes NFT50, Desal DL and Desal DK, respectively.

3.3. Membrane selectivity

The selectivity studies for both NF and NF90 membranes were carried out according to a 2^{4-1} fractional experimental design. The selectivity was evaluated with respect to the contaminants, represented here in a general way by amino acids, especially those that absorb at a wavelength of 280 nm, such as the aromatic ones. The retention coefficients, productivities and purification factors were evaluated against the following variables: pH, applied pressure, tangential velocity (agitation speed) and temperature. In addition, fermentation broths were used instead of the synthetic solutions used in previous experiments, allowing for a better evaluation of the process, so that the

best membrane could be chosen. Table 6 shows the variables and the results obtained. For the retention coefficient response, there was small variability in the results and no variables were significant at a10% level of significance. Figure 5 shows the performance of both membranes with respect to this response.

Table 6 – 2^{4-1} fractional factorial design for the membrane selectivity studies

					NF			NF90		
Exp.	P (MPa)	ω (rpm)	T (°C)	pH	R_C	Productivity ($[CA]_{RET}/[CA]_0$.L.h)	PF	R_C	Productivity ($[CA]_{RET}/[CA]_0$.L.h)	PF
1	-1	-1	-1	-1	0.9761	38.99	1.092	0.9963	9.25	1.005
2	1	-1	-1	1	0.9705	36.94	0.958	1.0019	30.22	0.889
3	-1	1	-1	1	0.9866	31.94	0.933	0.9990	17.86	0.945
4	1	1	-1	-1	0.9867	180.24	1.086	0.9993	62.77	1.108
5	-1	-1	1	1	0.9902	41.72	0.944	0.9982	25.28	0.924
6	1	-1	1	-1	0.9567	179.10	1.133	0.9936	69.85	1.031
7	-1	1	1	-1	0.9854	78.22	1.159	0.9970	29.09	1.096
8	1	1	1	1	0.9246	64.39	0.952	0.9943	34.25	0.936
9	0	0	0	0	0.9999	119.44	1.034	1.0000	61.08	1.129
10	0	0	0	0	0.9919	124.59	0.986	0.9946	63.82	1.003
11	0	0	0	0	0.9968	120.73	1.062	0.9988	65.03	0.985
Average ± standard deviation of central points					0.996 ± 0.004	121.59 ± 2.68	1.03 ± 0.04	0.998 ± 0.003	63.31 ± 2.02	1.04 ± 0.08

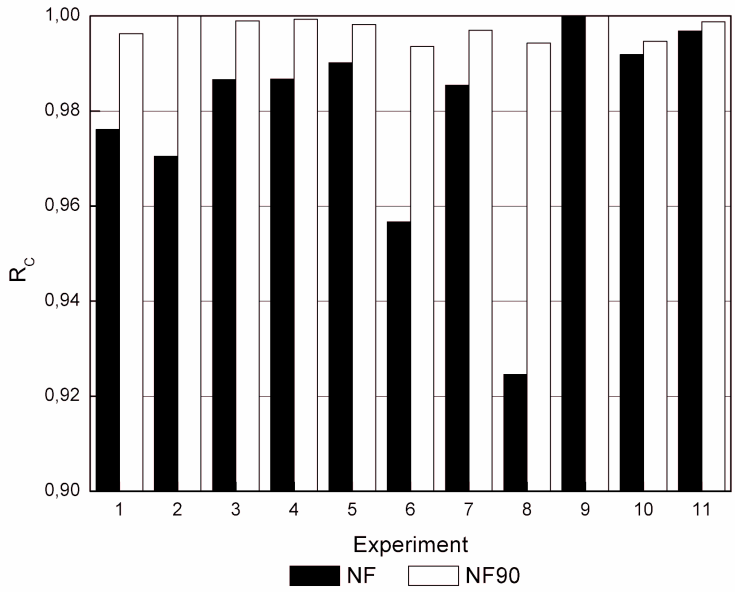

Figure 5 – Retention coefficients for both membranes.

As shown in Figure 5, the NF90 membrane showed greater retention than the NF one, which can be explained by the smaller pore size of the former, as previously explained. When comparing the results obtained from the fermentation broth with those obtained from the synthetic solution of clavulanic acid, it was found that the results for the NF90 membrane did not differ, however, the NF membrane showed lower retention rates than those found using a synthetic solution of CA. This apparent inconsistency may be explained by the presence of other substances in the fermented broth, which may have interacted with the NF membrane, changing the CA adsorption in its surface and altering its ability to retain the CA. The results concerning the influence of agitation speed and applied pressure on the separation and concentration of CA by nanofiltration, as reported in this work, have not been reported elsewhere, and it is also important to mention that the CA concentration in the fermented medium depended on the fermentation batch, which varied from 435 mg/L to 698 mg/L, and can obviously affect the filtration process.

Concerning the productivity of both membranes, the effect estimate analysis showed that the NF90 was affected positively by the applied pressure, whereas the NF membrane was also affected positively by the applied pressure and negatively by the pH of the solution, at a10% level of significance. However, the determination coefficients for these responses were relatively low (R^2

bellow 70 %), so the productivity was evaluated in the same way as the retention coefficient, as shown in Figure 6.

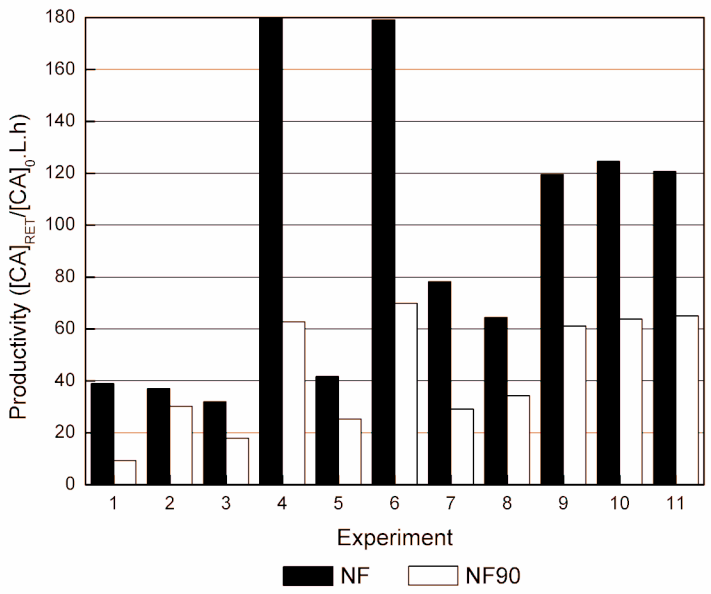

Figure 6 – Productivities ($[CA]_{RET}/[CA]_0$.L.h) for both membranes.

It is evident from Figure 6 that the productivity of the NF membrane was much higher than that of the NF90 membrane, suggesting that the former is more appropriate for this process. It can also be noted that both membranes showed greater productivity when using the fermented broth instead of the synthetic solution of clavulanic acid. It probably happened due to the increase in the applied pressure, which increased the water permeability of the membranes, leading to a higher discrepancy between the membranes productivities. However, it is imperative to evaluate the CA purification factor in order to choose the correct membrane.

Concerning the purification factor, the effect estimate analysis showed that both membranes were negatively affected by the pH of the solution at a 10 % level of significance. Although the determination coefficient for the NF membrane was representative for this response (R^2 = 92.06 %), the same cannot be said for the NF90 membrane (R^2 = 63.09 %). This pH effect can be attributed to the change in the molecules charge in the solution, since in the smaller pH used here (pH = 4.5) the CA is protonated, but some amino acids present in the solution may not be protonated, improving the purification factor. The response of purification factor can be evaluated for both membranes from Figure 7.

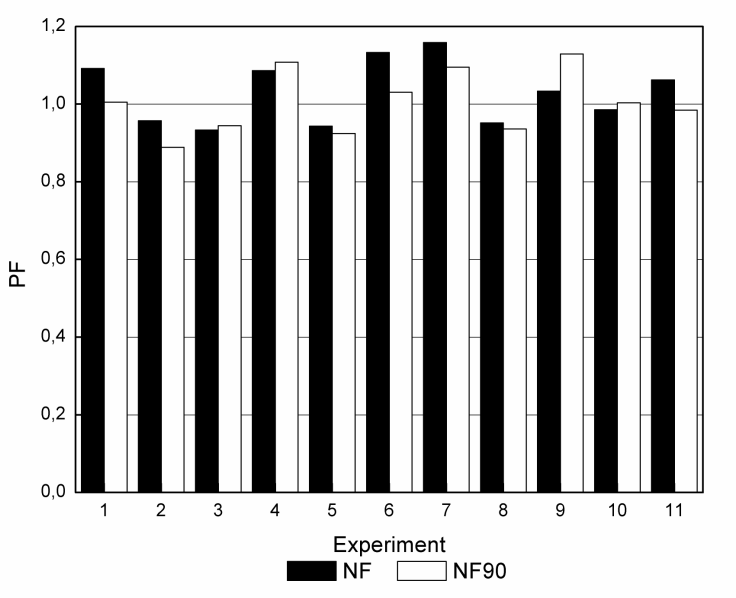

Figure 7 – Purification factor for both membranes.

According to Figure 7, both membranes showed similar results for the purification factor, since they are made from the same material, thus, presenting the same chemical behavior associated to the molecules adsorption by their surfaces. Therefore, since the retention coefficients and purification factors of both membranes were similar, as shown in Figures 5 and 7, and Table 6, the more appropriate membrane was determined according to the productivity, indicating that the NF membrane can be considered the more appropriate for the concentration and separation of CA.

4. Conclusions

According to the assays carried out for the selection of a membrane to separate clavulanic acid, both the NF and NF90 membranes could be indicated for the proposed objectives of this study, since they present the smallest pores and the clavulanic acid retention depends on the membrane pore size.

The optimal operational conditions for the NF and NF90 membranes were determined with respect to the pH value, clavulanic acid concentration in the feed phase and the process temperature, obtaining the following results: temperature of 30 °C and pH of 5.1 for NF; temperature of 17.5 °C and pH of 6.0 for NF90, and a CA concentration of 750 mg/L for both membranes.

In addition the results were validated under the selected conditions for each membrane. The average results for the NF and NF90 membranes were: retention coefficient above 0.99 for both membranes and productivities up to 121.59 $[CA]_{RET}/[CA]_0$.L.h and 63.31 $[CA]_{RET}/[CA]_0$.L.h for the NF and NF90 membranes, respectively.

The clavulanic acid rejection also depends on its adsorption on the membrane surface, which influences the membrane permeability. Therefore, under the best operational conditions, it was clearly demonstrated the effect of the permeability over the nanofiltration process, which was decisive to determine the best membrane for this process. Concluding, the NF membrane from Filmtec™ was more appropriate for the process under study.

Acknowledgements

The authors acknowledge the financial support from the State of São Paulo Research Foundation (FAPESP) and from the *Coordenação de Aperfeiçoamento de Pessoal de Nível Superior* (CAPES). The authors are also grateful for the membranes donated by Mycrodin Nadir® and Dow Filmtec™.

References

[1] Bersanetti, P.A.; Almeida, R.M.R.G.; Barboza, M.; Araújo, M.L.G.C.; Hokka, C.O. (2005) Kinetic studies on clavulanic acid degradation. *Bioch. Eng. J.*, 23: 31-36.

[2] Cavaco Morão, A.I.; Brites Alves, A.M.; Costa, M.C.; Cardoso, J.P. (2006) Nanofiltration of a clarified fermentation broth. *Chem. Eng. Sci.*, 61: 2418-2427.

[3] Almeida, R.M.R.G.; Barboza, M.; Hokka, C.O. (2003) Continuous clavulanic acid adsorption process. *Applied Bioch. and Biotechnol.*, 108: 867-879.

[4] Mayer, A.F.; Anspach, F.B.; Deckwer, W.D. (1996) Purification of clavulanic acid by ion-pairing systems. *Bioseparation*, 15: 25-39.

[5] Barboza, M.; Almeida, R.M.R.G.; Hokka, C.O. (2002) Kinetic studies of clavulanic acid recovery by ion exchange chromatography. *Bioseparation*, 10: 221-227.

[6] Brites Alves, A.M.; Morão, A.; Cardoso, J.P. (2002) Isolation of antibiotics from industrial fermentation broths using membrane technology. *Desalination*, 148: 181-186.

[7] Hilal, N.; Al-Zoubi, H.; Darwish, N.A.; Mohammad, A.W.; Abu Arabi, M. (2004) A comprehensive review of nanofiltration membranes: Treatment, pretreatment, modelling, and atomic force microscopy. *Desalination*, 170: 281-308.

[8] Matthiason, E. (1983) The role of macromolecular adsorption in fouling of ultrafiltration membranes. *J. Membr. Sci.*, 16: 23-36.

[9] Ochoa, N.A.; Prádanos, P.; Palacio, L.; Pagliero, C.; Marchese, J.; Hernández, A. (2001) Pore size distributions based on AFM imaging and retention of multidisperse polymer solutes: Characterisation of polyethersulfone UF membranes with dopes containing different PVP. *J. Membr. Sci.*, 187: 227-237.

[10] Schäfer, A.I.; Fane, A.G.; Waite, T.D. (2000) Fouling effects on rejection in the membrane filtration of natural waters. *Desalination*, 131: 215-224.

[11] Gekas, V. & Hallström, B. (1987) Mass transfer in the membrane concentration polarization layer under turbulent cross flow: I. Critical literature review and adaptation of existing sherwood correlations to membrane operations. *J. Membr. Sci.*, 30: 153-170.

[12] Vrijenhoek, E.M.; Hong, S.; Elimelech, M. (2001) Influence of membrane surface properties on initial rate of colloidal fouling of reverse osmosis and nanofiltration membranes. *J. Membr. Sci.*, 188: 115-128.

[13] Vrouwenvelder, J.S.; Kappelhof, J.W.N.M.; Heijman, S.G.J.; Schippers, J.C.; Van der Kooij, D. (2003) Tools for fouling diagnosis of NF and RO membranes and assessment of the fouling potential of feed water. *Desalination*, 157: 361-365.

[14] Tarabara, V.V.; Koyuncu, I.; Wiesner, M.R. (2004) Effect of hydrodynamics and solution ionic strength on permeate flux in cross-flow filtration: direct experimental observation of filter cake cross-sections. *J. Membr. Sci.*, 241: 65-78.

[15] Nghiem, L.D.; Vogel, D.; Khan, S. (2008) Characterizing humic acid fouling of nanofiltration membranes using bisphenol A as a molecular indicator. *Water Research*, 42: 4049-4058.

[16] Boussu, K.; Van der Bruggen, B.; Volodin, A.; Van Haesendonck, C.; Delcour, J.A.; Van der Meeren, P.; Vandecasteele, C. (2006) Characterization of commercial nanofiltration membranes and comparison with self-made polyethersulfone membranes. *Desalination*, 191: 245-253.

[17] Boussu, K.; Belpaire, A.; Volodin, A.; Van Haesendonck, C.; Van der Meeren, P.; Vandecasteele, C.; Van der Bruggen, B. (2007) Influence of membrane and colloid characteristics on fouling of nanofiltration membranes. *J. Membr. Sci.*, 289: 220-230.

[18] Wong, P.C.Y.; Kwon, Y.-N.; Criddle, C.S. (2009) Use of atomic force microscopy and fractal geometry to characterize the roughness of nano-, micro-, and ultrafiltration membranes. *J. Memb. Sci.*, 340: 117-132.

[19] Hirose, M.; Ito, H.; Kamiyama, Y. (1996) Effect of skin layer surface structures on the flux behavior of RO membranes. *J. Membr. Sci.*, 121: 209-215.

[20] Mänttäri, M.; Puro, L.; Nuortila-Jokinen, J.; Nyström, M. (2000) Fouling effects of polysaccharides and humic acid in nanofiltration. *J. Membr. Sci.*, 165: 1-17.

[21] Van der Bruggen, B.; Kim, J.H.; DiGiano, F.A.; Geens, J.; Vandecasteele, C. (2004) Influence of MF pretreatment on NF performance for aqueous solutions containing particles and an organic foulant. *Sep. Purif. Technol.*, 36: 203-213.

[22] Yagali-Quintanilla, V.; Sadmani, A.; McConville, M.; Kennedy, M.; Amy, G. (2009) Rejection of pharmaceuticlally active compounds and endocrine disrupting by clean and fouled nanafiltration membranes. *Water Research*, 43: 2349-2362.

[23] Bhattacharyya, D.; Hestekin, J.; Shan, D.; Ritchie, S. (2002) An overview of selected membrane techniques for environmental applications, *J. Chin. Inst. Chem. Eng.*, 33: 61-66.

[24] Van der Bruggen, B.; Vandecasteele, C.; Van Gestel, T.; Doyen, W.; Leysen, R. (2003) A review of pressure-driven membrane processes in wastewater treatment and drinking water production. *Environ. Progress*, 22: 46-56.

[25] Koyuncu, I.; Turan, M.; Topacik, D.; Ates, A. (2000) Application of low pressure nanofiltration membranes for the recovery and reuse of dairy industry effluents. *Water Sci. Technol.*, 41: 213-221.

[26] Nghiem, L. D.; Shafer, A. I.; Elimelech, M. (2005) Nanofiltration of hormone mimicking trace organic contaminants. *Sep. Sci. Technol.*, 40:2633–2649.

[27] López-Muñoz, M.J.; Sotto, A.; Arsuaga, J.M.; Van der Bruggen, B. (2009) Influence of membrane, solute and solution properties on the retention of phenolic compounds in aqueous solution by nanofiltration membranes. *Sep. Purif. Technol.*, 66: 194–201.

[28] Carvalho, A.L.; Maugeri, F.; Silva, V.; Hernández, A.; Palacio, L.; Pradános, P. (2010) AFM analysis of the surface of nanoporous membranes: aplication to the nanofiltration of potasium clavulanate. *J. Material Sci.*, Accepted.

[29] Bird, A.E.; Bellis, J.M.; Basson, B.C. (1982) Spectrophotometric assay of clavulanic acid in aqueous solution. *Analyst*, 107: 1241-1245.

[30] Almeida, R.M.R.G. (2003) *Estudo da purificação do ácido clavulânico utilizando processo contínuo de adsorção*, PhD Thesis; Federal University of São Carlos: São Carlos, BR.

[31] Hirata, D.B.; Oliveira, J.H.H.L.; Leão, K.V.; Rodrigues, M.I.; Ferreira, A.G.; Giulietti, M.; Barboza, M.; Hokka, C.O. (2009) Precipitation of clavulanic acid from fermentation broth with potassium 2-ethyl hexanoate salt. *Sep. Purif. Technol.*, 66: 598-605.

[32] Cavaco Morão, A.I.; Brites Alves, A.M.; Afonso, M.D. (2006) Concentration of clavulanic acid broths: Influence of the membrane surface charge density on NF operation. *J. Membr. Sci.*, 281: 417-428.

NANOFILTRATION PROCESS SCALE-UP: PURIFICATION OF CLAVULANIC ACID

A. L. Carvalho*; F. Maugeri

Departament of Food Engineering, Faculty of Food Engineering, Rua Monteiro Lobato 80, Barão Geraldo, University of Campinas – UNICAMP, CEP: 13083-862, Campinas, SP, Brazil

*e-mail: limoeiro@fea.unicamp.br, telephone: +551935214052, fax: +551935214027

Abstract

In this work, the concentration of clavulanic acid using both a conventional bench-scale and a crossflow pilot plant nanofiltration systems, were studied. These processes were compared in order to evaluate the effectiveness of using a conventional system with a stirrer, in which is promoted the convection movement common at crossflow processes, and at what extension its results can be reproduced in a pilot scaled-up process. Therefore, data obtained in bench-scale in previous work were compared to data arising from pilot plant assays in which different transmembrane pressure and tangential velocity on the membrane surface were used. The results of high productivity and retention coefficient were reproduced in both systems, with equivalent operational conditions. Based on these results, it can be stated that the system in a bench-scale can be the basis for a reliable scale up to a crossflow pilot plant.

Keywords: nanofiltration, membrane, clavulanic acid, scale up

1. Introduction

Clavulanic acid (CA) is a β-lactamase inhibitor, used in combination with β-lactamase sensitive penicillins, to protect the β-lactam ring of the antibiotic against hydrolysis [1,2]. CA is produced industrially by fermentation using *Streptomyces clavuligerus*, and presents low yields in the production process, particularly in the separation and purification step, due to its thermal instability and sensitivity to changes in pH [1,3]. Associated with its low concentration in the fermented broth, studies on its extraction and purification have to consider the kinetic degradation of CA, in order to minimize losses and maximize recovery yields and productivity.

Recent studies on the purification of CA were focused on the evaluation of procedures for its isolation and purification when produced by fermentation with *Streptomyces clavuligerus*. Some separation studies have used Amberlite XAD resin, Amberlite IRA 400 ion exchange resin pre-treated with NaCl, ultrafiltration (UF) followed by nanofiltration, and nanofiltration processes with different membranes and conditions [2,4-7]. Currently, several high-value bio-products have been produced by fermentation, bringing new challenges for the recovery and purification processes. UF processes are an efficient way of separating the biomass from the CA fermentation broth, producing a free protein permeate containing CA, which can be subsequently concentrated using nanofiltration membranes [2,6].

Nanofiltration is a process in which the driving force is the pressure difference between the two sides of the membrane. The main advantages of this process are the operation at low pressures when compared to reverse osmosis, high flow rate, considerable retention of multivalent anionic salts and organic molecules of molecular weight higher than 300 Da, and relatively low investment and low operational and maintenance costs [8]. The performance of nanofiltration is affected by steric and electrostatic effects through the membrane, the Donnan equilibrium, dielectric exclusion, and a steric effect at the membrane surface.

Membrane test cells are extensively used for quality assurance, screening tests and in many research projects. However, many practitioners will agree that test cell results may vary considerably and their accuracy can be inadequate for scale-up to larger membrane units [9]. The test cell usually is carried out in dead-end process while the pilot plant in a crossflow unit. In dead-end filtration, the feed is perpendicular to the membrane surface. As separation occurs the retained solids build up into a layer, which causes resistance to the liquid flow. In crossflow, on the other hand, the mixture flows across the surface of the membrane. The liquid permeates through the

membrane at right angles to the direction of flow of the feed and cake formation can be reduced by a transmembrane sheer stress [10,11]. In their work Lawrence *et al.* [12] have found that all results using the laboratory scale membrane unit under conditions of constant concentration gave flux curves indicative of fouling cake formation, with slight declines in value over the experimental period.

Taking into account the mass transfer on the membrane, it depends on several factors; one of them is the adsorption in the inner of the pores, which causes pore blockage and fouling on the membrane surfaces during the process [13-15]. Another factor is the concentration polarization of the solutes on the high-pressure side of the membrane forming a cake or a gel layer [14-16], leading to an increase in the operation and maintenance costs, permeate flux decline, and energy demands, turning down the membrane performance and eventually reducing membranes life [17-19].

The cake structure otherwise has been predicted to vary as a function of particle transport and surface potential. Moreover, this structure may be modified as a function of the relative balance between applied pressure and surface forces. Thus, the propensity of membrane cakes for reorganization and collapse is determined by a balance of forces acting on the particles in the cake [19].

In the comparison between the dead-end and crossflow processes, the second one shows a better performance, since its characteristics allow the particles to stay in a suspended state above the outer surface instead of being deposited, enhancing control over the fouling and the membrane concentration polarization [10,20,21]. Chun *et al.* [21] also demonstrated that both the cake layer thickness and the particle concentration in the cake layer, for the dead-end case, show higher values than those for cross-flow one. Becht *et al.* [22], conversely, have noticed a higher concentration polarization layer in the crossflow system than in the dead-end cell, since it was used a stirred dead-end cell.The use of the best operational conditions such as temperature, pressure and tangential flow should also be considered. Those conditions should be sought in order to optimize the process, especially in the case of a large scale application [23].

Accordingly, the moving from laboratory experiment to pilot plant operations and finally to a demonstration unit becomes progressively more complicated. Each step brings an increase in membrane area requirement, equipment, quantity of required feedstocks, time for execution, analytical facilities, technical issues, and operating personnel. Design advantages for the pilot plant over lab-scale operations included continuous monitoring of process conditions with a data collection system [24]. Those steps, however, can work as an indication of the economical feasibility of the implementation on full industrial scale in the following days [25].

Therefore, even with a large number of nanofiltration applications suggested [7,26-29], only few were implemented on an industrial scale, showing the necessity of investigate the scale up in membrane process. So, the aims of this work are the scale-up study of a nanofiltration process for clavulanic acid purification, from a lab scale to a pilot plant, and the optimization of the filtration conditions taking into account the transmembrane pressure and the tangential flow velocity.

2. Methodology

2.1. Material

A stainless steel stirred dead-end cell was used in the first studies of CA nanofiltration. The system consists of a cylindrical container jacketed, with a membrane located at the base, whose area was 1.52 x 10^{-3} m^2, and a magnetic stirrer that promotes the convection movement in the process. The pressure difference was applied by a change in the internal atmosphere with the application of nitrogen gas, as shown in Figure 1. In this step CA from microfiltered and ultrafiltered fermentation broth was used.

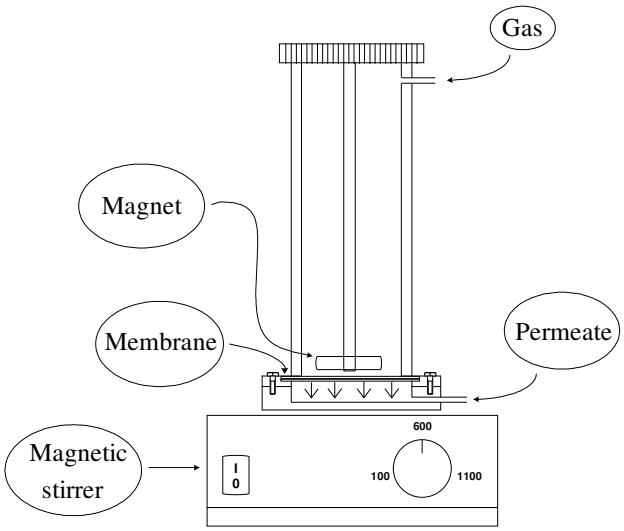

Figure 1 – Schematic representation of the bench-scale stirred dead-end cell.

The pilot plant used is a nanofiltration system which works recirculating the solution at the tank feed to improve the efficiency of filtration and to allow the continuous flow on the membrane surface, as presented in Figure 2. Is this step, a solution of CA prepared from the medicine Clavulin® (revested pills with 125 mg of potassium clavulanate and 500 mg of amoxicilin), from GlaxoSmithKline Brasil Ltda, was used. In some of those experiments a solution of peptone 5.5 g/L was added.

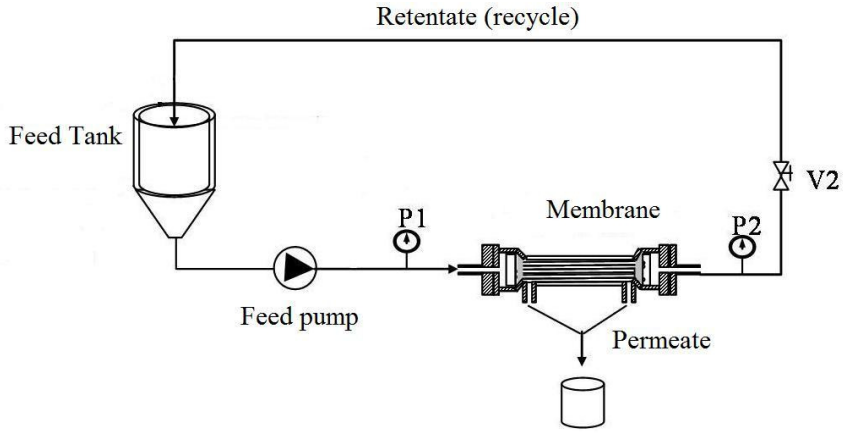

Figure 2 – Schematic representation of the pilot plant.

It was used a spiral module of the membrane NF-2540 (polypiperazine amide), from Filmtec™. The Table 1 shows its characteristics, according to the manufacturer. The pH of the CA solutions was adjusted using 0.2 M hydrochloric acid and 1 M potassium hydroxide, prepared using analytical grade reagents. The hydrochloric acid solutions were prepared using 36.5-38 % pure hydrochloric acid.

Table 1 – Characteristics of the membrane NF

MWCO (Da)	>200
Active area (m^2)	2.6
Max. pressure (bar)	41
Max. temperature (ºC)	45
pH range	3-10
Pore size (nm)[a]	1.39
Lp (10^{-11}m/Pa.s)[a]	3.39
Rejection of $MgSO_4$ (%)	>99

[a] Carvalho *et al.* [30]

The imidazole used in the analysis of the concentration of CA in the feed, permeate and rejection phases, was ultrapure. The results were analyzed using the statistical software Statistica 7.0® from StatSoft®.

2.2. Experimental procedure

The stirred dead-end cell was carried out using an ultrafiltered fermentation broth, in which the concentration of CA varied according to the fermentation process between 435 mg/L and 698 mg/L. In this case the initial volume was 100 mL, the applied pressure varied from 1 MPa to 3 MPa and the surface flow velocity from 0.76 m/s to 2.72 m/s. In the pilot plant experiments, aqueous solutions of potassium clavulanate were used, instead of fermentation broth, due to the elevated quantity of solution needed to carry out the experiment, which was around 10 L. These solutions were vacuum filtered and microfiltered through 14 μm and 0.45 μm pore membranes, respectively. Different from the former, the transmembrane pressure varied between 1 MPa and 2 MPa and the tangential flow velocity varied between 0.016 m/s and 0.11 m/s. The maximum pressure (3 MPa) was not used in pilot scale because it could damage the membrane due to the strong pulsations performed by the lobular pump used.

In some of the pilot plant assays a peptone solution was used in order to simulate amino acids and small peptides as contaminants in fermentation broth, since they can hinder the process as a whole. For these experiments four different conditions were used (1.5 MPa and 2 MPa, in two different permeate fluxes for each pressure).

In all cases the retention coefficient (R_C), the process productivity and the volumetric flux by membrane area (J_V) were evaluated. Since previous results showed that both temperature and pH were not relevant to the performance of the dead-end cell, they were not evaluated in the larger scale experiments [7].

2.3. Mathematical considerations

The retention coefficients were calculated from the CA mass found in the retentate and permeate phases, since the concentration factor was kept constant for all experiments. The productivities were calculated according to the CA concentration in the retentate and feed phases,

the feed tank volume and the time elapsed at the end of the process. Equations (1) and (2) show these relationships.

$$R_C = 1 - \frac{M_{PER}}{M_{REJ}} \tag{1}$$

$$Productivity = \frac{[CA]_{REJ}}{[CA]_0 \times V_0 \times t} \tag{2}$$

where R_C is the retention coefficient, M_{PER} is the CA mass in the permeate, M_{REJ} is the CA mass in the retentate, $[CA]_{REJ}$ is the CA concentration in the retentate, $[CA]_0$ is the CA concentration in the feed phase, V_0 is the volume in the feed phase, t is the process time (h).

2.4. Analytical methodology

The concentration of CA was determined according to Bird *et al.* [31], using a Beckman Coulter™ model DU®640 spectrophotometer. The antibiotic was reacted with imidazole (60 g/L, pH 6.8) and the absorbance of the reaction product measured at 312 nm. The product of this reaction is more stable than CA and its formation is directly proportional to the CA concentration present in the reaction mixture. Potassium clavulanate, also from the medicine Clavulin®, was used as standard.

3. Results and discussion

3.1. Experiments in the stirred dead-end cell and the pilot plant

In the experiments carried out in the stirred dead-end cell, in bench-scale, Carvalho *et al.* [7] have studied some nanomembranes considering their effectiveness at concentrating clavulanic acid, as well as their selectivity concerning peptides and amino acids, especially the aromatic ones. According to these the authors, the NF membrane was the best one for this process. Threfore, this membrane was selected to be used in this work, for the process of scaling up and parameter optimization.

The results of both works were assembled and shown in the following figures. In Figure 3, it can be seen that the NF membrane is effective in retaining over 97%, practically 100% for some conditions, of the clavulanic acid in the feeding solution, when suitable operational conditions are applied, either in bench or pilot scale.

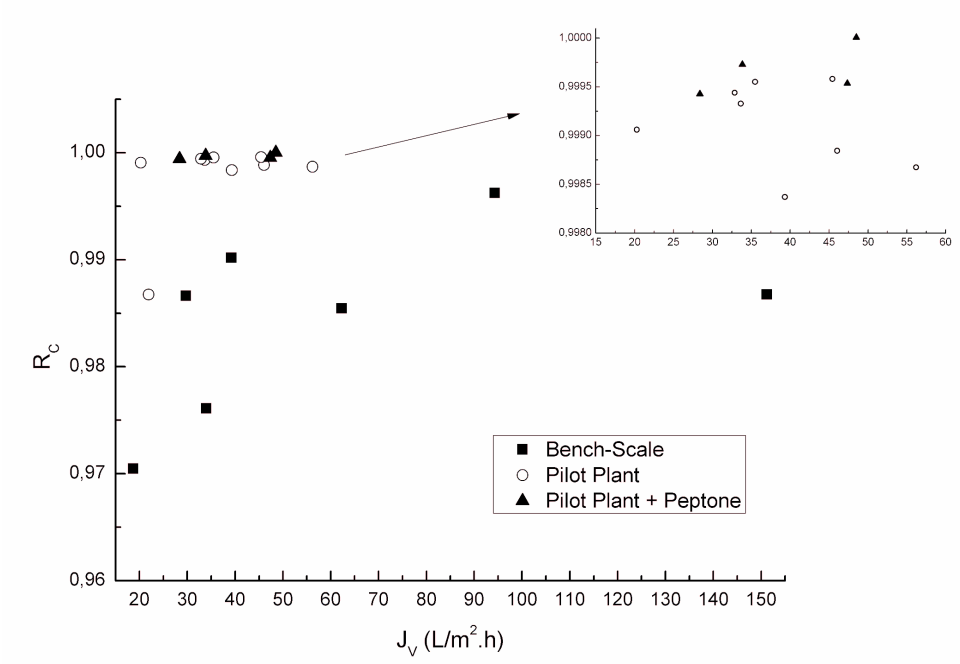

Figure 3 – Retention coefficient (R_C) as a function of permeate flux (J_V) for the different processes.

Particularly, when the experiments were carried out in the pilot plant, the retention coefficient was over 98.6%, at any tangential velocity or transmembrane pressure and a lower variability in the results was observed, which seems related to enhanced stability of the pilot plant, compared to the bench scale, allowing a better reproducibility.

According to Lawrence *et al.* [12], systems of dead-end cells have demonstrated the formation of a cake over the membrane surface with time of use due to the occurrence of a high concentration polarization in this kind of process. Thus, to reduce this effect, higher agitation speeds than those used in pilot scale were used, since the higher the speed the higher the mass transfer coefficient [32]. Therefore, this precaution enables a similar, or even higher, permeate flux for the stirred dead.end cell to those obtained at the pilot plant, as shown in Figure 3. However, even with agitation being promoted on the membrane surface the solutes accumulated on it, since the shear stress does not affect the CA molecule, which has a molecular mass of 199.16 g/mol,

leading to an increase in clavulanic acid permeability through the membrane, hampering the effectiveness of process, as seen through the lower retention coefficient in bench-scale when compared with that obtained in the pilot plant.

Furthermore, the addition of peptone did not hamper the retention behavior; on the contrary, it improved it, as shown in the inserted graphic, probably due to an increase in the concentration polarization layer with the formation of a gel layer of peptone, which decreased the transport of clavulanic acid through the membrane. This should have happened since the peptone is rich in polar substances, such as amino acids, which were preferably attracted to the membrane surface.

Comparing the results from both scales, it can be noticed that there is a small change in the retention coefficient from the bench-scale to the pilot plant process, as shown in the Figure 3, but high enough to suppose that this causes increments in productivity, as shown in the Figure 4. It has been suggested that in pilot plant experiments the retention coefficient is improved due to the reduction of the concentration polarization, though this is less evident in spiral membranes, such as those used in the pilot plant experiments, due to the induction of turbulent flows in between the layers of the membrane, caused by a polymer mesh filamentous interlaced comprising its structure [12].

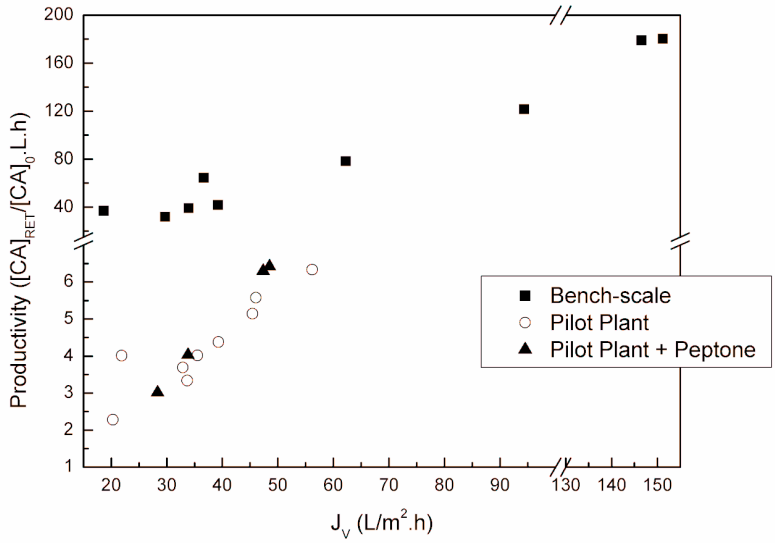

Figure 4 – Productivity for both processes as a function of permeate flux (J_V).

The productivity, as defined by Eq. 2, is an important parameter when denaturing bioproducts are concerned, since it relates the concentrating effect, the feed tank volume and the process time elapsed, so that higher the productivity, higher the chances of good product recovering.

It is relevant to point out that in the bench-scale process the productivity was extremely higher than in the crossflow process, achieving up to 180 $[CA]_{RET}/[CA]_0$.L.h, probably due to the smaller volume used in those assays, since the productivity is defined as the concentration factor by feed volume per hour and in the bench-scale processes were used volumes 100 times smaller than in the crossflow processes. In both processes it was noticed an increase in the productivity with the permeate flux. This phenomena was more accentuated in the bench-scale process, due to the larger transmembrane pressure used in some experiments in this step, which are those that corresponds to the higher permeate fluxes in the Fig. 4.

Additionally, it was observed that the presence of amino acids and peptide contaminants in the crossflow process, represented here by the peptone, improved the productivity, in concordance with the increase in the retention coefficient, reaching up to 6.4 $[CA]_{RET}/[CA]_0$.L.h. This behaviour can be better observed in Fig. 5 for transmembrane pressures from 1.5 MPa to 2 MPa used in the pilot plant experiments, with and without peptone, in which the same permeate flux corresponds to the same assay. It is also noticed that the permeate flux decreased with the presence of peptone, probably due to the higher viscosity of the CA solution, and that the transmembrane pressure affect more the productivity than the R_C, probably due to the increment in the permeate flux observed.

On the other hand, the permeate flux in the bench-scale was equal or superior to that obtained in the pilot plant, as shown in the Fig. 3 and 4. This result is consistent with that obtained by Lawrence *et al.* [12]. These authors suggested that this difference can be attributed to mechanical distinctions between the two systems and how the transmembrane pressure is applied, as in the case of the pilot plant, in which the pressure adjacent to the membrane surface on the permeate side is relatively higher than the ambient pressure, which suits as reference for calculating the transmembrane pressure, due to the high permeate flux in this type of process, which restricts the flow that could be obtained. Also, when the permeate flux is plotted against the transmembrane pressure an increase is observed in the former, which is predictable, since the higher the transmembrane pressure the higher the driving force to push water through the membrane, leading to the best results at a pressure of 2 MPa, as shown in the Fig. 6.

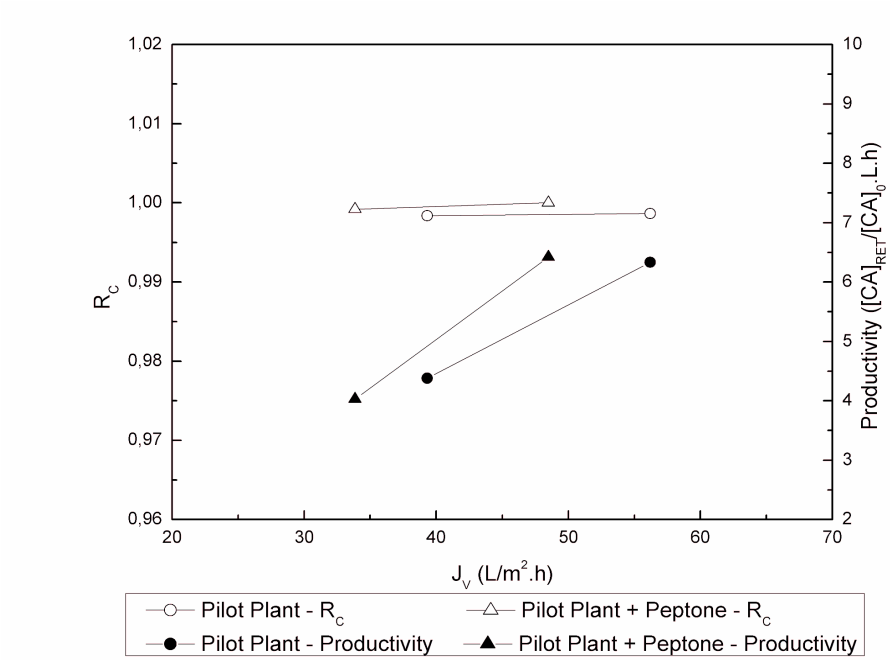

Figure 5 – Retention coefficient and productivity as a function of the permeate flow (J_V) for the pilot plant with and without the addition of peptone in the CA solution, in applied pressure of 1.5MPa and 2 MPa.

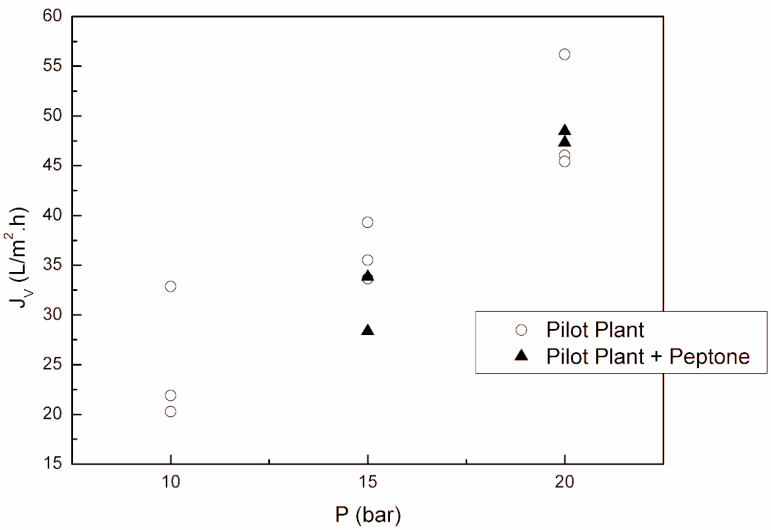

Figure 6 – Flow of permeate (J_V) for the pilot plant as a function of transmembrane pressure.

3.2. Scale-up procedure

The process scale-up from the bench-scale to the pilot plant needed some precautions, for instance the choice of a more adequate superficial velocity for the spiral membrane, in order to preserve its structure and assuring a longer life. Thus, velocities from 2 cm/s to 11 cm/s were used. The most convenient would be the use of a velocity around 6 cm/s, however this was exceeded in some cases when a larger pump rotation and small transmembrane pressure were used. Additional precaution was taken concerning the system pressures, which should not be higher than 2 MPa, in order to avoid any damage to the system, since the pump normally promoted strong pulsations. These pulsations made pressure oscillate, so that working pressure above 2 MPa led to pulses that exceeded the pump maximum operation pressure, which was 3 MPa.

The results of such measures were positive since the pilot plant reproduced consistent data when compared to those found in bench-scale. The differences found in retention coefficient, permeate flux and productivity can be attributed to the differences between the two process, mainly considering how the transmembrane pressure is applied, as explained before.

Therefore, even with the differences between bench and pilot plant scales, it is possible to predict the behaviour of a membrane process in the pilot plant with data from bench-scale, since the changes are predictable and can be circumvented. As a result, it is reasonable to affirm that the studies made in a stirred dead-end system in a bench-scale can be used reliably in the scale-up process from bench-scale to a pilot plant, targeting an industrial application of the process.

4. Conclusions

Based on the studies of scale-up of a clavulanic acid nanofiltration process from bench-scale to a pilot plant, it can be concluded that data from bench scale can be used to design the scale-up to a pilot plant nanofiltration process, even though some variations can occur, which can be circumvented, allowing the use of the bench-scale operational conditions to predict the pilot plant behaviour.

The peptone, used as peptide and amino acid contaminant source, possibly improved the process productivity, which indicates that peptide molecules could enhance the clavulanic acid concentration process by nanofiltration.

The NF membrane was extremely effective in this process, achieving retention coefficients of almost 100%. The pilot plant process was advantageous concerning the productivity, reaching up to 6.4 $[CA]_{RET}/[CA]_0$.L.h, meaning that the recovery of clavulanic acid by this kind of membrane can be very efficient and allows the prediction of a successful application in industrial scale.

Acknowledgements

The authors acknowledge the financial support from the State of São Paulo Research Foundation (FAPESP).

References

[1] P.A. Bersanetti, R.M.R.G. Almeida, M. Barboza, M.L.G.C.Araújo, C.O. Hokka, *Bioch. Eng. J.* 23 (2005) 31-36.

[2] A.I. Cavaco Morão, A.M. Brites Alves, M.C. Costa, J.P. Cardoso, *Chem. Eng. Sci.* 61 (2006) 2418-2427.

[3] R.M.R.G. Almeida, M. Barboza, C.O. Hokka, *Applied Bioch. and Biotechnol.* 108 (2003) 867-879.

[4] A.F. Mayer, F.B. Anspach, W.D. Deckwer, *Bioseparation* 15 (1996) 25-39.

[5] M. Barboza, R.M.R.G. Almeida, C.O. Hokka, *Bioseparation* 10 (2002) 221-227.

[6] A.M. Brites Alves, A. Morão, J.P. Cardoso, *Desalination* 148 (2002) 181-186.

[7] A. L. Carvalho, M. I. Rodrigues, F. Maugeri, *Sep. Sci. Technol.* (2010) Submitted.

[8] N. Hilal, H. Al-Zoubi, N.A. Darwish, A.W. Mohammad, M. Abu Arabi, *Desalination* 170 (2004) 281-308.

[9] T. Schipolowski, A. Jeżowska, G. Wozny, *Desalination* 189 (2006) 71-80.

[10] M.S. Le & T. Atkinson, *Process Biochem.* 20 (1985) 26-31.

[11] S. Eberhard, *Kluwer Academic/Plenum Publishers, New York* (2000) 19-40.

[12] N.D. Lawrence, S.E. Kentish, A.J. O'Connor, A.R. Barber, G.W. Stevens, *Sep. Purif. Technol.* 60 (2008) 237-244.

[13] E. Matthiason, *J. Membr. Sci.* 16 (1983) 23-36.

[14] N.A. Ochoa, P. Prádanos, L. Palacio, C. Pagliero, J. Marchese, A. Hernández, *J. Membr. Sci.* 187 (2001) 227-237.

[15] A.I. Schäfer, A.G.; Fane, T.D. Waite, *Desalination* 131 (2000) 215-224.

[16] V. Gekas & B. Hallström, *J. Membr. Sci.* 30 (1987) 153-170.

[17] E.M. Vrijenhoek, S. Hong, M. Elimelech, *J. Membr. Sci.* 188 (2001) 115-128.

[18] J.S. Vrouwenvelder, J.W.N.M. Kappelhof, S.G.J. Heijman, J.C. Schippers, D. Van der Kooij, *Desalination* 157 (2003) 361-365.

[19] V.V. Tarabara, I. Koyuncu, M.R. Wiesner, *J. Membr. Sci.* 241 (2004) 65-78.

[20] H. Strathmann, *Trends Biotechnol.* 3 (1985) 112-118.

[21] M.-S. Chun & W.C. Park, *J. Membr. Sci.* 243 (2004) 417-424.

[23] M.V. Tres, S. Mohr, M.L. Corazza, M. di Luccio, J.V. Oliveira, *J. Membr. Sci.* 333 (2009) 141-146.

[22] N.O. Becht, D.J. Malik, E.S. Tarleton, *Sep. Purif. Technol.* 62 (2008) 228-239.

[24] L.S. White, *J. Membr. Sci.* 286 (2006) 26-35.

[25] W.-J. Lau & A.F. Ismail, *Desalination* 245 (2009) 321-348.

[26] B. Van der Bruggen, J.H. Kim, F.A. DiGiano, J. Geens, C. Vandecasteele, *Sep. Purif. Technol.* 36 (2004) 203-213.

[27] D. Bhattacharyya, J. Hestekin, D. Shan, S. Ritchie, *J. Chin. Inst. Chem. Eng.* 33 (2002) 61-66.

[28] B. Van der Bruggen, C. Vandecasteele, T. Van Gestel, W. Doyen, R. Leysen, *Environ. Progress* 22 (2003) 46-56.

[29] I. Koyuncu, M. Turan, D. Topacik, A. Ates, *Water Sci. Technol.* 41 (2000) 213-221.

[30] A.L. Carvalho, F. Maugeri, V. Silva, A. Hernández, L. Palacio, P. Pradános, *J. Material Sci.* (2010) Accepted.

[31] A.E. Bird, J.M. Bellis, B.C. Basson, *Analyst* 107 (1982) 1241-1245.

[32] A.L. Carvalho, F. Maugeri, V. Silva, P. Prádanos, A. Hernández, (2011) Not submitted yet.

4. CONCLUSÕES GERAIS

Na etapa de seleção das membranas em células agitadas do tipo dead-end (escala de bancada), foram encontradas as melhores condições operacionais para as membranas NP010, NP030, NF e NF90, considerando-se o pH e a concentração de ácido clavulânico na fase alimentação, e a temperatura de processo. Nessas condições o pH não afetou o processo, permitindo o uso de qualquer dos valores contidos na faixa de estudo. Entretanto, devido à degradação do ácido clavulânico, recomenda-se trabalhar em pH 6,2. Assim, as melhores condições operacionais obtidas são as apresentadas na Tabela 1.

Tabela 1 – Melhores condições operacionais para as membranas estudadas

	NP010	**NP030**	**NF**	**NF90**
Temperatura (ºC)	30	30	30	17,5
C_0 (mg/L)	750	750	750	750

Os resultados nessas condições foram validados e suas respostas comparadas. As médias obtidas para cada membrana se encontram na Tabela 2.

Tabela 2 – Melhores resultados obtidos para as membranas estudadas.

	NP010	**NP030**	**NF**	**NF90**
C_R	0,718	0,862	0,990	0,999
Produtividade ($[CA]_{RET}/[CA]_0$.L.h)	42,97	33,05	34,05	30,34

A partir do teste de Tukey de comparação de médias, verificou-se que as membranas NF e NF90 apresentaram os melhores resultados para os objetivos propostos por este trabalho. Ambas foram avaliadas na etapa de estudo de seletividade das membranas, com o qual verficou-se que a membrana NF é melhor para esse processo por permitir uma maior produtividade, 121,59 $[CA]_{RET}/[CA]_0$.L.h, duas vezes a obtida pela membrana NF90, mantendo a mesma retenção de 0,99.

As quatro membranas foram caracterizadas através da morfologia de suas superfícies e das suas densidades volumétricas de carga através de visualização em microscópio de força atômica e de medidas do potencial elétrico. Foi também avaliada a retenção de KCl em variadas concentrações e valores de pH para determinar, em uma etapa posterior a constante dielétrica dentro dos poros e assim finalizar a etapa de caracterização das membranas.

Das análises microscópicas, tem-se que o diâmetro dos poros de cada membrana são, para as membranas NF90, NF, NP030 e NP010, 0,99 nm, 1,39 nm, 1,48 nm, 1,49 nm, respectivamente. O que já era esperado devido aos rendimentos de processo de concentração de ácido clavulânico obtidos na etapa anterior de seleção de membranas, que indicaram melhores resultados para a membrana NF90 e piores para a NP010, uma vez que o ácido clavulânico tem massa molar de 199,16 g/mol. Os resultados mostraram também que os poros têm o formato elíptico. Notou-se ainda que para as membranas com valores de rugosidade similares quando limpas:

- A permeabilidade se relaciona linerarmente com o tamanho dos poros.
- Em elevada adsorção de ácido clavulânico, a rugosidade tende ao mesmo valor para todas as membranas.
- A dimensão fractal aumenta com a adsorção, em acordo com o aumento da densidade superficial.
- A redução da permeabilidade é alta quanto maior é a diferença na dimensão fractal antes e depois de ocorrer a adsorção.

Verificou-se ainda que o ponto isoelétrico das membranas estudadas se encontram entre o pH 5,0 e pH 6,0 em todas elas, e que as membranas NF90 e NF apresentam comportamento negativo, e que as membranas NP030 e NP010 apresentam um comportamento neutro.

Observou-se também que a permeabilidade à água das membranas segue a seguinte ordem: NP010 > NP030 > NF > NF90, como apresentado na Tabela 3:

Tabela 3 – Permeabilidade a água para cada membrana avaliada, antes e depois do seu uso para permear clavulanato de potássio

Lp (10^{-11}m/Pa.s)	NF90	NF	NP030	NP010
Antes	1,53	3,39	4,36	6,47
Depois	1,10	2,46	1,96	1,38
Lp (usada)/Lp (nova) (%)	72%	73%	45%	21%

Os coeficientes de transferência de massa para as membranas NP030 e NP010 não diferem entre si e as membranas NF e NF90 mostraram valores maiores, especialmente a NF90 com valores até três vezes superiores às membranas NP030 e NP010. Têm-se ainda que a rejeição de ácido clavulânico variou com o pH para as membranas NF e NF90, passando de 0,5 em pH 4 para 0,95 em pH 8.

Quanto à seletividade das membranas, as mesmas apresentaram seletividade ao KCl e ao ácido clavulânico na mesma tendência da densidade volumétrica de cargas: NF > NF90 > NP030 ≈ NP010.

A partir da resolução do modelo SEDE-VCh foi possível determinar a constante dielétrica dentro dos poros e, assim como a permeabilidade, a constante dielétrica dentro dos poros é diretamente proporcional ao diâmetro médio dos poros até a mesma atingir o valor da água livre.

Com base nos estudos feitos para avaliar a ampliação de escala de um processo de nanofiltração de ácido clavulânico de um sistema de bancada para uma planta piloto, conclui-se que as variações previstas podem ser contornadas e que os resultados da ampliação foram satisfatórios, uma vez que as condições de processo utilizadas na escala de bancada puderam servir de base para os estudos em escala piloto, permitindo o uso desse sistema convencional que simula o sistema de fluxo tangencial em outros estudos de avaliação de processos e de seleção de membranas.

A peptona adicionada para atuar como contaminante, em substituição aos peptídeos e aminoácidos presentes nos caldos fermentados, agiu de forma a melhorar a produtividade do processo, o que indica que substâncias protéicas podem operar melhorando o processo de concentração de ácido clavulânico por nanofiltração.

O processo de concentração de ácido clavulânico por nanofiltração com a membrana NF foi bastante eficaz com coeficientes de retenção de quase 1,0. O processo em escala piloto também se mostrou bastante vantajoso, como se verifica através da produtividade que foi de até 6.4 $[CA]_{RET}/[CA]_0$.L.h. A partir desses resultados pode-se concluir que o processo é promissor para implantação industrial, podendo seguir para as próximas etapas de ampliação de escala.

Considerando a purificação de uma solução de ácido clavulânico em relação aos aminoácidos, nas condições estudadas não foi possível purificar o produto de interesse, entretanto ao se considerar sais monovalentes, como o cloreto de potássio, como contaminantes, os resultados foram positivos, com uma seletividade em torno de 30.

5. SUGESTÕES PARA TRABALHOS FUTUROS

Para o futuro sugere-se que sejam feitos trabalhos para averiguar com mais atenção o efeito dos compostos protéicos sobre o transporte de ácido clavulânico através da membrana NF, considerando-se a adsorção de ambos na superfície da mesma e estudos eletrocinéticos.

Testar o efeito da presença de outros compostos sobre o processo, como alguns sais mono e divalentes, e averiguar se ocorre melhora na purificação do ácido clavulânico.

Efetuar mais experimentos na planta piloto com o intuito de avaliar a polarização da concentração na superfície da membrana com o tempo de uso da mesma.

Testar outras condições de processo, como a diafiltração, para avaliar se ocorre alguma melhora na purificação do ácido clavulânico.

Trabalhar o modelo matemático SEDE-VCh com os dados obtidos com os experimentos feitos na planta piloto visando a uma futura ampliação de escala para uma planta de demonstração.